Adaptive Power Amplifier Linearization by Digital Pre-Distortion with Narrowband Feedback using Genetic Algorithms

A Thesis
Presented to
The Academic Faculty

by

Roland Sperlich

In Partial Fulfillment
of the Requirements for the Degree
Doctor of Philosophy

School of Electrical and Computer Engineering
Georgia Institute of Technology
August 2005

Adaptive Power Amplifier Linearization by Digital Pre-Distortion with Narrowband Feedback using Genetic Algorithms

Approved by:

Dr. J. Stevenson Kenney, Advisor
School of Electrical and Computer Engineering
Georgia Institute of Technology

Dr. Robert K. Fenney
School of Electrical and Computer Engineering
Georgia Institute of Technology

Dr. G. Tong Zhou, Co-Advisor
School of Electrical and Computer Engineering
Georgia Institute of Technology

Dr. James A. Sills
KhiMetrics Inc.

Dr. William M. Leach
School of Electrical and Computer Engineering
Georgia Institute of Technology

Date Approved June 22, 2005

To my parents, Raymonde and Roland,

my sisters Catherine and Madeleine,

and all of my friends.

ACKNOWLEDGEMENTS

I want to express my appreciation to the following people for their help over the past several years. Their support has made my completion of this program possible.

First and foremost, I would like to thank my advisor whom through knowledge, experience and passion guided my graduate studies. Dr. Kenney has ensured my academic development while emphasizing the importance of collaborative work with fellow students and peers instilling strong personal skills.

I would also like to thank Dr. Jim Sills, Mr. Greg Copeland, Mr. Al Wegener and Texas Instruments for their continued involvement without which none of this work would have been possible.

My gratitude is also extended to my family, whose expectations in me and unwavering support have been a foundation upon which I can always trust.

Finally, I would like to thank all my friends, who contributed in countless ways to my achievements. Their social and moral support allowed me to maintain my perspective over the past few years.

TABLE OF CONTENTS

LIST OF TABLES

LIST OF FIGURES

SUMMARY

This dissertation presents a study of linearization techniques that have been applied to power amplifiers in the cellular communication industry. The objective of this work is to understand the limitations of power amplifiers, specifically the limitations introduced by the use of spectrally efficient modulation schemes. The digitization of communication systems has favored the use of new techniques and technologies capable of increasing the efficiency of costly power amplifiers. The work explores traditional and digital linearization systems; an algorithm based on the principles of natural recombination is proposed to directly address the limitations of previous embodiments. Previous techniques, although effective, have significant implementation costs that increase exponentially with the increasing signal bandwidths. The proposed software-hardware architecture significantly reduces implementation costs and the overall complexity of the design without sacrificing performance.

To fulfill the requirements of this study, multiple systems are implemented through simulation and closed-loop hardware. Both simulation and hardware embodiments meet the expected performance metrics, providing validation of the proposed algorithm. The application of the algorithm to memory power amplifier linearization is a new approach to adaptive digital pre-distortion using narrowband feedback. The work will show performance improvements on an amplifier with memory effects suggesting that this technique can be employed as a lower-cost solution to meet requirements when compared to typical system implementations.

CHAPTER I

INTRODUCTION

1.1 Motivation

Efficiency is and has always been a primary concern in electrical engineering and many other industries. Most often this greatly sought after efficiency comes at a financial cost. In the automotive industry, for example, if an assembly line is operating at its highest possible level of efficiency, the quality control over each vehicle may diminish. The cellular industry is no different from other business in its efforts to reduce cost by maximizing efficiency. In the case of the cellular industry, a large portion of the costs are attributed to basestations. The basestation is the infrastructure that is responsible for transmitting and receiving speech and data between cellular devices. A significant portion of the costs are attributable to the high power amplifiers (HPA) located within these infrastructures. When a PA is operating at higher efficiency, the linearity of the PA is adversely affected. The motivation for this work is to maximize the efficiency and linearity of HPAs thus breaking the antipodal relationship between the two.

To compound the problem, the rapidly increasing number of mobile communication system users has driven the demand for spectrally efficient modulation schemes. In first-generation systems, constant envelope modulation techniques such as frequency modulation (FM) were employed because they allowed the power amplifier (PA) to operate near saturation with increased PA efficiency. These modulation techniques do not generate spectral regrowth or intermodulation distortion (IMD) products in the nearby channels; however, they are spectrally inefficient with low data to bandwidth ratios. Wireless systems share a common transmission medium

thus maximizing the information that can be carried over a particular bandwidth will effect the profit of the system. Second-generation systems addressed the problem with the introduction of time domain multiple access (TDMA) modulation schemes. These schemes allowed for multiple users to be multiplexed over a particular bandwidth, in the case of Global System for Mobile Communications (GSM) as many as eight users were multiplexed. Finally, the growth in users stimulated the development of varying envelope modulation schemes that we now see in third-generation (3G) systems.

Non-constant envelope digital modulation techniques such as universal mobile telecommunications system (UMTS), code-division multiple access (CDMA) and wide-band CDMA (WCDMA) are spectrally more efficient [1]; however, they are subject to severe IMD when the PAs are operated near saturation. The increase in channel capacity has driven the need for linear PAs; therefor, the increased spectral efficiency has resulted in less efficient PAs. Higher linearity is necessary because distortion is strictly limited by FCC and ETSI regulations [2] that define maximum levels for adjacent channel leakage ratio (ACLR). A second type of distortion resulting from nonlinear operation is harmonic distortion, contrary to IMD, this appears far from the fundamental band and is easily filtered out.

The most recent advances in modulation techniques have also favored the trend towards multicarrier power amplifiers (MCPA) in basestation architecture. As opposed to single carrier power amplifier which require expensive combiners to achieve equivalent bandwidth, MCPAs are more cost effective and easily scalable. They are however predisposed to the tradeoff between linearity versus efficiency. A simple method to maintain linearity is to operate the PA at a lower average power level, this technique is referred to as backoff. The term *headroom* is used to indicate the difference between average power and saturation level at the output of a PA. The backoff technique increases the amount of headroom, thus decreasing efficiency. A second

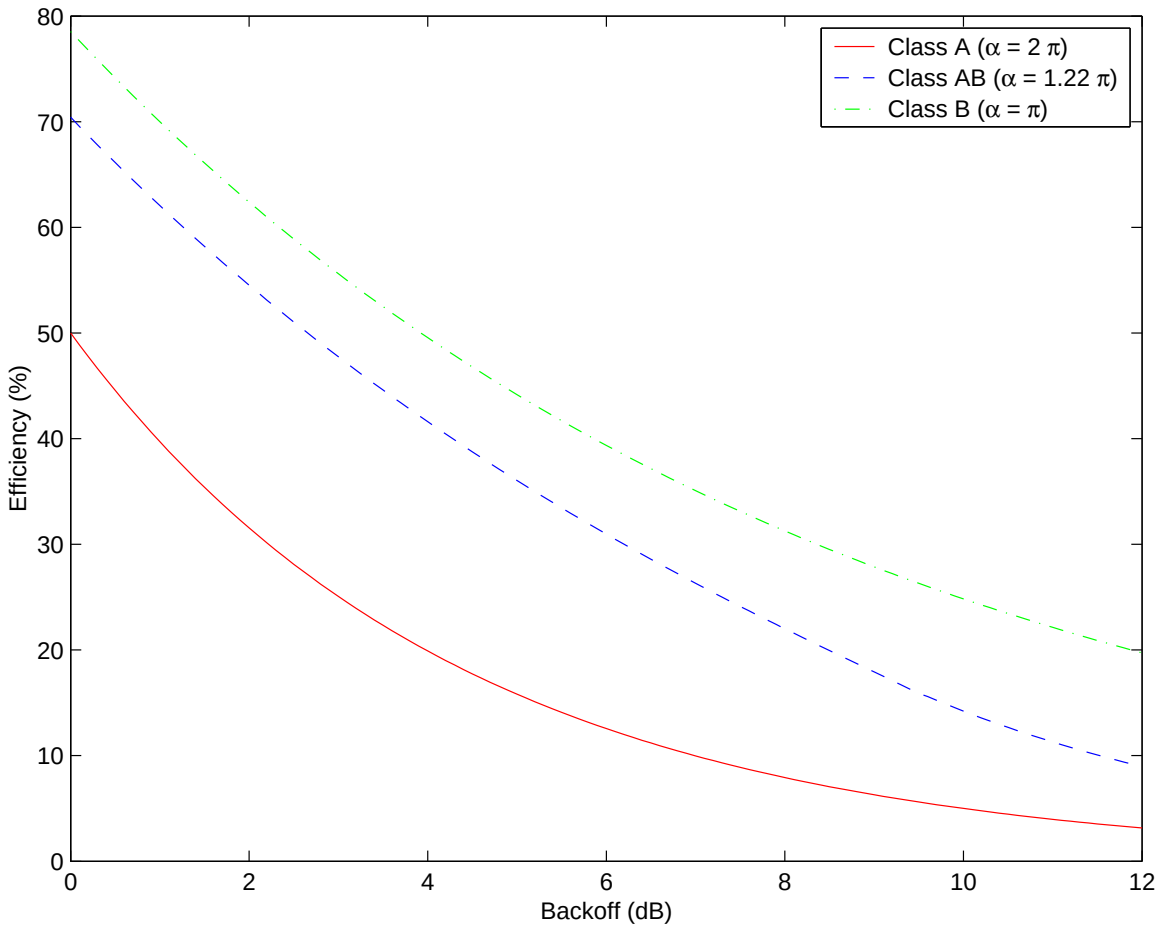

Figure 1: Amplifier efficiency performance.

obvious disadvantage to this technique is the increased cost of a more powerful amplifier with a higher saturation level. The inefficiency of these HPAs also contributes to cooling problems within the basestations due to high power dissipation.

Fortunately, there are linearization techniques [3–5] that allow a PA to be operated at higher power with minimal ACLR to meet efficiency and linearity requirements. Since power and cost are directly related, linearization allows for a lower-cost more-efficient PA to be used in place of a high-cost less-efficient PA. PAs in the field today are predominately linearized by some form of feedforward technology, a concept originally proposed by Black during the 1930's [6]. In recent years, there has been growing interest in linearization by digital pre-distortion (PD). Compared to

feedforward, designs based on digital pre-distortion are showing higher efficiency at lower cost, and with recent advances in technology, digital pre-distortion can now support signal bandwidths in excess of 20MHz. Adaptive PD designs utilize a feedback signal to compensate for variations in the PA nonlinearity over time. Faulkner describes adapting a PD look-up table (LUT) [7] by comparing the PD input and PA output on a sample by sample basis in both amplitude and phase [8, 45]. This technique is applied to the adaptation of a PD polynomial in [10]. Accounting for intermodulation products in the PA output, the feedback bandwidth for sample-by-sample comparison can reach 100MHz. In such cases, system cost is largely driven by the high-performance analog-to-digital converters (ADC) in the feedback path. Such a high performance ADC can end up being the most expensive component in the transmitter and can greatly diminish any power amplifier cost savings gained using pre-distortion. A less costly alternative adapts the PD using only narrowband feedback. Stapleton et al. propose a direct search algorithm to adjust polynomial coefficients to minimize out-of-band emissions in [11]. This method is slow to converge and requires a quadratic cost function. Results are given for third-order polynomials where the linear gain term is fixed.

This work presents adaptation results using narrowband feedback and a genetic algorithm (GA). Genetic algorithms are optimization techniques that use natural selection and recombination to generate new sample points in a search space [12–14]. These algorithms are well-suited to nonlinear optimization problems and converge well even on complicated non-convex cost functions [15, 16]. Typical wideband, or sample-by sample optimization methods are undesirable because their adaptation is prone to locating false peaks in multimodal search spaces. The GA adapts using a rich database of points or population of strings; many peaks are therefore climbed in parallel, consequently reducing the probability of locating a false peak. This technique readily affords the adaptation of higher-order polynomials with varying linear gain.

We also investigate the use of crest factor reduction (CFR) as a preprocessor to PD. This linearization technique further improves the PD performance. The 3G digital modulation schemes also result in signals with a larger peak-to-average ratio (PAR), the CFR technique reduces the crest factor of the input signal in such a way that the signal spectrum, particularly the adjacent channel spectrum, is preserved. Thus, using CFR, a PA may be operated at higher output levels by decreasing the amount of headroom required to maintain acceptable levels of ACLR. The work also reveals the importance of *memory effects* which are often present in HPAs and severely limit the performance of linearization techniques. The causes of these memory effects are reported followed by efforts targeted at suppressing them through system and algorithm development.

1.2 Thesis Organization

The goal of this dissertation is to study both algorithms and systems used to increase the efficiency and linearity of power amplifiers. Previous techniques used to address this problem will be discussed and their limitations will be identified to create a starting point for the research. The research presented here will address the limitations of the previous techniques and demonstrate new methods of linearization. A new system architecture and algorithm are proposed which address critical issues in pre-distortion systems, such as cost and overall complexity of the design. This new architecture will be characterized and its limitations will be identified.

In Chapter 2, the origin and history of the problem are discussed. Some fundamentals will be discussed along with PA modeling and characterization techniques. The reader will also be introduced to a state-of-the-art digital pre-distortion architecture in which the advantages and short comings of such an implementation are highlighted. Chapter 3 introduces the genetic algorithm and its application to PA linearization. The chapter also compares the GA to more conventional adaptation

algorithms. Chapter 4 describes adaptive digital pre-distortion of power amplifiers through simulation and implementation of a closed-loop system. The chapter will also characterize the limitations of the proposed system and algorithm. Chapter 5 will introduce crest factor reduction and present performance results when applied with a typical pre-distortion system. Chapter 6 will show the expansion of the algorithm to include memory effects. This chapter will also introduce a system architecture capable of linearizing PAs with memory effects. Finally, in Chapter 7, a brief summary of the work is presented along with a discussion of the major contributions of the work and potential future directions for research in the field.

CHAPTER II

ORIGIN AND HISTORY OF THE PROBLEM

2.1 Linearization Fundamentals

Power amplifiers are one of the most expensive and power-consuming devices in communication systems. Conflicting design objectives in PAs make optimal performance difficult to achieve. Specifically, the trade-off between efficiency and linearity is the primary concern for PA design. For a PA operating at a high percentage of its power rating, an external linearization technique must be employed to maintain linearity. For a given RF output power level, a lower-power amplifier operating more efficiently consumes substantially less dc power than an inefficient high-power amplifier. PA efficiency is described by Equation 1 [17].

$$\eta = \frac{P_{OUT}}{P_{dc}} \tag{1}$$

The desired linearity performance is achieved by maintaining appropriate levels of output power. This is commonly referred as "back-off". The resulting efficiency of Class A, AB, and B amplifiers falls of rapidly as back-off increases, as illustrated previously in Figure 1. The illustration results from the analysis given in [17] for a PA governed by a strong nonlinearity in transconductance [18]. The minimum back-off required for linear operation is equal to the peak-to-average ratio (PAR) of the transmitted signal for an ideal strong nonlinearity. Further back-off is required in real-world PAs due to the existence of weak nonlinearities. The linearization of the PA reduces back-off, thus increasing efficiency. Typical values for added efficiency due to linearization are summarized in Table 1. The benefits are even more pronounced for multicarrier applications where PARs tend to be large. Linearization of such systems

may be improved further through crest factor reduction (CFR), a method capable of reducing the PAR of the signal [19].

Table 1: Linearization Benefits

Pre-distortion	No	Yes
TX Power	10W	10W
PAR	9dB	9dB
Backoff	12dB	9dB
PA Power Rating	160W	80W
Efficiency	9%	18%
Power Dissipation	101W	45W

2.2 Power Amplifier Modeling

The typical PA is designed to achieve maximum efficiency. Thus, understanding the nonlinear behavior of the PA is critical to applying an external linearization technique. An accurate representation of the nonlinear effects in PAs is achieved using a polynomial expression. The output of such a system could be determined using a 3rd degree polynomial as shown in Equation 2

$$y = a_1 \cdot x + a_2 \cdot x^2 + a_3 \cdot x^3 \tag{2}$$

where a_1 describes the linear small signal gain, and a_2 and a_3 are the gain constants for the quadratic and cubic nonlinearities, respectively. If the coefficients are real valued, the system is considered nonlinear and memoryless. It is important to distinguish the difference between a system with memory and memory effects. The use of complex valued coefficients indicates a constant, frequency-independent phase shift which is used to model a nonlinear system with memory [17, 20]. The term memory effects refers to the bandwidth-dependant nonlinear effects often present in PAs. These encompass envelope memory effects and frequency memory effects. Envelope memory effects are primarily a result of thermal hysteresis, and electrical properties inherent to PAs. Frequency memory effects are due to the variations in the frequency spacing

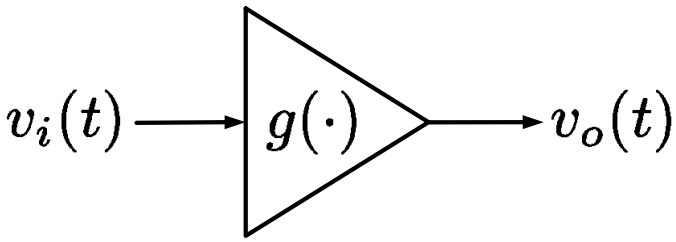

Figure 2: Power amplifier input-output diagram.

of the transmitted signal [21]. Memory effects are omitted from our simple model, however they are subject to further discussion in this work.

2.3 Power Amplifier Characterization

The input-output block diagram of a PA is illustrated in Figure 2, where $v_i(t)$ and $v_o(t)$ are the input and output signals respectively. The two-tone test, where the input signal is composed of two distinct frequency components, has long been employed as an effective PA characterization method. It is especially useful for defining the spectral regrowth in a nonlinear and memoryless system, such as a PA. The polynomial model in Equation 2 can be characterized with the two-tone input generated by the following equation.

$$v_i(t) = Acos(w_1 t) + Acos(w_2 t) \tag{3}$$

The mathematical expansion is found in Appendix A. By grouping the terms at the fundamental frequencies or IM1 and third-order frequencies or IM3, it is easily observed that Equations 4 and 5 describe the PA output at such frequencies.

$$v_o^{IM1}(t) = [a_1 A + \frac{9}{4} a_3 A^3 + \frac{25}{4} a_5 A^5] cos(w_{1,2} t) \tag{4}$$

$$v_o^{IM3}(t) = [\frac{3}{4} a_3 A^3 + \frac{25}{8} a_5 A^5] cos((2w_{1,2} - w_{2,1})t) \tag{5}$$

The resulting spectral regrowth from the two-tone test is shown in Figure 3 using

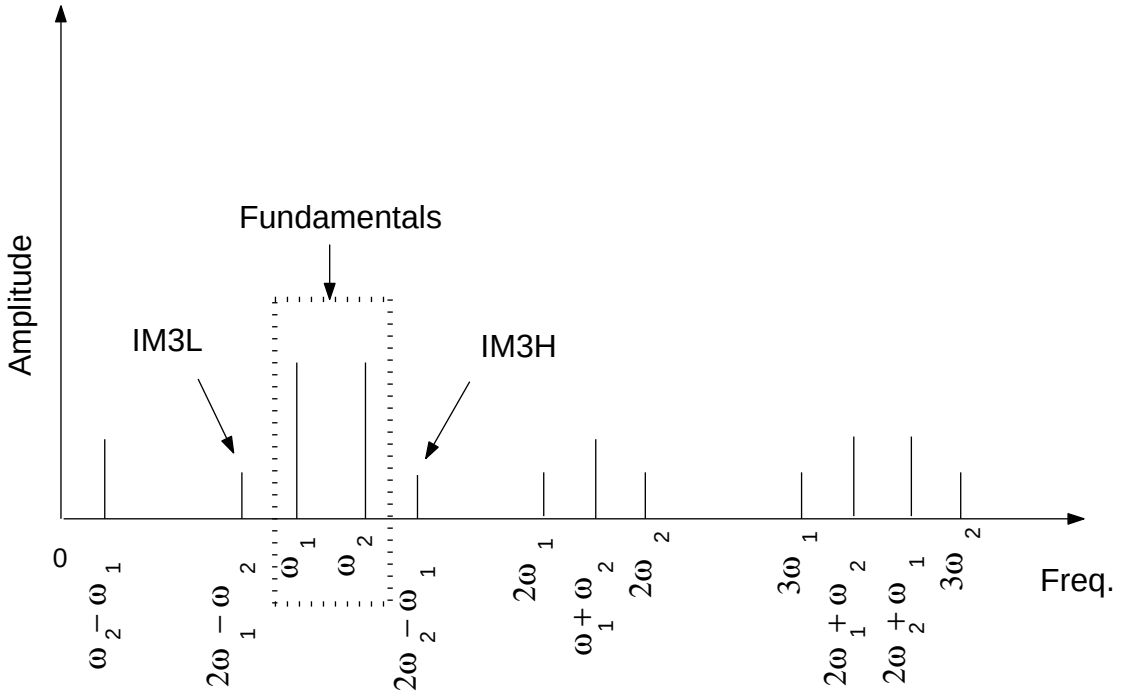

Figure 3: Spectral regrowth of a two-tone signal.

the polynomial PA model previously defined by Equation 2, with real-valued coefficients.

From these results one can determine that the linear term $a_1 x$ amplifies the fundamental tones, while the quadratic nonlinearity $a_2 x^2$ rectifies the signal down to dc band and is responsible for generating the second harmonic band. Finally, the cubic nonlinearity $a_3 x^3$ generates the IM3 terms and is also responsible for generating the third harmonic band. As previously indicated, the second and third harmonic bands are of no concern as they are easily filtered out. Only odd-order nonlinearities will generate in-band distortion products, thus one can eliminate the quadratic nonlinearity from the polynomial PA. A common simplification is to further eliminate all even power terms from our polynomial model because our amplifier is assumed to have narrow fractional bandwidth, greater but comparable to the carrier spacing [22, 25]. The simplified polynomial model is shown in Equation 6 for real-valued coefficients.

$$v_o(t) = a_1 \cdot v_i(t) + a_3 \cdot v_i^3(t) + a_5 \cdot v_i^5(t) \tag{6}$$

The two-carrier excitation is represented in [25] by the following equation

$$v_i(t) = 2Acos(w_m t)cos(w_c t) \tag{7}$$

Using the simplified polynomial model, the n^{th} degree term can be written as shown in Equation 8 from which the modulation on the fundamental carrier is summarized into Equation 9. The magnitude of the IM_{n-2k} products for the n^{th} degree of nonlinearity is described by the bracketed term from which the results are summarized in Table 2, these are also called power series coefficients.

$$v_o(t) = a_n 2^n A^n cos^n(w_m t)cos^n(w_c t) \tag{8}$$

$$\begin{aligned} v_o(t) = a_n 2^n A^n \frac{n!}{2^{n-1}(\frac{n-1}{2})!(\frac{n+1}{2})!}\frac{1}{2^{n-1}} \\ \left[cos(nw_m) + ncos(w_m t(n-2)) + \frac{n!}{(n-k)!k!}cos(w_m t(n-2k))\right] cos(w_c t) \end{aligned} \tag{9}$$

Table 2: Power Series Coefficients

n	3	5	7
	a_3A^3	a_5A^5	a_7A^7
IM1	9/4	25/4	1225/64
IM3	3/4	25/8	735/64
IM5	-	5/8	245/64
IM7	-	-	35/64

The distortion components caused by 3rd and 5th degree nonlinearities are illustrated in Figures 4(a) and 4(b).

The previous two figures are indicative of the relationship between input power and resulting intermodulation products. The relationship is shown with respect to input-output power in Figure 5. The figure illustrates that for low signal amplitudes, where the 5th order intermodulation products can be neglected, the amplitude of the IM3 tones vary at a 3:1 rate with respect to the input power; as such, are proportional to the 3rd power of the input amplitude. Therefor, a decrease of 3dB in input power should decrease the IM3 tones by 9dB. As the input signal amplitude increases, the

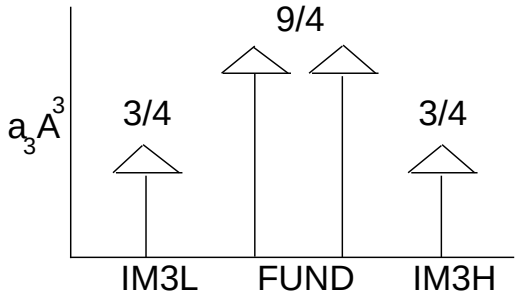

(a) 3rd degree nonlinearities.

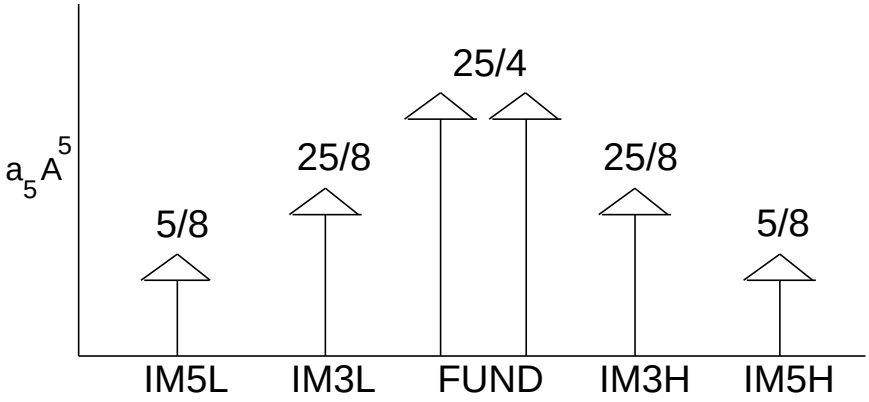

(b) 5rd degree nonlinearities.

Figure 4: Distortion components from 3rd and 5th degree nonlinearities.

5th order distortion products begin to affect IM3 levels. Depending on the phases between the 3rd and 5th degree nonlinearities, the IM3 distortion may increase or be reduced.

Often the performance of a PA is characterized by its amplitude-amplitude (AM-AM) and amplitude-phase (AM-PM) transfer characteristics. The nonlinear polynomial model specified in Equation 6 is adequate for determining AM-AM transfer characteristics however, it is unable to model AM-PM effects. Volterra proposes a general form for Equation 6 which has the ability to model these effects [24]. The work states that each degree of nonlinearity has a corresponding constant phase angle, φ_1, φ_3, φ_5 in the case of a fifth degree polynomial above.

The 1dB compression point (P_{1dB}) is defined as the input power at which the

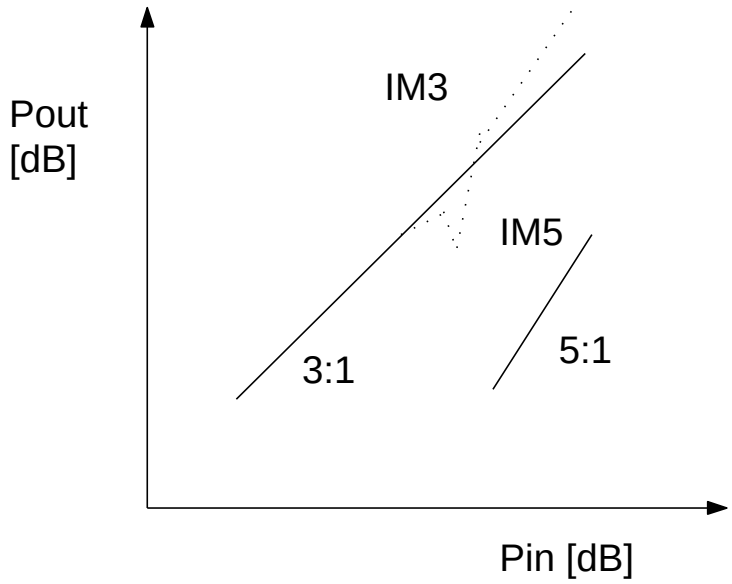

Figure 5: Intermodulation components as a function of input amplitude.

amplifier's output power is 1dB below the linear response. The saturation point is simply the input level that results in the largest output power. A sinusoid may be applied to an amplifier to determine P_{1dB} by increasing the amplitude of the sinusoid until the measured gain at the output decreases by 1dB. The PA output at the fundamental frequency is easily shown by Equation 10 where the small signal gain is equal to a_1.

$$v_o^{fund}(t) = \left\{ a_1 A + \tfrac{3a_3 A^3}{4} \right\} cos(wt) \tag{10}$$

A compression of 1dB corresponds to a linear voltage gain degradation of $10^{(-1/20)}$ or 0.89125. Thus, at P_{1dB}, Equation 10 is described as follows

$$a_1 A + \frac{3a_3 A^3}{4} = A(0.89125)a_1 \tag{11}$$

from which $A_{1dB} = \sqrt{0.145|a_1/a_3|}$. For typical linearization efforts, the approximate small signal gain a_1 and P_{1db} of the PA are known. Using Equation 12 to determine the third order coefficient, the transfer characteristic of the PA can be determined to propose initial inverse transfer functions for pre-distortion efforts.

$$|a_3| = 0.145 \frac{|a_1|}{A_{1dB}^2} \tag{12}$$

A complex baseband model from [11, 18, 22] is considered in which the output can be expressed by Equation 13. The amplifiers AM-AM and AM-PM transfer characteristics are represented by $g_a\left(|v_i(t)|^2\right)$ and $g_\phi\left(|v_i(t)|^2\right)$, respectively. Without memory effects, nonlinearities depend only on the instantaneous input power and not its phase which justifies the use of the magnitude squared of the real bandpass input signal [23].

$$v_o(t) = g\left(|v_i(t)|^2\right) v_i(t) = g_a\left(|v_i(t)|^2\right) e^{j g_\phi\left(|v_i(t)|^2\right)} v_i(t) \tag{13}$$

From Volterra's work, the summation of the nonlinear components is accomplished vectorially. The AM-AM and AM-PM polynomials can be expressed as follows in Equations 14 and 15, respectively.

$$g_a\left(|v_i(t)|^2\right) = a_1 + a_3 \cdot |v_i(t)|^2 + a_5 \cdot |v_i(t)|^4 \tag{14}$$

$$g_\phi\left(|v_i(t)|^2\right) = \varphi_1 + \varphi_3 \cdot |v_i(t)|^2 + \varphi_5 \cdot |v_i(t)|^4 \tag{15}$$

2.4 The Simple Case

The simplest possible case is now investigated to show a typical PA model characterization in which only the third degree nonlinearity is considered in the AM-AM and AM-PM characterizations. Generally, the constant phase offset φ_1 is of no concern and will be omitted from further models. As such, Equations 14 and 15 can be expressed as follows

$$g_a\left(|v_i(t)|^2\right) = G\left(1 - 1|v_i(t)|^2\right) \tag{16}$$

where G corresponds to a gain of 35 dB and

$$g_\phi\left(|v_i(t)|^2\right) = -0.3|v_i(t)|^2 \tag{17}$$

The amplifier's linear characteristic is defined by

$$\bar{g}_a\left(|v_i(t)|^2\right) = G \tag{18}$$

and

$$\bar{g}_{\phi}\left(|v_i(t)|^2\right) = 0 \tag{19}$$

The linear region is defined as that set of inputs for which $g_a \simeq \bar{g}_a$ and $g_{\phi} \simeq \bar{g}_{\phi}$. From the above equations, the AM-AM and AM-PM characteristic curves are plotted in Figures 6(a) and 6(b) with respect to the input power. These figures, although simulations, are typical of measurements for PAs. For this particular model, the 1dB compression point occurs at 20dBm input power while the saturation point occurs at 25dBm. The PAR of a two-tone signal, or sinusoid, is calculated as the name implies where the peak of the normalized signal is 1 and the average of a sinusoid is 0.707 giving a PAR of 3dB. The input tones are defined with $w_1 = 5MHz$ and $w_2 = 9MHz$ and an average power of 17dBm. Figures 7(a) and 7(b) illustrate the input and output spectra from the defined PA model. Figures 8(a) and 8(b) illustrate the individual amplitude and phase components at the output of the PA.

It is evident from Figures 8(a) and 8(b) that the phase response has an infinite number of spectral components, but the amplitude of these components falls off rapidly. The amplifier's output can be equivalently shown to be the convolution of the input spectrum with the amplitude and phase spectra.

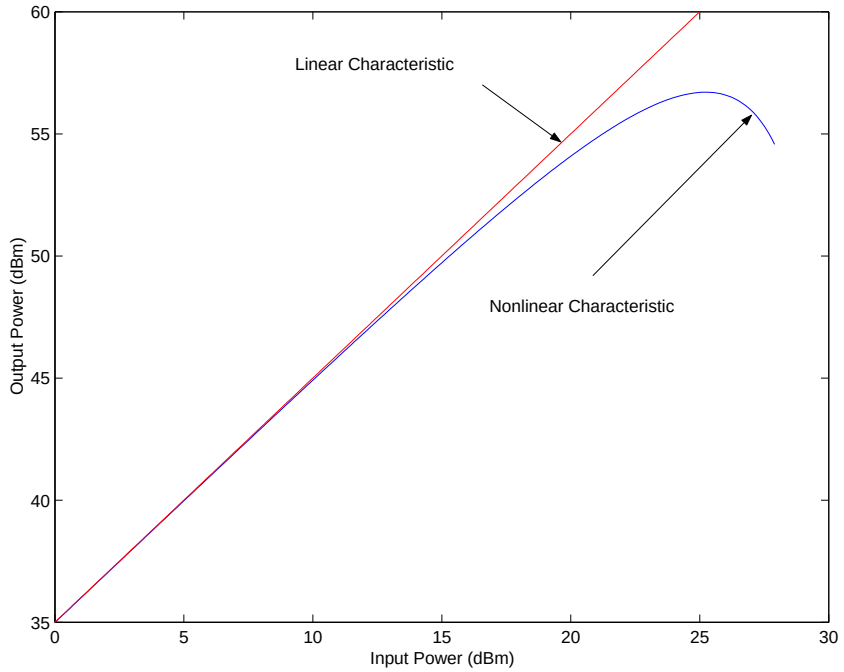

(a) AM-AM characteristic.

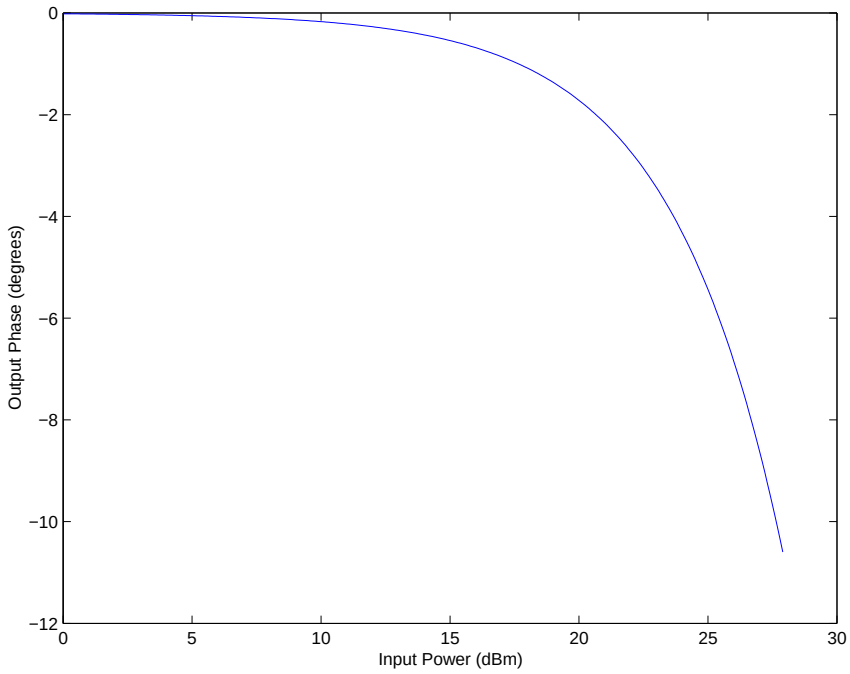

(b) AM-PM characteristic.

Figure 6: Characterization of a memoryless nonlinearity.

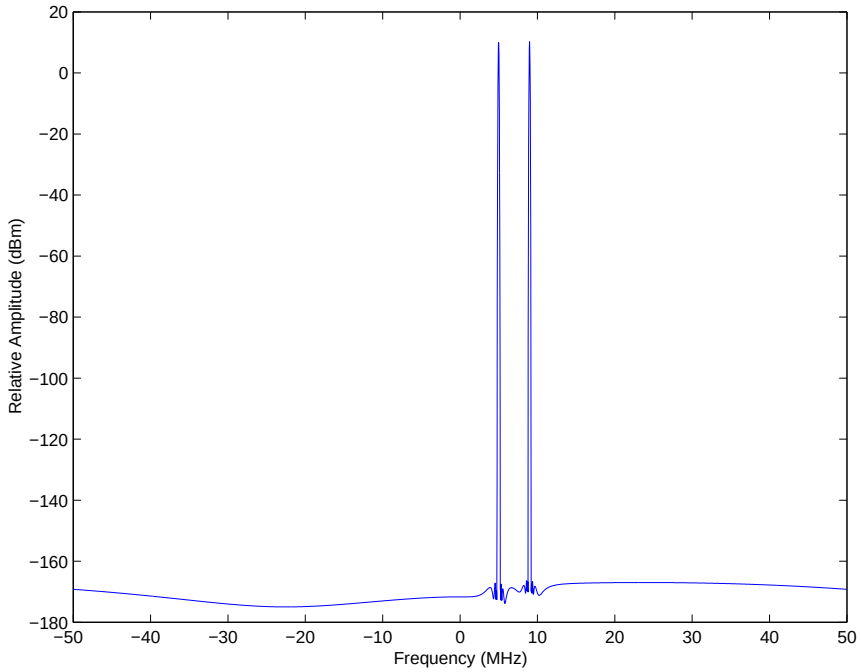

(a) Spectrum of two-tone input.

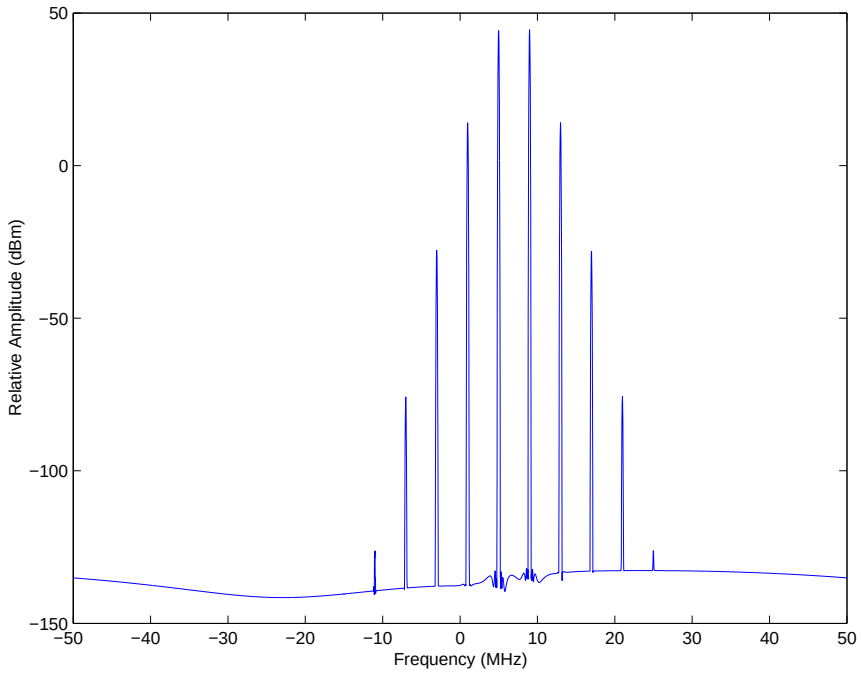

(b) Spectrum of two-tone PA output.

Figure 7: Input and output spectral response of two-tone test.

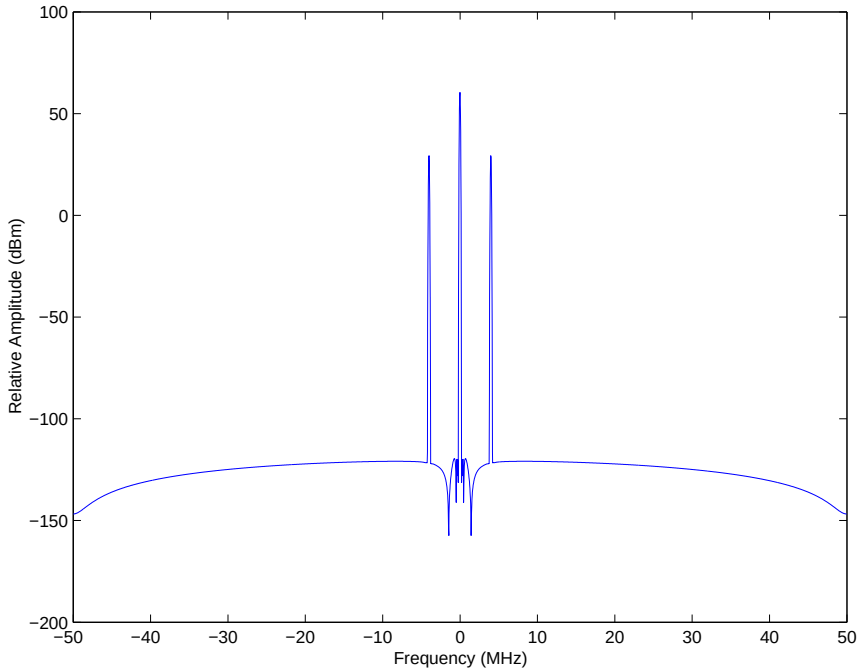

(a) Spectrum of PA amplitude component.

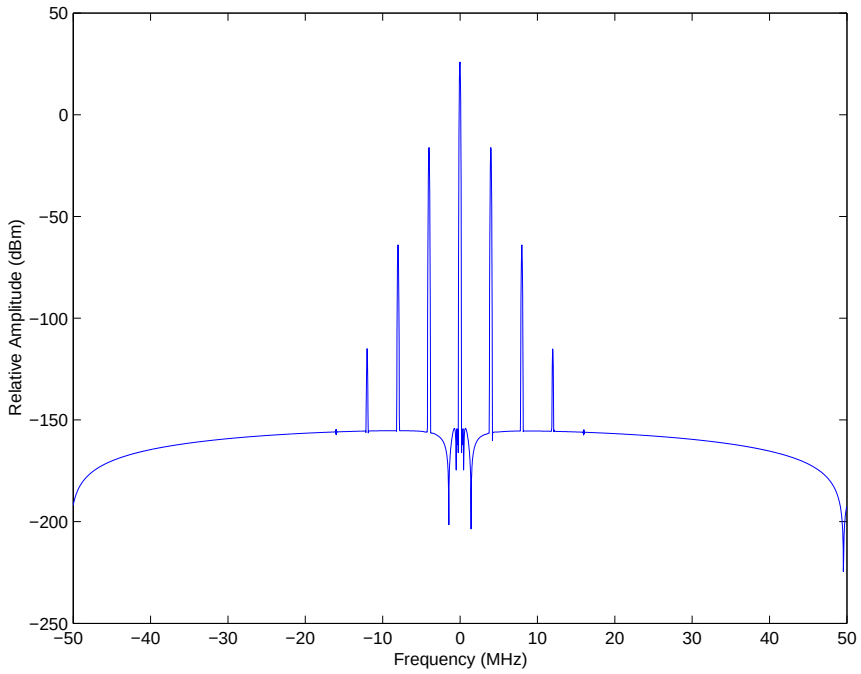

(b) Spectrum of PA phase component.

Figure 8: Amplitude and phase spectral response of two-tone test.

2.5 Digital Pre-Distortion

To maintain linearity and efficiency, one can apply linearization to the PA through several techniques such as feedback [26,27], feedforward [6,28,29], and pre-distortion [5,8, 10,11,18,30,45]. Typical performance indices of the basic linearization techniques are illustrated in Table 3. It is pre-distortion that is the focus of this research, specifically digital base-band pre-distortion.

Table 3: Comparison of the three linearization techniques

Technique	IMD Cancellation	Bandwidth	Power Added Efficiency	Size
Feedback	Good	Narrow	Medium	Medium
Feedforward	Good	Wide	Low	Large
Pre-distortion	Medium	Wide	High	Small

A pre-distortion system effectively performs a mathematical inversion of the PA Volterra model described in the previous section. The implementation of a PD-PA cascade is illustrated in Figure 9.

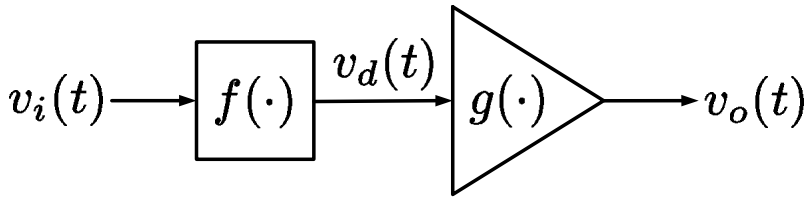

Figure 9: PD-PA cascade.

The PD output is $v_d(t)$ and the output of the PD-PA cascade is expressed by the following.

$$v_o(t) = g\left(\left|f\left(|v_i(t)|^2\right)v_i(t)\right|^2\right) f\left(|v_i(t)|^2\right) v_i(t) \tag{20}$$

Clearly, the PA is linearized when

$$G = g\left(\left|f\left(|v_i(t)|^2\right)v_i(t)\right|^2\right) f\left(|v_i(t)|^2\right) \tag{21}$$

A pre-distorter applies distortion to the input signal in order to drive the PA harder. The PD-PA cascade attempts to combine two nonlinear systems into one linear result

which allows the PA to operate closer to saturation. Beyond this point, no increase in power will suffice to linearize the PA. The PAR of the signal greatly restricts optimal performance of the PD system. A CDMA signal, for example, may have a PAR as high as 13dB. A PA transmitting such a signal must operate with significant back-off to prevent peaks from occurring beyond saturation. There are two common types of PD implementations, the first is an analog implementation using a physical nonlinear device [32, 33]. The second and perhaps more popular choice, is a digital signal processor (DSP) hardware implementation where the PD function is defined algorithmically through software [34, 35].

Digital pre-distortion (DPD) has become an effective linearization technique due to the renewed possibilities offered by the computational power of next generation DSP. Typical adaptive PD designs utilize feedback to compensate for variations in the PA nonlinearity over time. The application of DPD is often performed through the adaptation of a look-up table (LUT). Each sample of the complex baseband signal is modified according to the LUT which ideally contains the inverse of the PA characteristics [8, 31, 45]. Faulkner describes a gradient adaptation method which updates entries in the LUT by comparing the PD input and PA output on a sample-by-sample basis. The LUT is generated by a complex polynomial such that both AM-AM and AM-PM correction is applied; the PD functions can be expressed as follows

$$f\left(|v_i(t)|^2\right) = f_a\left(|v_i(t)|^2\right) e^{j f_\phi\left(|v_i(t)|^2\right)} \tag{22}$$

where

$$f_a\left(|v_i(t)|^2\right) = A_a + B_a \cdot |v_i(t)|^2 + C_a \cdot |v_i(t)|^4 + D_a \cdot |v_i(t)|^6 \tag{23}$$

$$f_\phi\left(|v_i(t)|^2\right) = B_\phi \cdot |v_i(t)|^2 + C_\phi \cdot |v_i(t)|^4 + D_\phi \cdot |v_i(t)|^6 \tag{24}$$

To account for 3rd and 5th order intermodulation products at the PA output, the feedback bandwidth for sample-by-sample adaptation must be 5 times the signal bandwidth. Multicarrier systems today can reach signal bandwidths of 20MHz, thus

the required feedback signal must have a minimal bandwidth of 100MHz as illustrated in Figure 10.

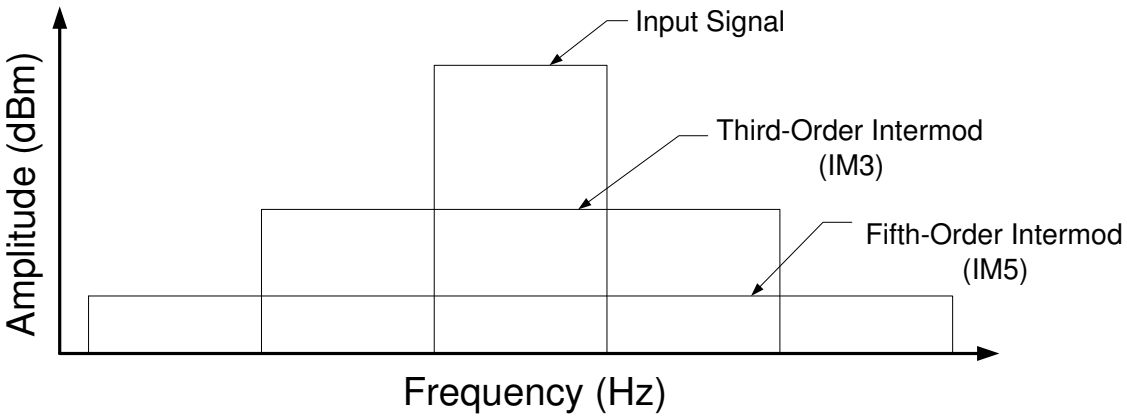

Figure 10: Input signal and intermodulation bandwidth.

The cost of a system with high bandwidth requirements is greatly driven by the high performance ADCs in the feedback path, which are required to provide intermodulation distortion and transmitted signal information to the DSP. The DSP, through a computational algorithm, then adjusts the PD function to achieve optimal linearization results. A digital pre-distortion architecture with wideband feedback is shown in Figure 11.

A popular, gradient based optimization algorithm is the least-mean-square (LMS) method. As previously mentioned, the implementation of this algorithm requires a costly feedback path. The algorithm is further restricted in that, although effective at determining a single minimum, it requires additional search schemes to determine the global minimum. The algorithm uses the gradient of the cost function to determine the steepest downhill path; however, the gradient cannot be calculated when dealing with cliffs and boundaries [13]. In attempting to reduce linearization costs, adaptation through narrowband feedback presents itself as an attractive alternative. Stapleton et al. propose a direct search algorithm to adjust polynomial coefficients which minimize IMD in [11]. This method is slow to converge and requires a quadratic

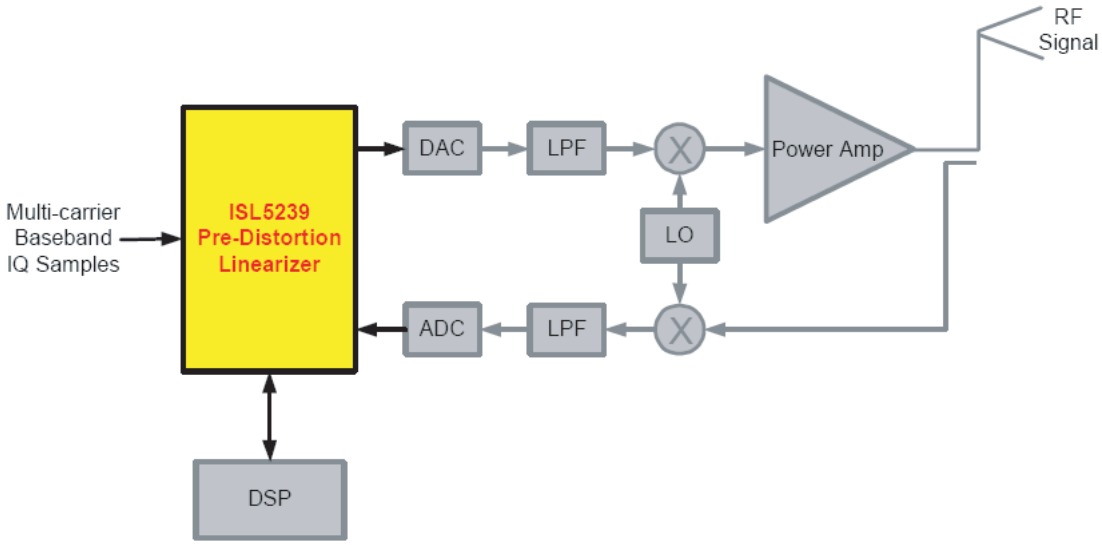

Figure 11: State-of-the-art digital pre-distortion using wideband feedback.

cost function. Genetic algorithms present themselves as an ideal alternative to typical gradient solutions and they are the focus of the presented research.

CHAPTER III

THE GENETIC ALGORITHM

3.1 Introduction

The term genetic algorithms (GA) refer to a subset of evolutionary algorithms that model biological processes to optimize highly complex cost functions. A GA allows a population of composed of individuals (population members) to evolve under specified genetic processes to a state which minimizes the cost function [12]. The algorithm itself has evolved from its first conception; however, it is suitable to define it as a population-based model that uses selection, recombination and mutation operators to generate new sample points in a search space. The GA is capable of yielding a robust search by implicitly sampling hyperplane partitions of a search space. A single hyperplane, commonly referred to as schema, is the theoretical foundation on which the algorithm was developed as first introduced by John Holland in 1975 [36]. The advances in DSP technology are largely responsible for the growing interest in GAs, specifically due to the computational complexity often associated with their use. GAs have most recently been applied to antenna design, power electronic circuit optimization, schedule optimization and even cancer detection and treatment [37,38].

3.2 Theoretical Foundations of Genetic Algorithms

The most general description of the GA indicates that optimization through this technique is achieved by identification, emphasis and recombination of good "building blocks" of solutions in a highly parallel fashion. These building blocks are also referred to as schemas or schemata. The algorithm bases itself on the notion that combining good schemata will lead to good solutions. A schema is a template made up of

ones, zeros and don't cares (*) used to describe a set of bit strings. The schema H = 1**0 describes all 4-bit strings that begin with a one and end with a zero. The strings that match the schema are called instances of H, in this case they are: 1000,1010,1100,1110. Oddly enough, if we consider a binary string of length 4 there exists 2^4 or 16 possible solutions from which the best can be located; however, by adding the *'s, there are 3^4 or 81 possibilities. It would seem that we have increased the difficulty in determining the best possible solution; however, the algorithm does not evaluate strings as individuals but instead in parallel, as a population. Schemas allow the algorithm to focus on the important bits rather than all at once. The following example in Table 4 clearly illustrates the point.

Table 4: Genetic Algorithm Interpretation

String	Fitness
1101	2197
1000	512
0100	64
0011	27

Looking at the strings as individuals rather than members of a population reveals four pieces of information, it may be difficult to see the relationship between the string and the fitness which is simply $f(x) = x^3$. However, if one looks at the strings, their fitness and the similarities between strings the importance of certain bits over others is revealed. The question remains, how does the GA mathematically process the information that we can observe? If any given bit string of l length is an instance of 2^l different schemas then the string 11 is an instance of ** which represents all four possible bit strings of length 2. Therefore, any population of N members has instances between 2^l and $N * 2^l$ different schemas. For any given population, while the GA is explicitly evaluating the fitness of the individual members, it is in fact implicitly estimating the fitness of a much larger number of schemas. It can be shown that the average fitness of a schema is evaluated by the average fitness of all the possible

instances of that schema [14]. The GA does not explicitly store the schemas that yield optimal levels of fitness, it does however increase their number of instances in future populations. The increase or decrease of schema instances from one population to the next is described by the Schema Theorem introduced by Holland [36].

The theorem can be broken down as follows. If H is a schema with at least one instance present in the population at generation or iteration i, then $m(H,i)$ is the number of instances of H at iteration i. The average fitness of the instances of H at iteration i is defined as $\hat{u}(H,i)$ and expressed as follows in Equation 25.

$$\hat{u}(H,i) = \sum_{k \epsilon H} f(k)/m(H,i) \tag{25}$$

Therefore, the expected number of instances of H at iteration i+1 is represented by $E(m(H,i+1))$. Through a selection process described later, the expected offspring of a particular population member k is equal to $f(k)/\bar{f}(i)$ where $f(k)$ is the fitness of k and $\bar{f}(i)$ is the average fitness of the population at iteration i. The expected number of instances is represented in Equation 26 and through simple substitution expressed in Equation 27.

$$E(m(H,i+1)) = \sum_{k \epsilon H} f(k)/\bar{f}(i) \tag{26}$$

$$E(m(H,i+1)) = \hat{u}(H,i)/\bar{f}(i) m(H,i) \tag{27}$$

The previous equations describe the expected instances in the next population i+1 due to a selection from the current population; however, it does not reflect the effects of recombination (often referred to as crossover) and mutation. These genetic operators can create and destroy the instances of H in following populations. For the sake of simplicity, we will only consider the lower bound or the destructive effects of these operators. The probability that the selected instance of H will "survive" after

crossover is expressed in Equation 28 where p_c is the probability that crossover will occur, $d(H)$ defines the length of the instance H and l remains the length of the bit strings in the search space. The shorter schemas have a higher probability of survival through crossover, as determined by their length $d(H)$.

$$S_c(H) \geq 1 - p_c \frac{d(H)}{l-1} \tag{28}$$

The mutation operator is now added to the analysis; similar to crossover, p_m is the probability that mutation will occur. The "survival" of H through mutation is described in Equation 29 where $o(H)$ is the number of defined bits in H (i.e., ones and zeros). Therefore, increasing the "don't cares" increases the probability of survival through mutation. The previous equations are consolidated to form the Schema Theorem, as shown in Equation 30.

$$S_m(H) = (1 - p_m)^{o(H)} \tag{29}$$

$$E(m(H, i+1)) \geq \frac{\hat{u}(H,i)}{\bar{f}(i)}(1 - p_c \frac{d(H)}{l-1})(1 - p_m)^{o(H)} \tag{30}$$

Although the previous analysis describes the fundamental basics of the genetic algorithm, there exist numerous interpretations that are modified to meet the requirements of the desired optimization. The following section describes a variation as it applies to the field of PA linearization and gives greater detail as to the functionality of the genetic operators customized for this application.

3.3 Application of the Genetic Algorithm

Linearization is achieved through the optimization of the coefficients in Equations 23 and 24. In this embodiment of the GA, adaptation is the result of a process similar to "natural selection" or survival of the fittest. The optimization or "evolution" of the PD solution occurs through the use of genetic operators, such as elitism, sampling,

crossover and mutation. Using biological terms, a "chromosome" is used to describe a PD solution consisting of 7 coefficients or "genes". Four of the genes are used for amplitude correction and the remaining three are for phase correction. Finally, a set of chromosomes is called a "population." Thus the k^{th} member of the i^{th} population is denoted as follows

$$A_a(k,i), B_a(k,i)), C_a(k,i)), D_a(k,i)), B_\phi(k,i)), C_\phi(k,i)), D_\phi(k,i)) \tag{31}$$

The adaptation process is initiated through the creation of a randomly generated population. The chromosomes are defined within a predetermined search space. Secondly, the chromosomes are individually evaluated to determine their fitness. For this PD application, the fitness is a normalized measure of the adjacent channel power (ACP), often referred to as adjacent channel power ratio (ACPR). The optimal chromosome is verified for convergence and the adaptation is then terminated if the fitness is acceptable. When the fitness is not acceptable, the GA must create a new population to evaluate.

Elitism is the first step to generating a new population. This genetic operator selects the best chromosomes of the current population and duplicates them into the new population. The number of chromosomes duplicated depends on the rate of elitism defined by the user. This operator prevents the GA from losing the optimal solution. To generate the remaining chromosomes of the new population, the algorithm must first select parents from which to model them. Stochastic sampling with replacement is performed on the current population to select two chromosomes as parents. In a manner similar to natural selection or what biologists call "viability selection", chromosomes are selected according to their fitness. Thus, the fitter chromosomes produce more offspring. The two selected parents are combined to form an offspring through uniform crossover. This genetic operator selects elements, called "alleles", from each parent chromosome to create a new offspring, roughly mimicking biological recombination between two single-chromosome organisms. The application

of crossover varies anywhere from single-point crossover to multi-point crossover. The type of crossover is typically application dependant; in this case, a random binary string p_c is generated in which the probability of 1 in each bit position is equal to the crossover rate. The implementation of crossover is represented by the following boolean expression in Equation 32. Other forms of crossover are available, but this is the preferred embodiment.

$$A_a(k_{cross}, i+1) = [A_a(parent_1, i) \cdot p_c] + [A_a(parent_2, i) \cdot \overline{p_c}] \tag{32}$$

The equation only describes the crossover of a single coefficient; however, the equation is also valid for the remaining complex coefficients. Finally, before the new member can join the population, it is subjected to the mutation operator. Similarly to crossover, the mutation rate creates a binary mutation string p_c which randomly changes the allele values of some locations in the new chromosome. This unique feature prevents the algorithm from "getting stuck" in a local minimum solution. The mutation operator is applied to the coefficients resulting from crossover, as described in Equation 33.

$$A_a(k, i+1) = A_a(k_{cross}, i+1) \oplus p_m \tag{33}$$

The genetic operators repeat themselves for the N members of the new population and over each successive new population, i, commonly referred to as an iteration. The entire GA is summarized by the following steps:

1. Generate random population of N chromosomes.
2. Evaluate the fitness of each chromosome in the population.
3. Test for convergence. Stop if fitness is acceptable.
4. Generate new population.

(a) Elitism. Select best K chromosomes of the current population.

(b) Selection. Identify parents by stochastic sampling with replacement.

(c) Crossover. Apply uniform crossover.

(d) Mutation. Apply random changes.

5. Loop to step 2 and repeat for new population.

The adaptation of the GA in problem solving is determined by its ability to converge to a desired solution. Convergence is achieved when the fitness of a solution reaches an adequate level. In the case of linearization, the desired solution is ACP reduction and the adequate level is when the ACP meets regulatory requirements. A simple example is proposed next to show the GAs iterative process. The example begins with the creation of a random population in Equation 34, in this case $N = 5$; however, practical experience will show that populations must be greater than 25 to achieve any kind of linearization improvement. The larger population size is necessary to evaluate enough of the search space on a given iteration, increasing the rate at which the algorithm is able to "learn" from erroneous solutions.

$$Pop.(i=0) = \begin{bmatrix} A_a(1,0) & B_a(1,0) & C_a(1,0) & D_a(1,0) & B_\phi(1,0) & C_\phi(1,0) & D_\phi(1,0) \\ A_a(2,0) & B_a(2,0) & C_a(2,0) & D_a(2,0) & B_\phi(2,0) & C_\phi(2,0) & D_\phi(2,0) \\ A_a(3,0) & B_a(3,0) & C_a(3,0) & D_a(3,0) & B_\phi(3,0) & C_\phi(3,0) & D_\phi(3,0) \\ A_a(4,0) & B_a(4,0) & C_a(4,0) & D_a(4,0) & B_\phi(4,0) & C_\phi(4,0) & D_\phi(4,0) \\ A_a(5,0) & B_a(5,0) & C_a(5,0) & D_a(5,0) & B_\phi(5,0) & C_\phi(5,0) & D_\phi(5,0) \end{bmatrix} \tag{34}$$

The fitness of each population member is evaluated and normalized as shown in Equation 35. The population members are sorted with respect to their fitness and shown in Equation 36. The results indicate that k=3 is the best member while k=2

is the worst.

$$Fitness(f) => \begin{bmatrix} f_1 \\ f_2 \\ f_3 \\ f_4 \\ f_5 \end{bmatrix} = \begin{bmatrix} 0.20 \\ 0.05 \\ 0.40 \\ 0.10 \\ 0.25 \end{bmatrix} \tag{35}$$

$$Pop.(i=0) = \begin{bmatrix} A_a(3,0) & B_a(3,0) & C_a(3,0) & D_a(3,0) & B_\phi(3,0) & C_\phi(3,0) & D_\phi(3,0) \\ A_a(5,0) & B_a(5,0) & C_a(5,0) & D_a(5,0) & B_\phi(5,0) & C_\phi(5,0) & D_\phi(5,0) \\ A_a(1,0) & B_a(1,0) & C_a(1,0) & D_a(1,0) & B_\phi(1,0) & C_\phi(1,0) & D_\phi(1,0) \\ A_a(4,0) & B_a(4,0) & C_a(4,0) & D_a(4,0) & B_\phi(4,0) & C_\phi(4,0) & D_\phi(4,0) \\ A_a(2,0) & B_a(2,0) & C_a(2,0) & D_a(2,0) & B_\phi(2,0) & C_\phi(2,0) & D_\phi(2,0) \end{bmatrix} \tag{36}$$

In a population of 5 members, an elitism rate set at 20% corresponds to duplicating exactly one member from the i^{th} iteration into the $i^{th}+1$. The remaining 4 members result from selection, crossover and mutation. In the given example, the generation of the 2^{nd} member of the $i^{th}+1$ results from crossover between the 3^{rd} and 1^{st} members of the i^{th} iteration. An example of crossover is shown in the Equation 37. Afterwards, mutation is applied to the respective offspring resulting in the 2^{nd} member of the $i^{th}+1$ iteration as shown in Equation 38.

$$\begin{aligned} A_a(3,0) &= 001110010011 \\ A_a(1,0) &= 100101100010 \\ p_c &= 100100100010 \\ \overline{A_a(2_{cross},1) = 000101010010} & \end{aligned} \tag{37}$$

$$
\begin{aligned}
A_a(2_{cross}, 1) &= 000101010010 \\
p_m &= 010000000000 \\
\overline{A_a(2,1) &= 010101010010}
\end{aligned} \tag{38}
$$

The genetic operators are repeated for the remaining coefficients and population members. The iterative process repeats itself until satisfactory results are achieved.

Although proven effective in various system implementations, the implementation of a GA as a polynomial solver is the desired investigation. This is a good starting point as linearization is often seen as a polynomial curve fit. In the case of a simple polynomial curve fitting, the GA uses Equation 39 to calculate the fitness of a chromosome. Although this calculation of fitness is effective for a simple curve fitting problem, careful consideration of the cost function is required for linearization efforts and will be examined further in great detail.

$$
f = \sum_{x=0}^{1} \sqrt{(Chromo_{Real}(x) - Ideal_{Real}(x))^2 + (Chromo_{Imag}(x) - Ideal_{Imag}(x))^2} \tag{39}
$$

Although the fitness, f, is calculated using LMS like in wideband architectures, the solution here adapts on the difference between the curve generated by the chromosome-polynomial and the curve generated by the ideal-polynomial and does so for both real and imaginary curves simultaneously. The initial population of solutions for both real and imaginary polynomials are shown in Figures 12(a) and 12(b), respectively. The solid-line curves show the elite chromosomes of the population.

Finally, Figures 13(a) and 13(b) show the final convergence of the real and imaginary polynomials versus the ideal case, respectively. The implementation, although simple, proves the algorithm is able to adapt the coefficients of two distinct polynomials simultaneously while provided with a single measure of fitness.

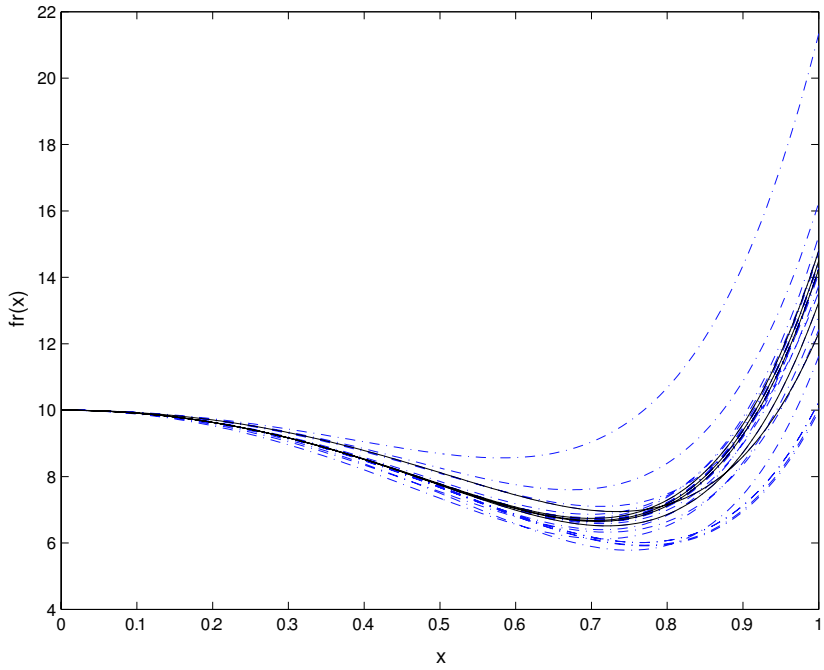

(a) Initial population real-valued polynomial curves.

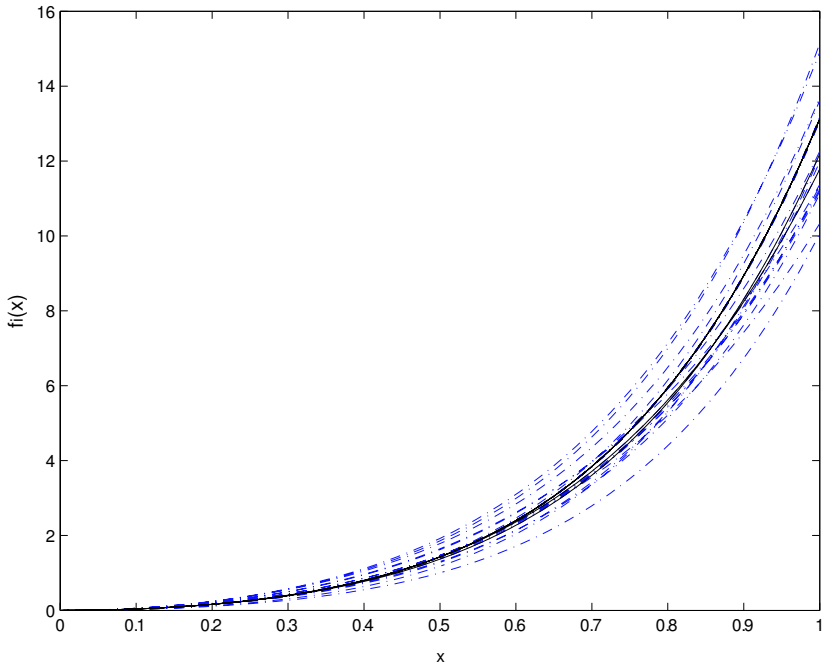

(b) Initial population imaginary-valued polynomial curves.

Figure 12: Initial polynomial solutions.

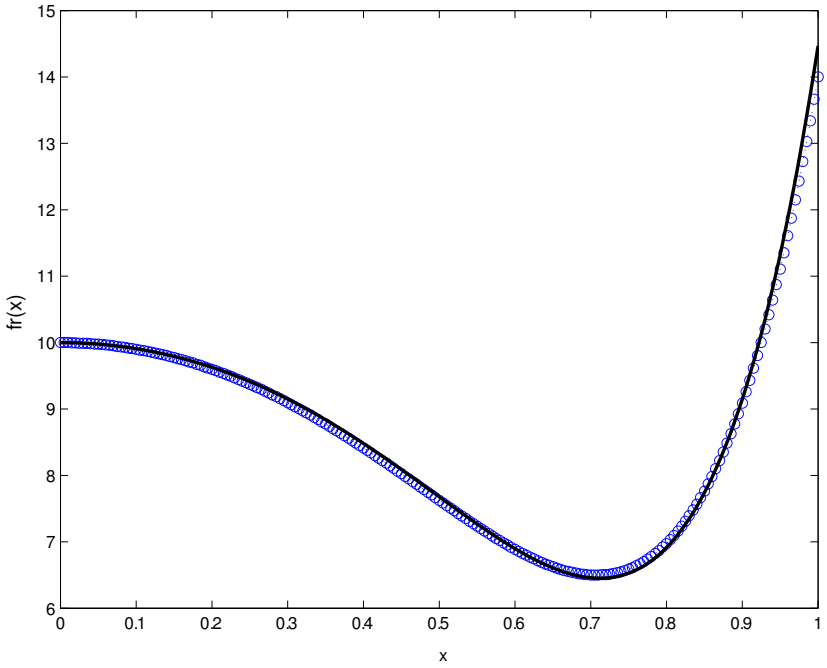

(a) Final real-valued polynomial solution versus ideal.

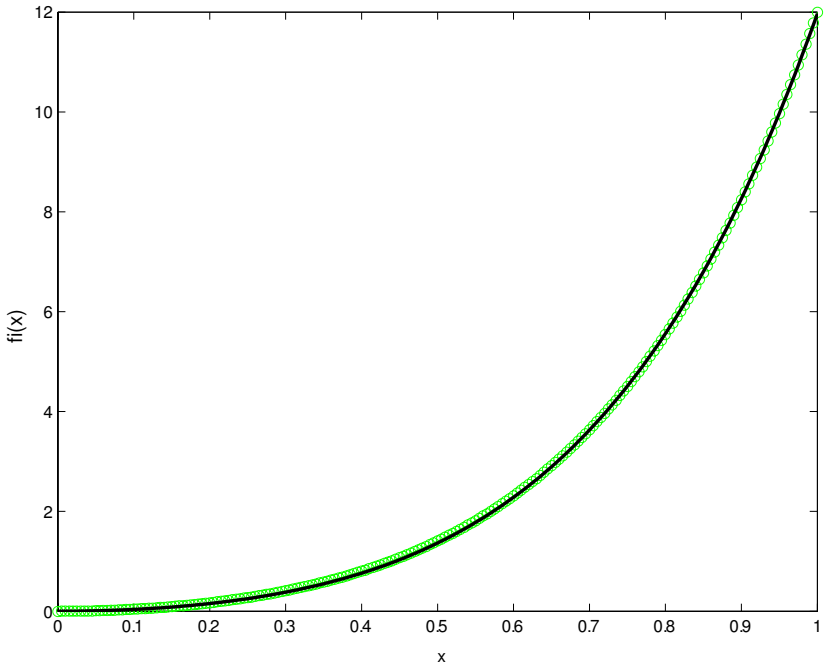

(b) Final imaginary-valued polynomial solution versus ideal.

Figure 13: Final polynomial solutions versus ideal curves.

The use of narrowband feedback in the adaptation of a polynomial PD is not a new one [11]; however, this is the first known application of GA adaptation to the field of PA linearization. As such, the simulated linearization of a polynomial PA model is the next focus of discussion.

CHAPTER IV

PRE-DISTORTION AND THE GENETIC ALGORITHM

4.1 Introduction

In the previous chapter, it was shown that the GA is effective at solving two polynomial curves simultaneously. The application of PD was previously described in Chapter 2; the platform used to implement PD solutions was based on a LUT architecture proposed by Intersil Corporation, the original supporter of these research efforts. The memoryless pre-distortion function implemented by Intersil's ISL5239 PD processor is shown in Figure 14. The LUT features 1024 entries, each with a 16 bit unsigned real and 16 bit signed imaginary value. The LUT is operated in the linear voltage mode, all the entries are confined to a range of 60dB with most entries allocated to the higher power region. All input levels below the 60dB range are mapped to the first entry in the LUT [47]. The adaptive scaling and indexing of LUTs can provide further improvement in terms of correction and efficiency performance [48]; however, in this work, this adaptation is not included to reduce the overall complexity of the implementation.

The following software model and hardware implementations adapt polynomial coefficients by generating complex LUTs. Each successive LUT is evaluated to determine the optimal PD coefficients.

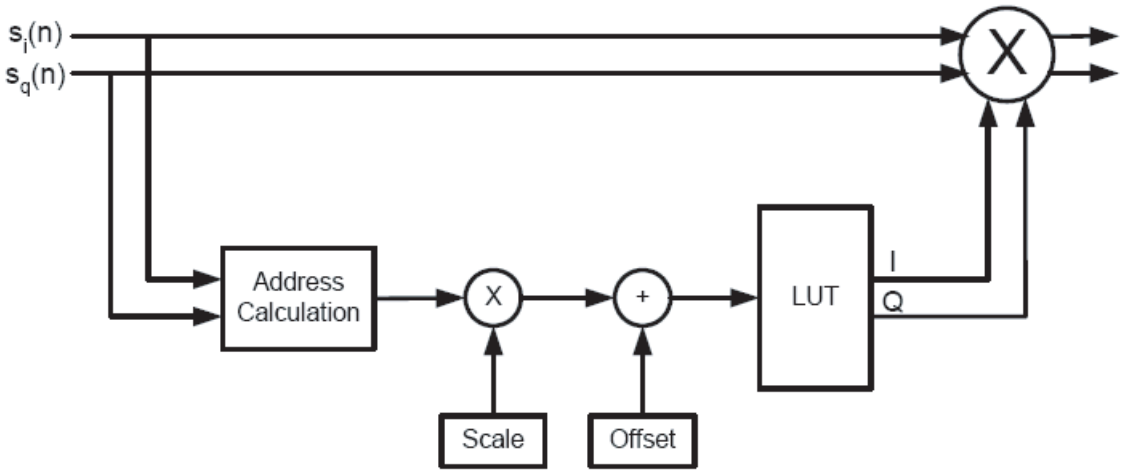

Figure 14: ISL5239 Memoryless pre-distortion function.

4.2 Simulation of LUT-based Pre-distortion

In simulation work, linearization is applied to the PA model represented by Figures 6(a) and 6(b) [56]. The chromosomes or polynomial coefficients are optimized over predetermined search spaces for AM-AM and AM-PM correction; these are shown in Figure 15. These further indicate that the search space for this GA includes PD solutions that may have up to 8dB of amplitude expansion and 30 degrees of phase shift. The convergence principles of genetic algorithms seem to be nothing more than a random search technique. To disprove this assumption, PD was applied using both a random search technique and the GA technique. The random search technique was constrained to the same search space as shown in Figure 15. Both techniques used identical initial populations with $N = 25$ chromosomes and the simulations were allowed to run over $i = 20$ iterations. The GA adaptation results were achieved by defining the genetic operators with an elitism rate of 15%, a mutation rate of 12% and a crossover rate of 50%. The simulation optimization was achieved by minimizing the cost function described in Equation 40 for each population member. The fitness was only dependant on the high-side intermodulation products (IM3H).

$$f = IM3H(dBm) \tag{40}$$

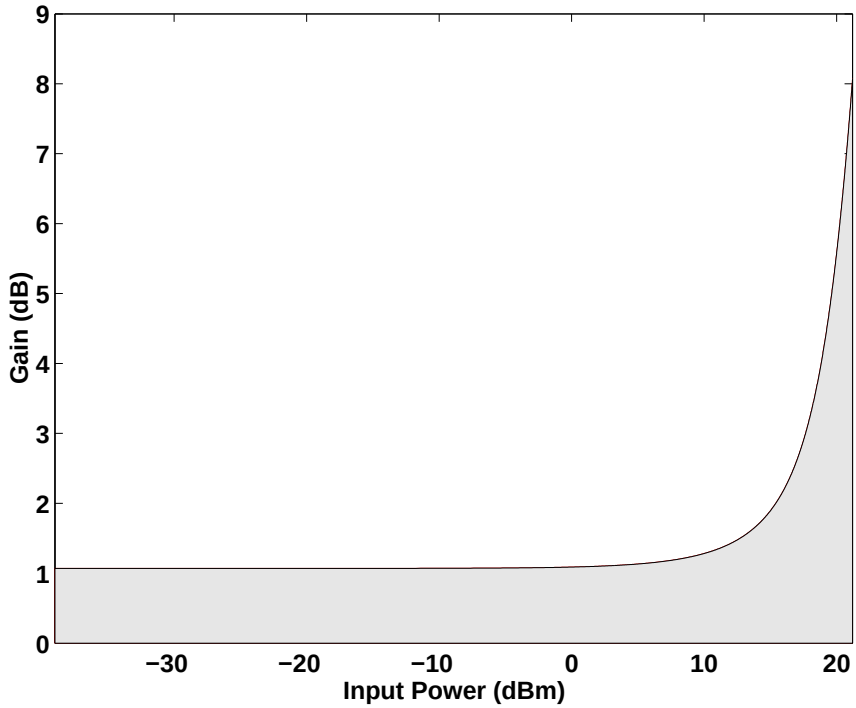

(a) Search space for f_a.

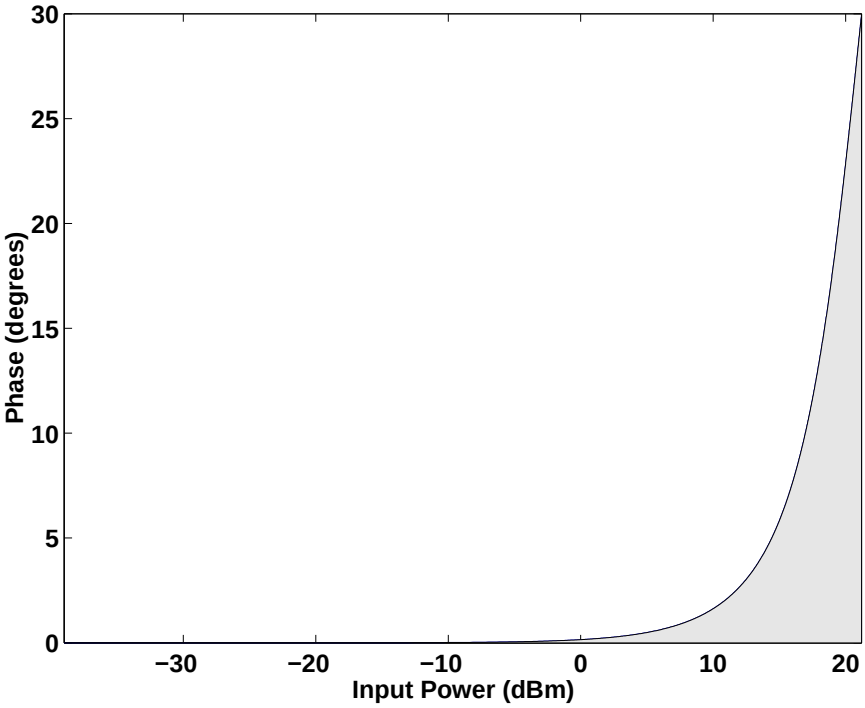

(b) Search space for f_ϕ.

Figure 15: Search space for the genetic algorithm.

For each population, the value of the minimum ACP is shown for both techniques in Figure 16 . The two techniques began with identical populations and therefore equal minimum ACP at iteration 0. With each iteration the GA solution is continually improving toward the lower bound, while the random search shows only minimal improvement. Also shown is the average ACP from which it is evident that the GA is improving while the random search average ACP remains relatively constant. It is this trend toward populations with improved fitness that allows the GA to outperform a random search. Figure 17 compares the final GA and random search solutions with non-linearized performance. Without linearization, the ACPR is 35 dBc. This improves to 43 dBc with the random search technique, and finally, to over 65 dBc with the GA. This is near the noise floor of 75 dBc, which corresponds with expected levels from the 13 bit DAC model used in the simulations. The noise floor defines the lower bound of optimization. ACP reduction here is limited by the noise floor which is governed by the DAC performance and the PA gain. The DAC performance is fixed therefore, the noise level into the PA is constant, but the signal level is not. Since the PA gain is a function of the total average input power, the output noise floor can vary with input signal power. The output noise floor is actually lower for a PA operating in compression than when operating in its linear region. PD solutions are allowed to vary gain over a 1dB range, a possibility uninvestigated in [11]. In this case, optimum ACP enhancement is achieved when the PD gain is at its maximum level and the resulting output noise floor is at a minimum. Results show nearly optimal performance in a limited number of iterations suggesting that this technique can be employed as a low-cost solution to meet ACLR requirements. The algorithm will now be applied to a typical basestation test bed.

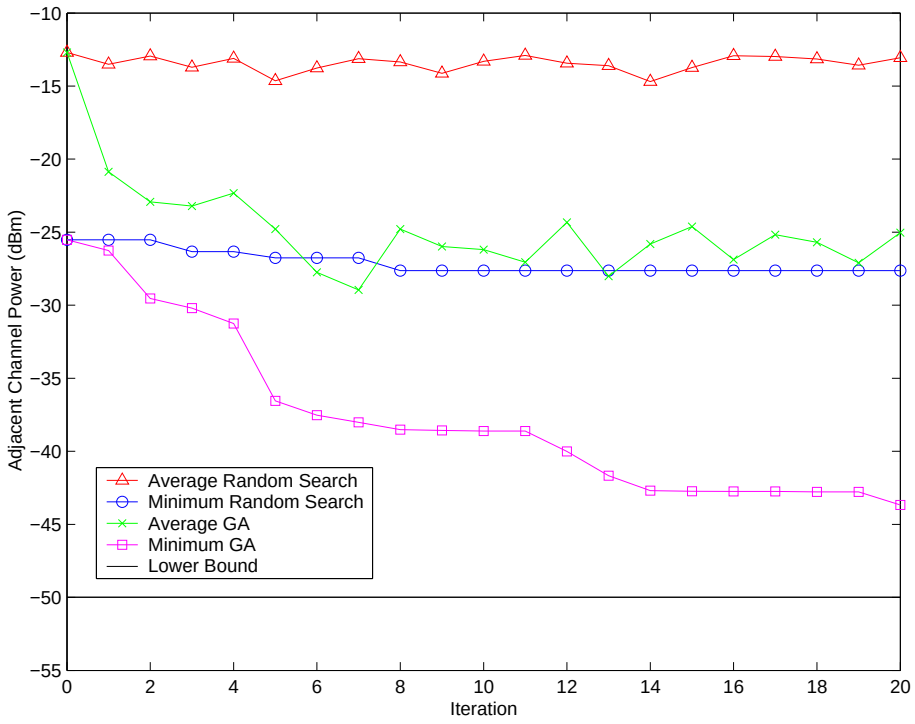

Figure 16: Convergence profile.

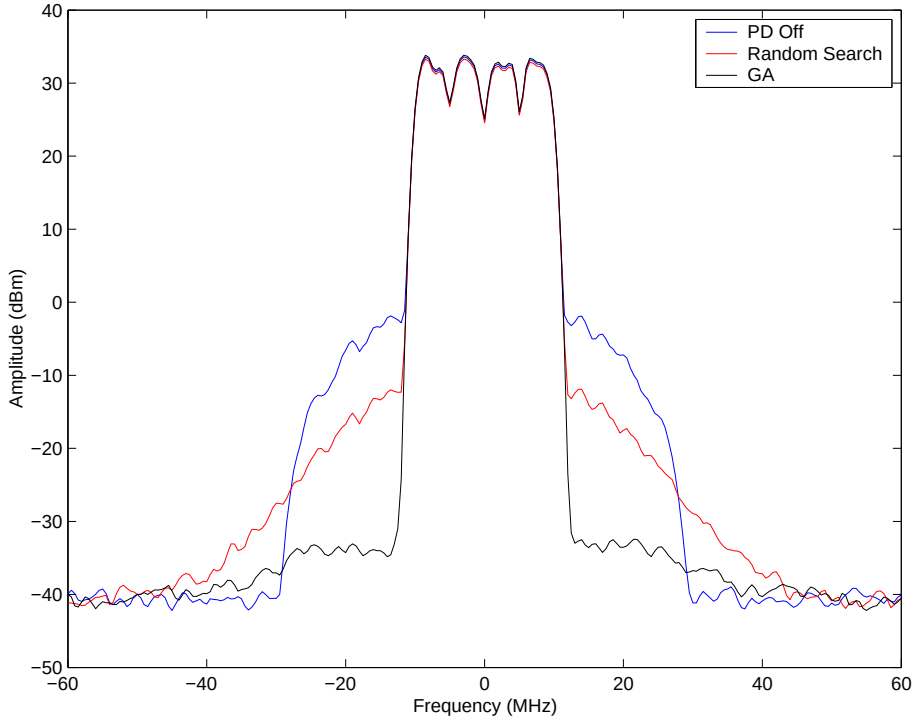

Figure 17: Linearization performance.

4.3 Closed-Loop Pre-distortion with Laboratory PA

The GA is used to linearize a 0.5W laboratory PA during transmission of a multi-carrier CDMA2000 waveform centered at 881MHz using narrowband feedback [57]. It is important to redefine the polynomial coefficients. A chromosome was previously defined in Equation 31. To facilitate convergence, each gene is now composed of two variables $\overline{A}_a$ and $\widetilde{A}_a$; these represent the nominal and delta coefficients, respectively. The bar terms represent the average of the search space, they are constant and chosen a priori in the neighborhood of an expected solution. The tilde terms represent a particular member of the population. These parameterizations restrict the search space to keep the algorithm stable. The algorithm may also be modified to allow optimization of the bar terms as well. The adaptation of the nominal coefficients is subject to future investigations.

The implementation of the digital pre-distortion hardware test bed is illustrated in Figure 19. Our forward path uses direct RF conversion. However, for our test bed, the spectrum analyzer is used to replace the feedback path. The Intersil ISL5217 evaluation board was used to generate a three-carrier CDMA2000 waveform, with each carrier having a signal bandwidth of 1.23MHz for a total bandwidth of 3.75MHz. The CDMA2000 waveform has a PAR of approximately 12.4dB. This waveform was pre-distorted using the Intersil ISL5239 evaluation board. The ISL5239 is a baseband look-up table (LUT) pre-distortion device. The ISL5239 also included gain, phase, and offset correction to improve image rejection and carrier leakage of the direct upconverter. The ISL5239 evaluation board includes the Intersil ISL5929 dual DAC and interfaces with the Sirenza [41] STQ-2016 direct upconverter to generate the 881MHz pre-distorted RF waveform, the evaluation platform described above is shown in Figure 18.

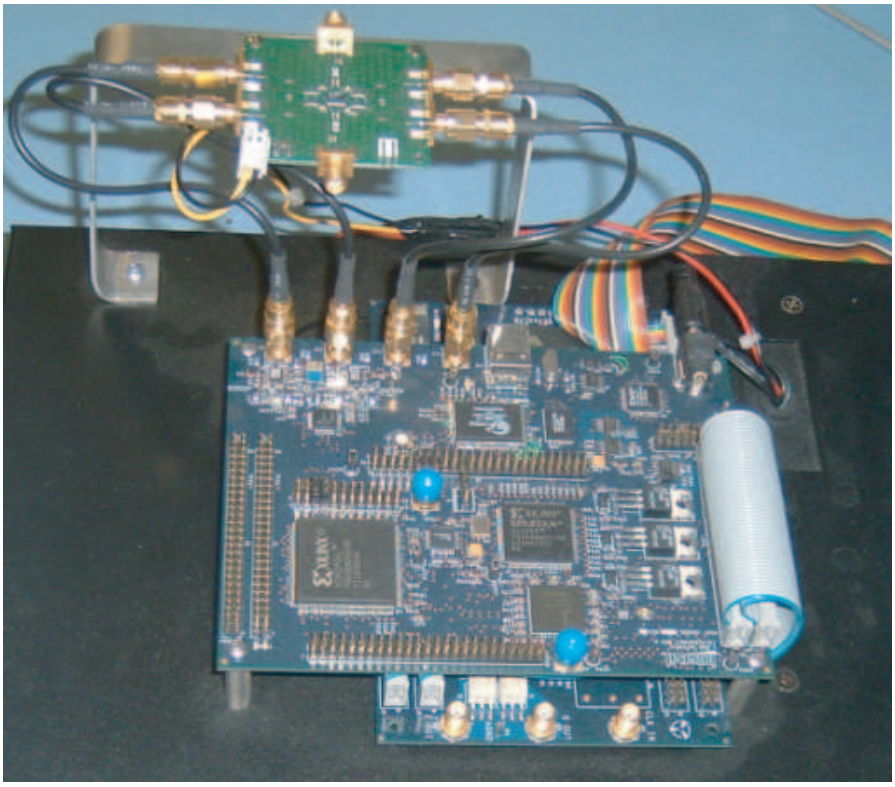

Figure 18: Intersil pre-distortion evaluation platform.

The waveform was driven by a Mini-Circuits [55] ZHF-1000 amplifier. The waveform was then amplified by a Sirenza SHF-0189 PA. The output was fed back to a computer through an Agilent E4404B Spectrum Analyzer. The data was processed in Matlab to implement a LUT solution in the ISL5239. In this implementation, linearization is achieved through the adaptation of a LUT in which polynomial functions are used to correct for amplitude and phase, as in [10].

Optimal linearization results were achieved by defining the genetic operators with an elitism rate of 20%, a mutation rate of 3% and a crossover rate of 50%. The initial populations were comprised of $N = 25$ members and the simulations were allowed to run over $i = 20$ iterations. Figures 20(a) and 20(b) show the AM-AM and AM-PM correction curves of the LUT after the algorithm has converged. The P_{1dB} of the laboratory PA is $-3.5dBm$ thus both tables remain constant up to an input power of approximately -4dBm after which correction is applied. The hardware

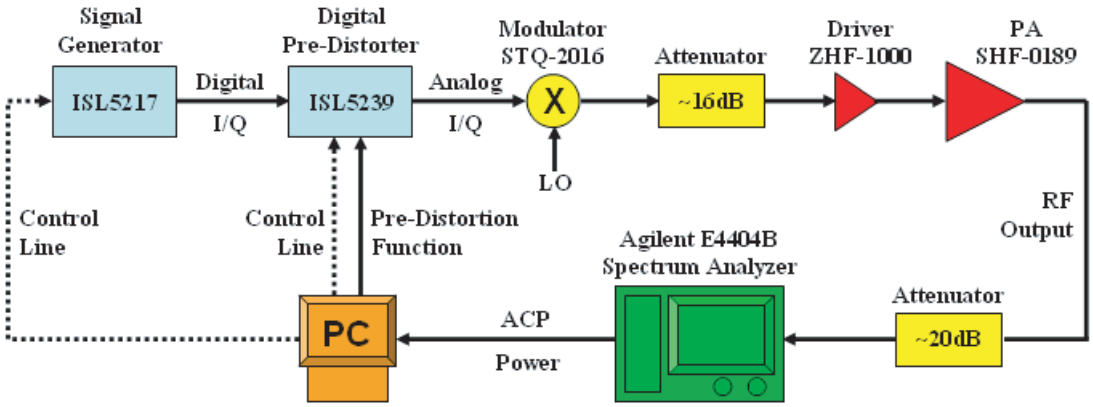

Figure 19: Testbed of the closed-loop adaptive digital pre-distortion system.

optimization was achieved by minimizing the cost function described in Equation 41 for each population member. The fitness, similar to the software model, depends on the difference between the IM3H and the in-band power (IM1).

$$f = IM1 - IM3H \tag{41}$$

The GA adaptation curves are shown in Figure 21 demonstrating the progress of the algorithm as a function of the number of iterations. The results shown prior to iteration 0 indicate ACP measurements without pre-distortion. The uppermost line shows the average adjacent channel power for the population. The second line corresponds to the GA optimal solution. Even though the adjacent channel power decreases for each iteration the optimal solution does not remain constant due to varying input power levels. Finally, the lowest line represents the minimum possible adjacent channel power as defined by the noise floor of the system. As explained in [2], the output noise floor is lower for a PA operating in compression than for a PA operating in its linear region. As was shown through simulations, optimum ACP performance is achieved when the PD gain is at its maximum level and the resulting output noise floor is at a minimum. The increase in PD gain also causes the PA to operate with higher efficiency.

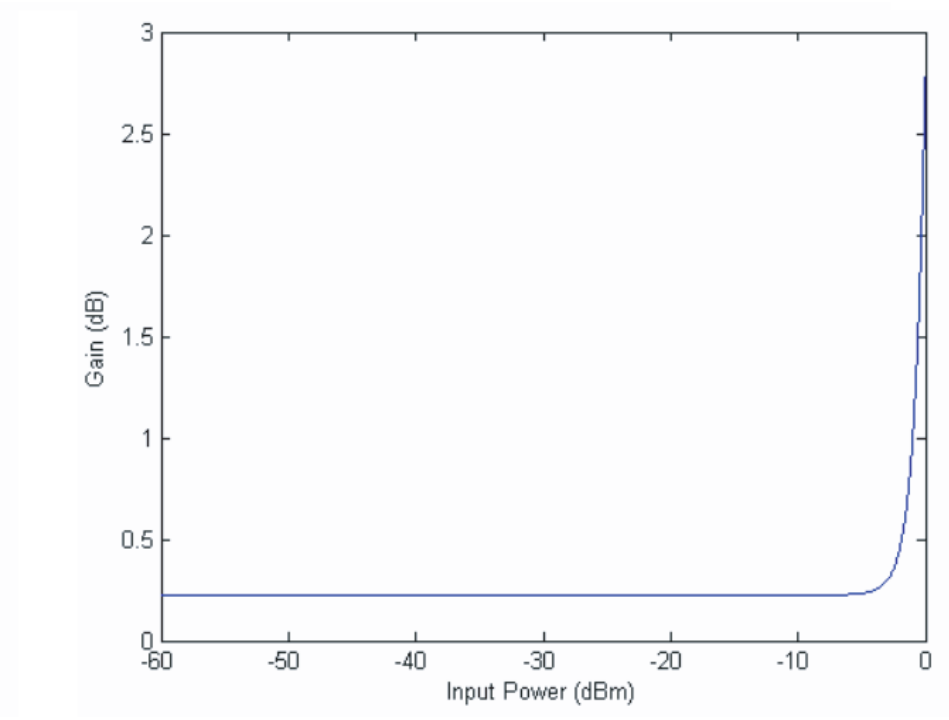

(a) AM-AM Pre-Distortion Curve for the 0.5W PA.

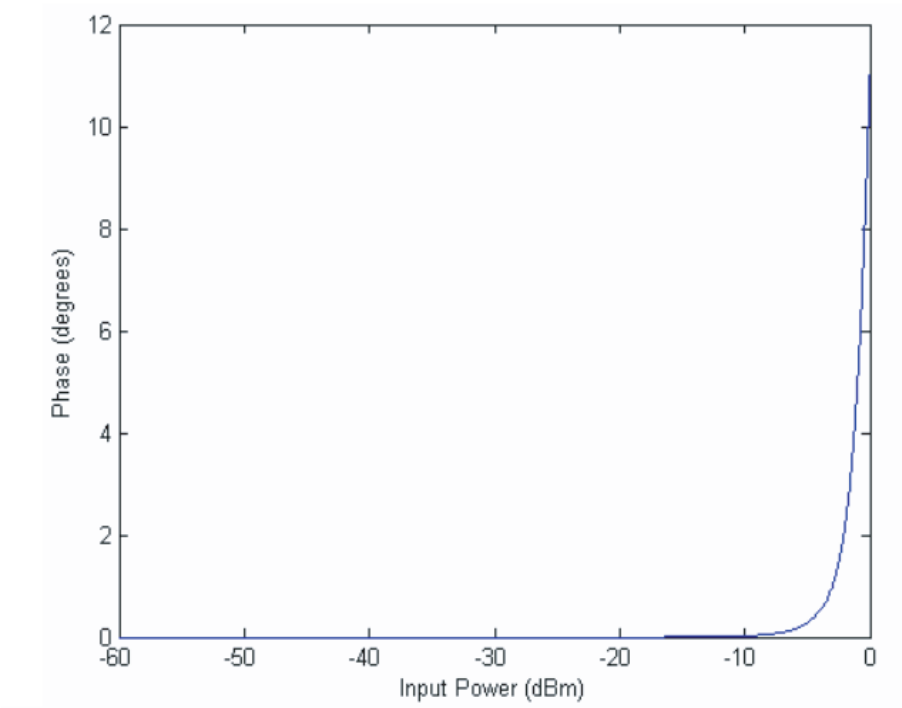

(b) AM-PM Pre-Distortion Curve for the 0.5W PA.

Figure 20: Pre-Distortion Curves for 0.5W Laboratory PA.

Figure 22 shows the PA output with and without pre-distortion. The PA output power is held constant for both cases. Without linearization the ACPR is measured to be 34dBc. This improves to 49dBc with the pre-distortion defined by the GA. The low-cost implementation is able to improve APC performance by approximately 15dB, thus meeting the 3GPP specifications.

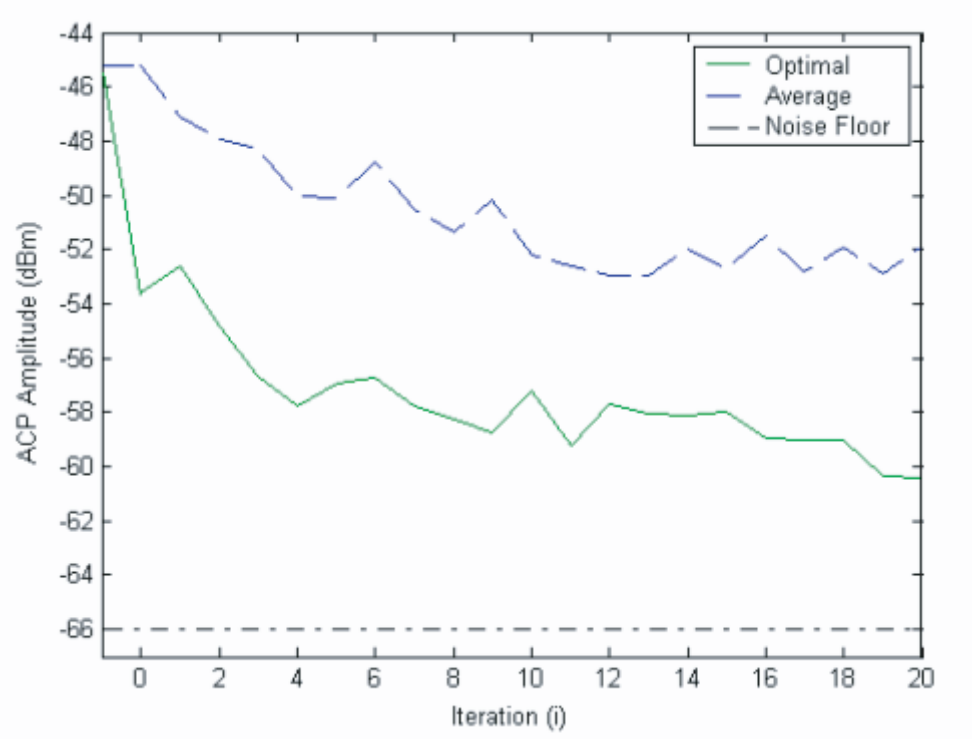

Figure 21: Convergence profile.

It can be observed from Figure 22 that this laboratory PA does not show spectral regrowth asymmetry in the adjacent and alternate channels which indicates a virtually memoryless amplifier. The ideal behavior of the PA facilitates the convergence of the algorithm. The same architecture is used to evaluate the performance of a high power amplifier (HPA).

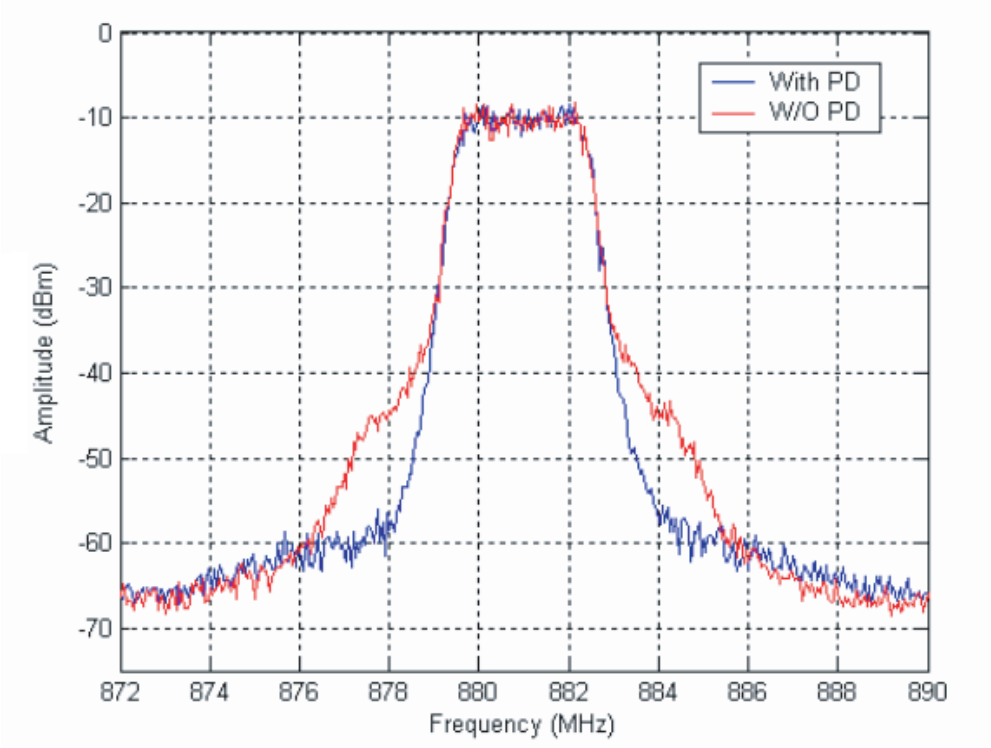

Figure 22: Linearization performance.

4.4 Closed-Loop Pre-distortion with a Basestation PA

The laboratory PA from the previous section was shown to be quite linear with no indication of spectral regrowth asymmetry in the adjacent and alternate channels, thus a virtually memoryless amplifier. The ideal conditions of the 0.5W amplifier facilitate the convergence of the algorithm. The HPA used in the second implementation is a 45W device that is known to show memory effects [43]. Consequently, this results in significant asymmetry in the adjacent and alternate channels as explained in [42]. The algorithm uses measurements of adjacent channel power, as before. Thus, incongruities between the low and high side will affect the convergence of the originally proposed formulation of the GA. The setup described in the previous section is used again; however, in this configuration a Stealth Microwave linear PA is used to drive

the device-under-test (DUT). Prior to pre-distortion efforts this amplifier was characterized using a network analyzer to determine the AM-AM and AM-PM transfer curves shown in Figures 23(a) and 23(b), respectively. The seemingly odd behavior for a input power of 37dBm is due to a built-in protection circuitry.

To compensate for the asymmetry, the algorithm was modified such that it measures both high and low side ACLR and then seeks to minimize the higher of the two, ideally forcing the pre-distortion function to linearize the PA symmetrically. This was achieved by modifying the cost function of the GA such that the fitness of each population member now depends on the sum of the differences between the linear measurements for IM3L, IM3H and the IM1 as described in Equation 42. The use of linear terms ensures that the imbalance between the high and low side will be properly weighted.

$$f = 10^{(IM1-IM3L)/20} + 10^{(IM1-IM3H)/20} \tag{42}$$

However, it was observed that this modification was unable to completely eliminate the asymmetries in the adjacent and alternate channels. The adaptation curves for the 45W PA are shown in Figure 24. As in Figure 21, the average, optimal and noise floor curves are shown. The convergence of the optimal solution is impeded by the significant memory effects which account for the irregular results. The results indicate the presence of memory effects; these are responsible for the observed asymmetry in Figure 25. The GA implementation applies pre-distortion functions to this PA and achieves approximately 12dB of ACP improvement on the low-side (ACPL). However, the high-side ACP (ACPH) improvement is only 10dB. The results are significant as previous wideband implementations in [44] were only able to achieve approximately 3dB of ACP improvement.

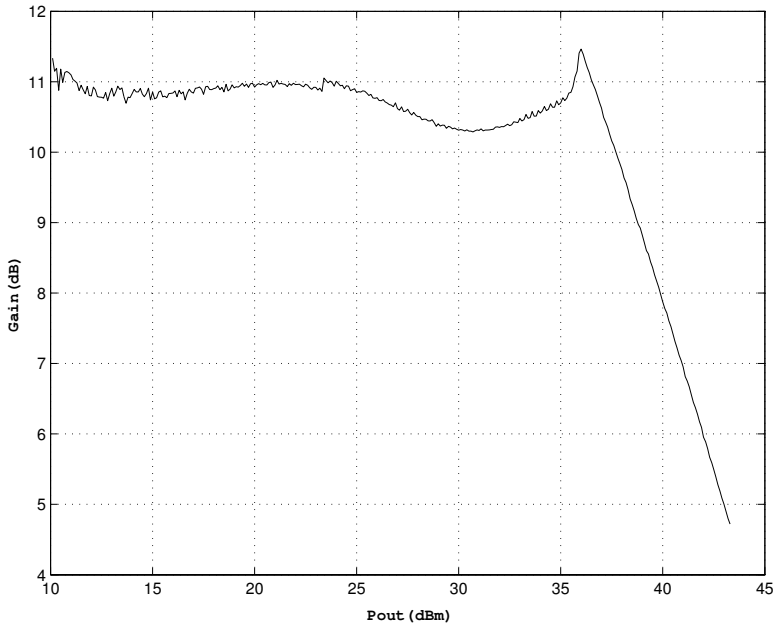

(a) AM-AM Characteristic Curve for the 45W PA.

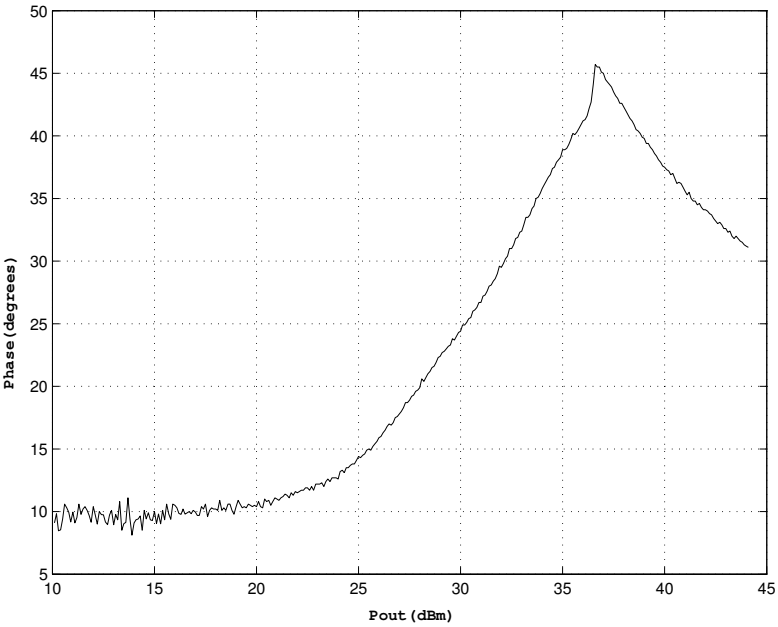

(b) AM-PM Characteristic Curve for the 45W PA.

Figure 23: Characteristic Curves for 45W Basestation PA.

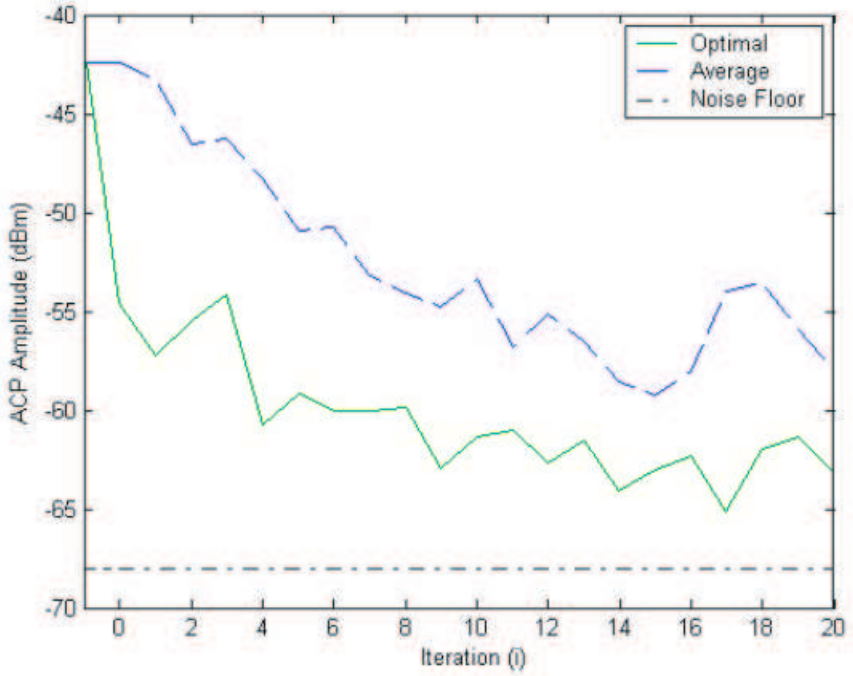

Figure 24: Convergence profile.

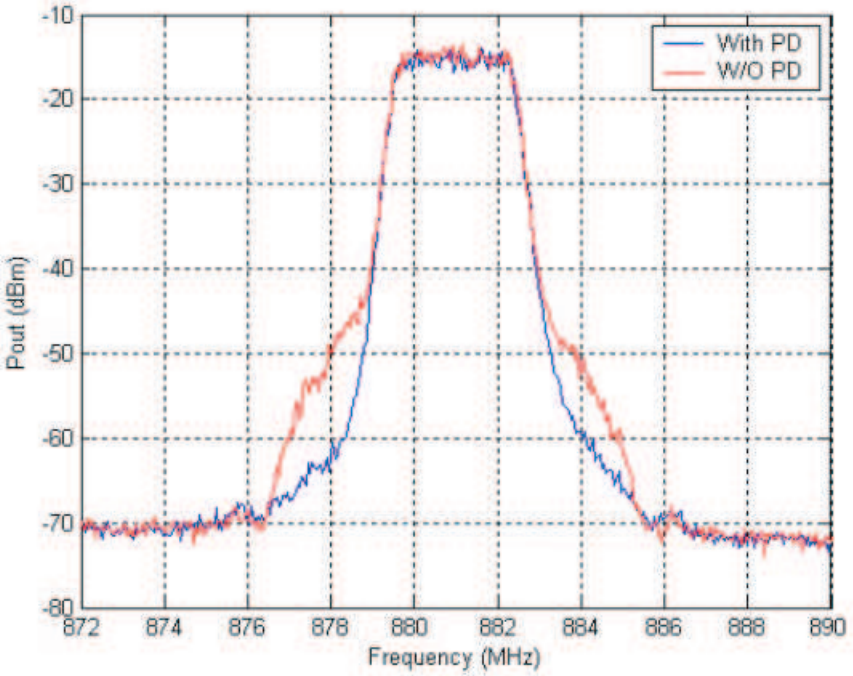

Figure 25: Linearization performance.

CHAPTER V

CREST FACTOR REDUCTION AND PRE-DISTORTION

5.1 Introduction

The effectiveness of the PD technique is substantially dependant on signal characteristics. A CDMA signal, for example, may have a PAR as high as 13dB. A basestation PA transmitting CDMA signals must operate with significant back-off to allow for the high PAR while maintaining linearity. The back-off levels in this case translate into undesirable power efficiency losses. The PAR of a signal can be calculated with Equation 43 using typical mathematical manipulations where $\sigma(x)$ is the standard deviation of the signal x.

$$PAR = 20log_{10}(\frac{max|x|}{\sigma(x)}) \tag{43}$$

The PAR of the transmitted signal is also often referred to as the crest-factor (CF) of the signal calculated as the peak-to-rms voltage. The relationship between the two terminologies is described by Equation 44.

$$CF = \sqrt{PAR} \tag{44}$$

A crest factor reduction (CFR) technique has been described which allows the PA to operate at higher input/output power levels while maintaining linearity at the output of the amplifier [19]. When CFR is applied to typical modulated signals, significant efficiency improvements can be observed through the PA.

It is important at this time to introduce yet another system requirement that needs to be met by the basestation transmitter. With linearization efforts the tradeoff for added efficiency is increased levels of ACP. Similarly, the tradeoff for reducing

the CF of the signal could include signal degradation measured as error vector magnitude (EVM), or composite EVM (cEVM). These are measures of the difference between the input waveform prior to CFR and the modified output waveform. For the measurement to be accurate, the input and output signals must be time aligned to account for processing and filter tap delay length. The amplitude of the signals must also be normalized. The EVM calculations are summarized in Equations 45 and 46. The composite EVM calculation function can be found in Appendix B.

$$error(n) = out(n-d) * \frac{\frac{1}{N}\sum_{n=1}^{N}|input(n)|}{\frac{1}{N}\sum_{n=1}^{N}|output(n-d)|} - in(n) \tag{45}$$

$$EVM(\%) = \frac{\frac{1}{N}\sum_{n=1}^{N}|error(n)|^2}{\frac{1}{N}\sum_{n=1}^{N}|in(n)|^2} * 100 \tag{46}$$

Peak code domain error (PCDE) is also regulated, it is a measure of how much cross-talk exists between different channels within the signal. Although PCDE is a concern, measurement requires specific instrumentation that was unavailable at the time of publication. The application of CFR can also affect the ACP measurements. The WCDMA standards are summarized in Table 5. In this chapter, results for CFR implementation are reported; wideband DPD is also applied both with and without CFR to show performance improvements.

Table 5: WCDMA Standards

Requirement	Limit
IM3	$\geq 45dBc$
IM5	$\geq 50dBc$
EVM	$\leq 17.5\%$
PCDE	$\leq -33dB$

5.2 Crest Factor Reduction

It is perhaps relevant at this point to look at the conceptual principles of WCDMA modulation. It can be shown that the linear combination of sinusoids of equal amplitude but different frequency create a combined waveform in which the amplitude of the signal has significantly increased, however the average power has not changed significantly. The average power grows by a factor of N when N contributors of equal average power are combined. Simultaneously, the peak voltage increases by a factor of N and equivalently the peak power increases by N^2. The resulting combined waveform has a PAR that increases by N for every added contributing signal. The typical Vin-Vout performance of a PA transmitting a CDMA signal can be observed in Figure 26.

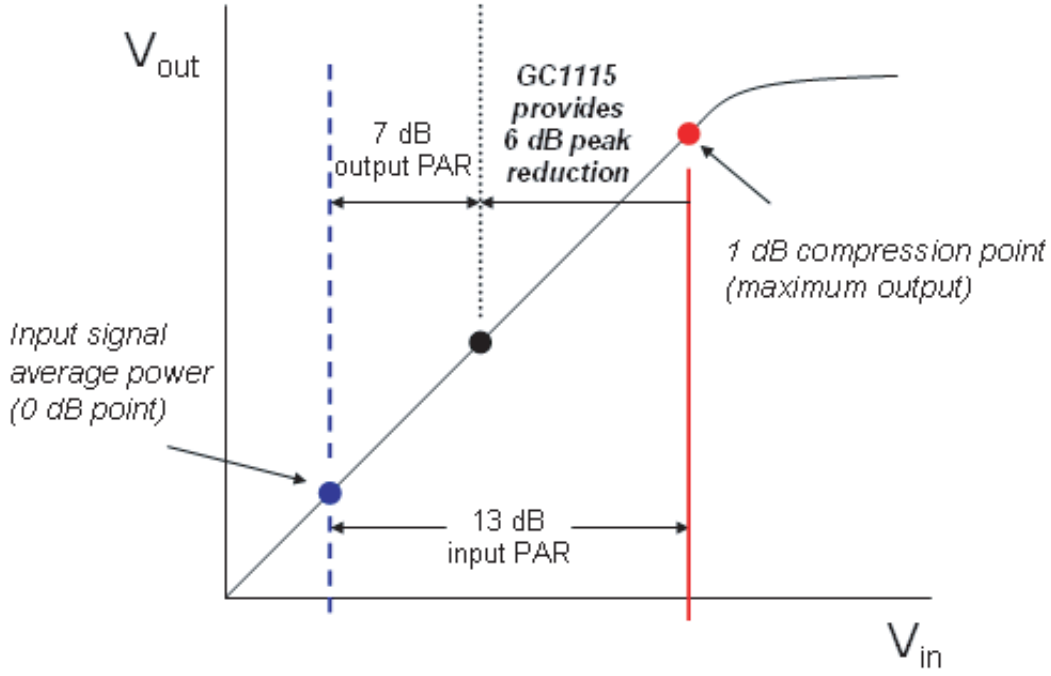

Figure 26: PA Vin-Vout response for a typical CDMA signal.

There exist numerous methods to achieve CFR; code selection, digital clipping

and pulse injection are among the most popular methods [39, 40]. The chosen implementation uses pulse injection in combination with digital clipping to achieve optimal results. Figure 27 illustrates the method by which a peak is reduced.

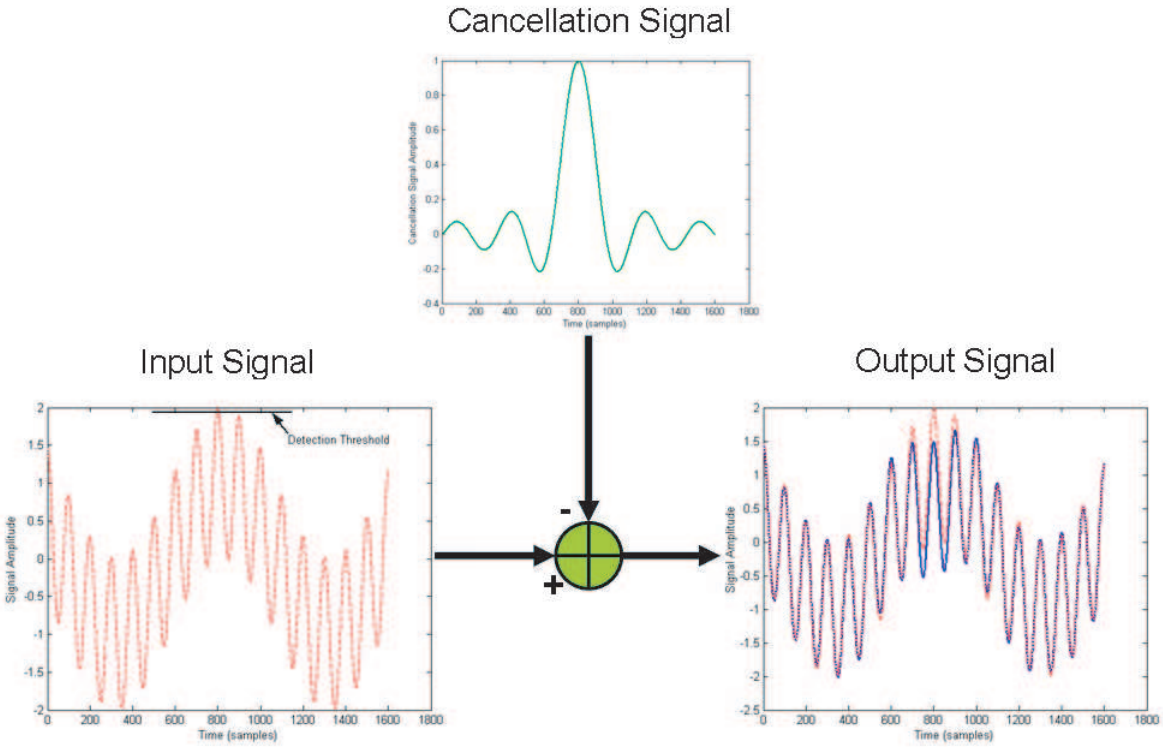

Figure 27: Typical peak cancelation through pulse injection.

When CFR is applied to a signal prior to amplification, the added efficiency illustrated in Figure 28 is observed. Added efficiency results for an ideal PA model are summarized in Table 6

Table 6: Typical Efficiency Improvement using CFR

-	Without CFR	With CFR
Average PA Output Power	$10W$	$20W$
DC Power	$125W$	$125W$
Efficiency	8%	16%

Figure 29 illustrates the complementary cumulative distribution function (CCDF) of the transmitted signal before and after CFR implementation. The research will investigate the added improvement to PD with the implementation of CFR.

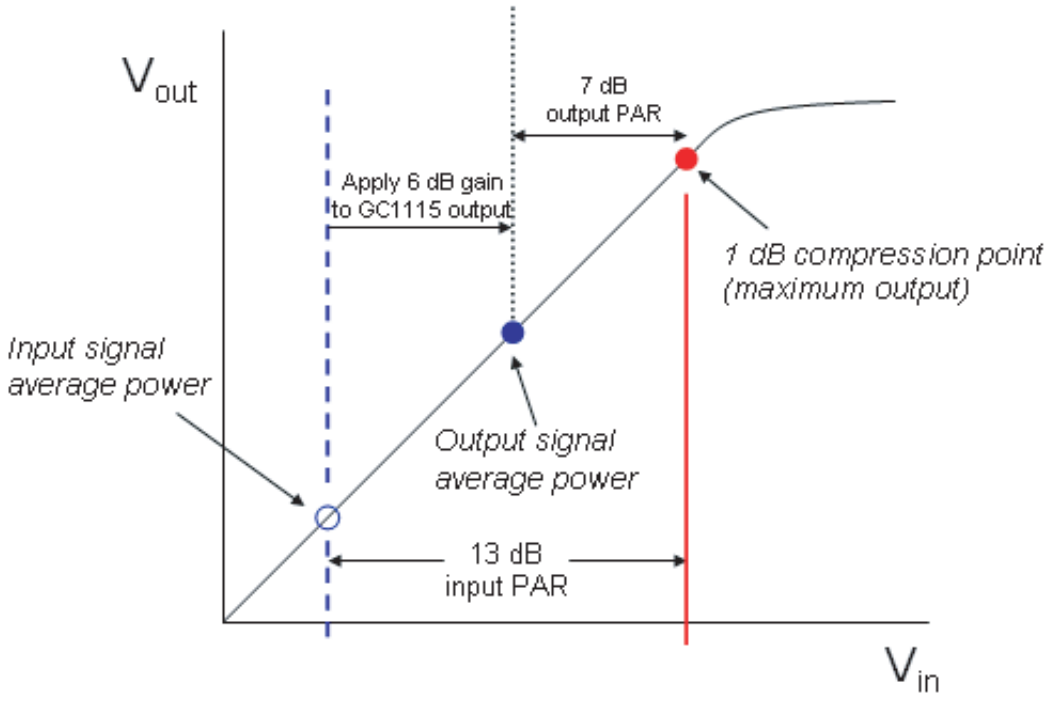

Figure 28: PA Vin-Vout response for a CDMA signal with CFR.

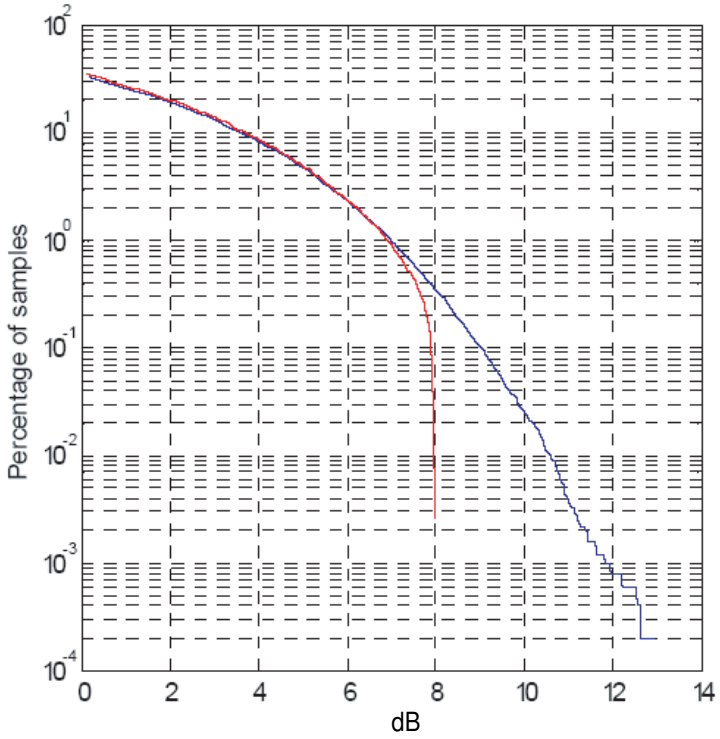

Figure 29: CCDF of the transmitted signal with and without CFR.

The architecture of the CFR approach is proposed by Texas Instruments through the use of their GC1115 preprocessor. The preprocessor identifies peaks in the input signal that are above a specific level. The detected peak location is within 1/256th of the sample rate. The peak location is then used to drive a digital signal generator which effectively generates a scaled waveform that locates and cancels the pre-existing peak. Figure 30 illustrates the real and imaginary components of the generated pulse. Care must be taken in choosing a waveform to cancel the envelope peak so as to preserve out-of-band spectrum, and hence the ACP.

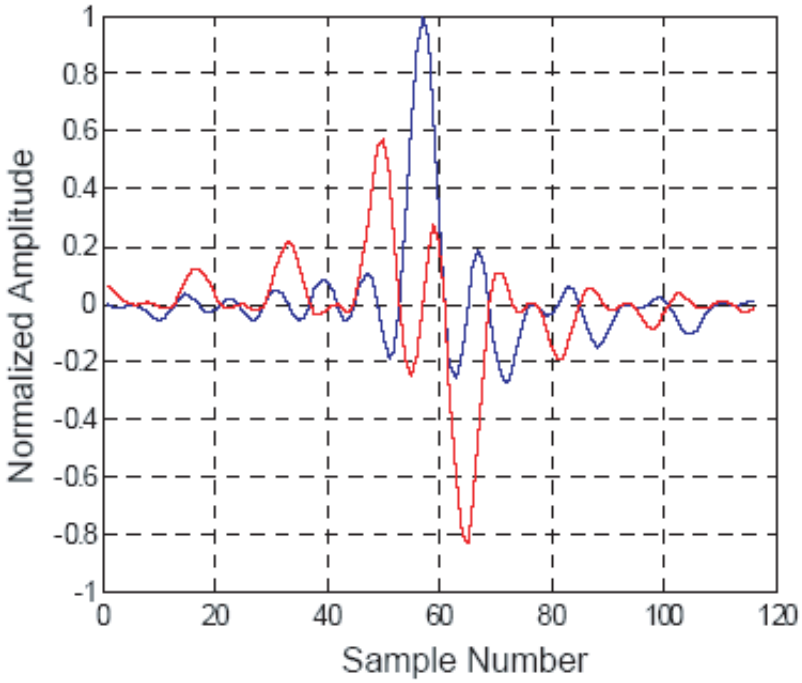

Figure 30: Real and imaginary components of canceling pulse.

The CFR process includes four processing stages used to cancel new peaks that may result from the added cancelation peaks in the previous stage. Digital clipping is implemented through an output limiter to eliminate the rare occurrence of peaks after the fourth stage. A detailed block diagram of the four-stage CFR is illustrated in Figure 31. The peak detection limits are defined by specifying the desired output PAR to levels of 5 to 8dB. Signal processing of the input signal in the time domain is

shown in Figure 32. The detection threshold is set below $6x10^4$, thus any peaks that trigger the threshold are processed. The gain threshold is set to a limit slightly lower than the detection threshold; after processing, the peaks will not surpass this second specification. The peak canceling waveform is also shown in the same figure for the given input signal.

The CFR technique is applied to a 4-carrier UMTS signal, a 1-carrier CDMA signal, and a 15-carrier CDMA signal to show the effective PAR after preprocessing has been applied to the original signals. The figures also show the corresponding EVM levels that increase as the PARs of the signals decrease. The results are also summarized by the following tables.

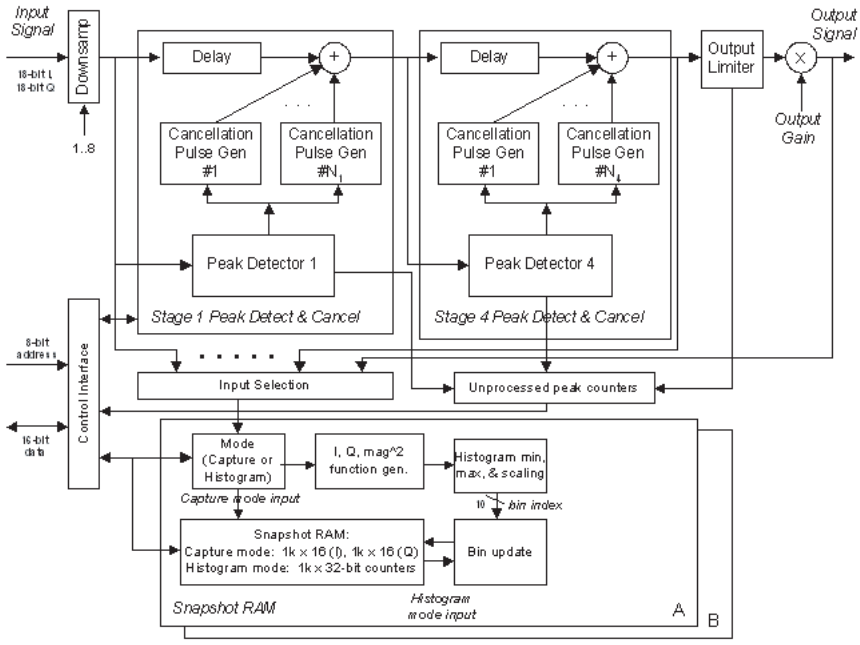

Figure 31: Block diagram of GC1115 CFR processor.

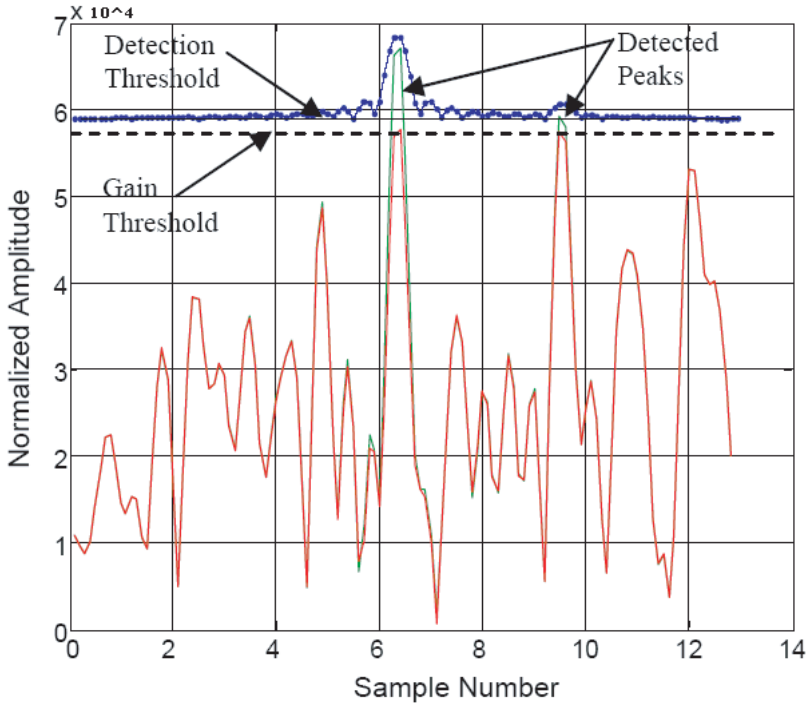

Figure 32: Corrected and uncorrected signal with canceling peaks and detection threshold.

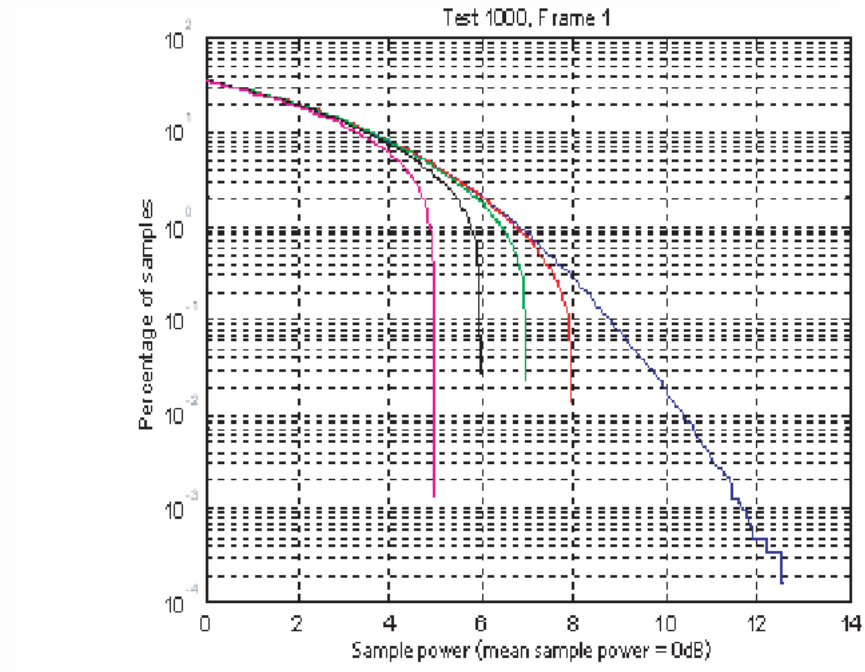

(a) CCDF for CFR data using a 4-carrier UMTS signal.

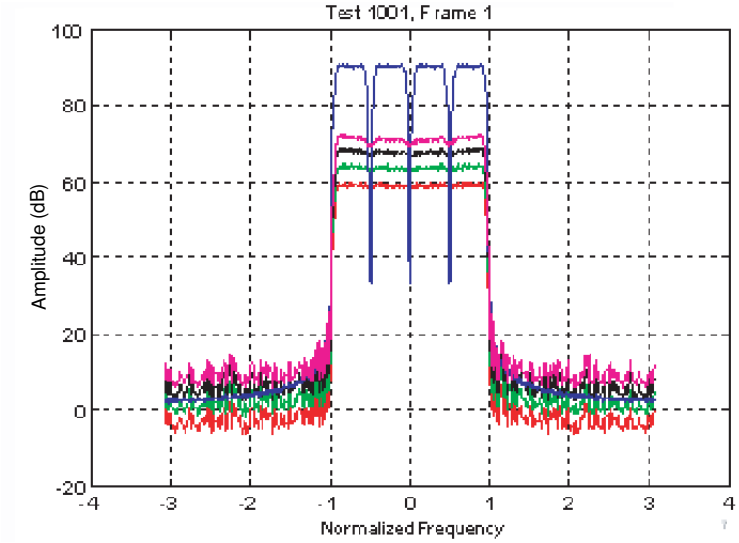

(b) PSD for CFR data using a 4-carrier UMTS signal.

Figure 33: GC1115 performance with 4-carrier UMTS signal of PAR=11.2dB.

Table 7: PAR and EVM of 4-carrier UMTS signal.

Desired PAR	8dB	7dB	6dB	5dB	4dB
Effective PAR	8.01dB	7.07dB	6.18dB	5.4dB	4.75dB
Estimated EVM	1.91%	3.87%	6.9%	11.15%	16.71%

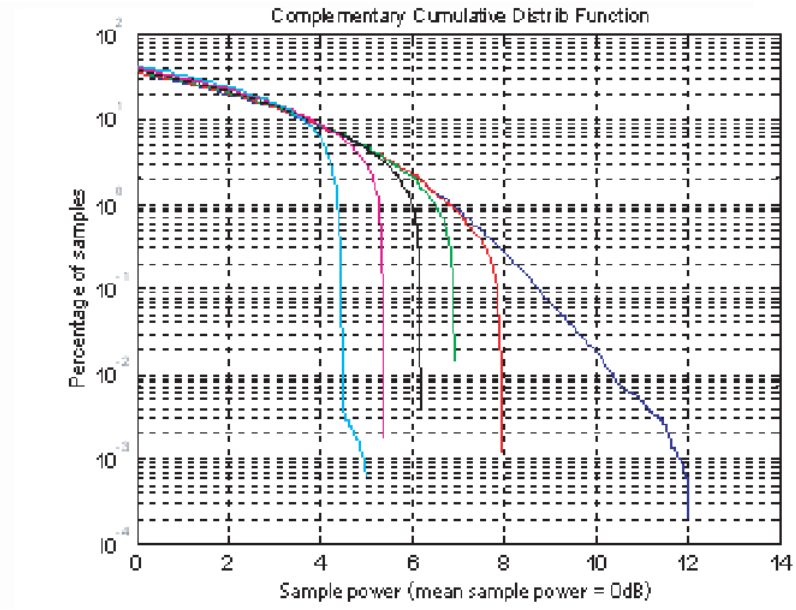

(a) CCDF for CFR data using a 1-carrier CDMA signal.

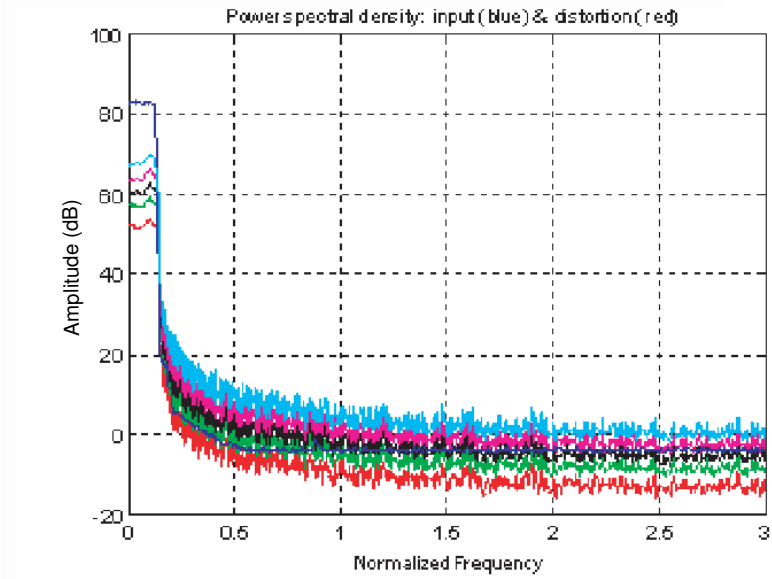

(b) PSD for CFR data using a 1-carrier CDMA signal.

Figure 34: GC1115 performance with 1-carrier CDMA signal of PAR=12.03dB.

Table 8: PAR and EVM of 1-carrier CDMA signal.

Desired PAR	8dB	7dB	6dB	5dB	4dB
Effective PAR	7.99dB	6.94dB	6.22dB	5.42dB	5.02dB
Estimated EVM	2.96%	5.43%	8.17%	12.66%	20.61%

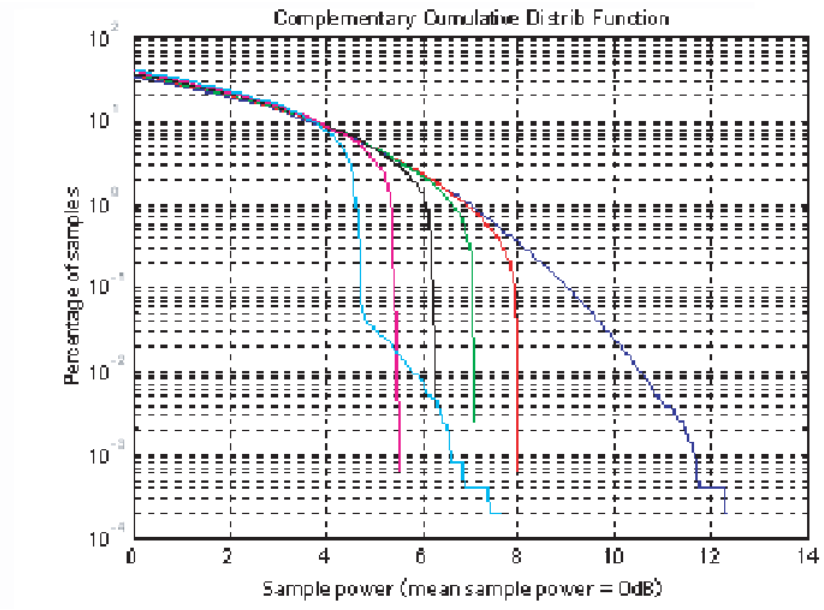

(a) CCDF for CFR data using a 15-carrier CDMA signal.

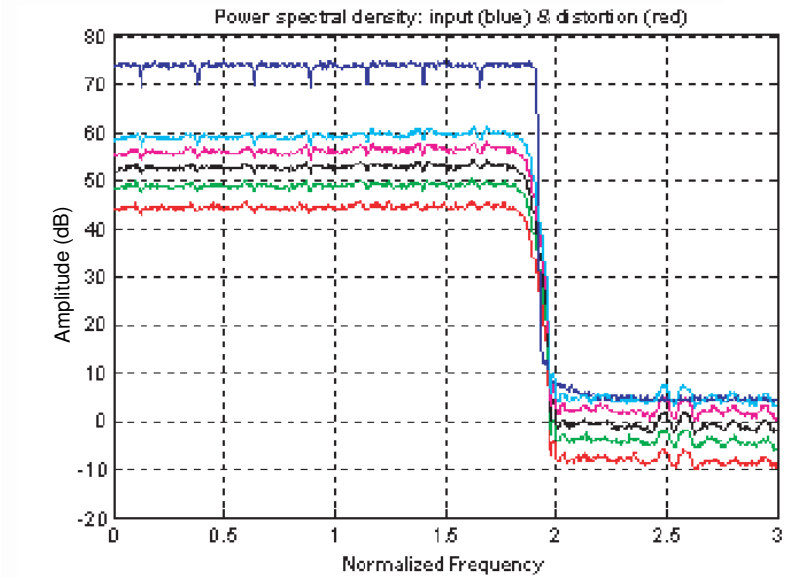

(b) PSD for CFR data using a 15-carrier CDMA signal.

Figure 35: GC1115 performance with 15-carrier CDMA signal of PAR=12.41dB.

Table 9: PAR and EVM of 15-carrier CDMA signal.

Desired PAR	8dB	7dB	6dB	5dB	4dB
Effective PAR	8.02dB	7.11dB	6.29dB	5.53dB	7.71dB
Estimated EVM	3.44%	5.87%	9.17%	13.97%	20.56%

Finally, CFR is applied to a Mini-Circuits ZRL-2300 laboratory PA using the UMTS test signals shown in Figure 33(a) [58]. The results for added available output and corresponding ACP levels are shown in Figure 36. It is important to understand that although the application of CFR decreases the peak signal power, the improvement does not linearly translate to added PA output power. Experimental results indicate that, for constant ACP levels, a signal which has a 6dB reduction in PAR will increase the PA output power by no more than 3dB. When CFR is applied to the signal, a higher percentage of samples will be located closer to the 1dB compression point of the PA. CFR is a technique that allows the PA to operate more efficiently and is not a linearization technique. As such, PA backoff is still required to maintain appropriate ACP levels. DPD will be responsible for linearizing the PA after CFR has been applied to the input signal.

The following section describes the application of both CFR and DPD while reporting performance improvements for the individual techniques along with their combined enhancement.

5.3 Adaptive Pre-Distortion with Crest Factor Reduction

The application of CFR and pre-distortion were investigated to determine the added linearization performance. In this implementation, linearization results for the LMS algorithm introduced in [45] are compared to results obtained exclusively by CFR. Finally, the two implementations will be cascaded from which increased output power and added efficiency are quantified while maintaining the 3GPP specification for ACP.

The combined techniques are applied to a CREE Microwave 30W PA module operating at 1.96GHz [46], this particular PA shows very little memory effects. The PAR of the IS-95 signal is reduced from 9.6dB to 5dB prior to the pre-distortion process when CFR is applied. Figure 37 shows the hardware test bed that is used

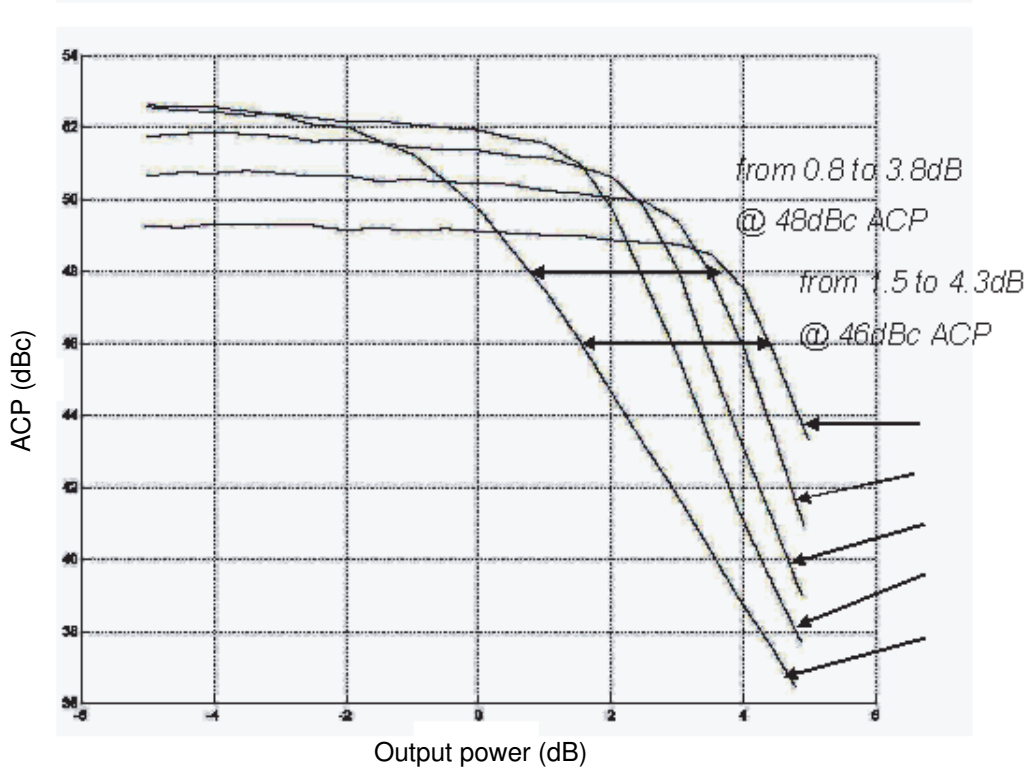

Figure 36: CFR performance as applied to a Mini-Circuits ZRL-2300 PA.

to implement a LUT based approach to digital pre-distortion. The process of CFR is performed by the PC along with the pre-distortion; the linearized signal is then loaded into the Agilent arbitrary waveform generator. The feedback data collected by the oscilloscope adjusts values in the LUT such that optimal linearization is achieved. The investigation compares CFR results for both the original signal with 9.6dB PAR, and the processed signal with 5dB PAR. Performance results are also shown with and without pre-distortion. Figure 38 compares ACP improvement results for output power levels with the given test conditions.

Figure 38 indicates an increased output power for a given ACP (or ACPR) of 45dBc in a 30kHz bandwidth at an offset of 885kHz. This increase in ACP can be translated to added PA efficiency. As the increasing input power level approaches P_{1dB} of the PA, the performance of the PD degrades as shown by a decrease in output power. The limited dynamic range of the test bed prevents measurements at lower

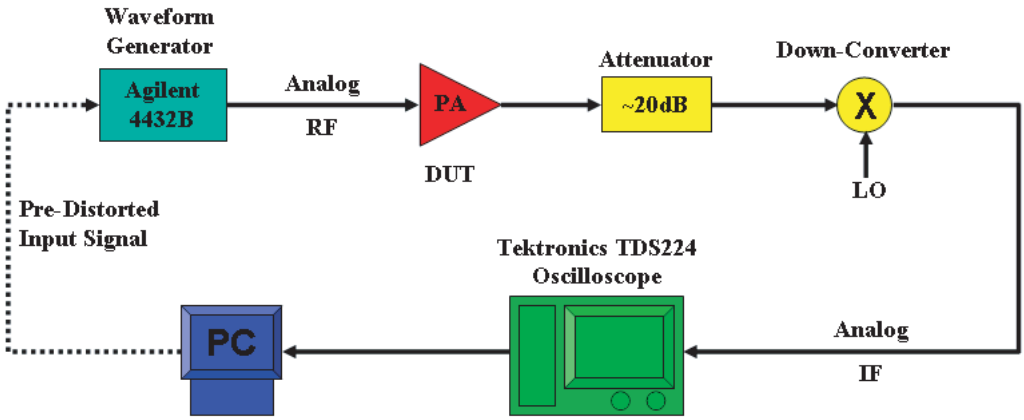

Figure 37: CFR-DPD linearization platform.

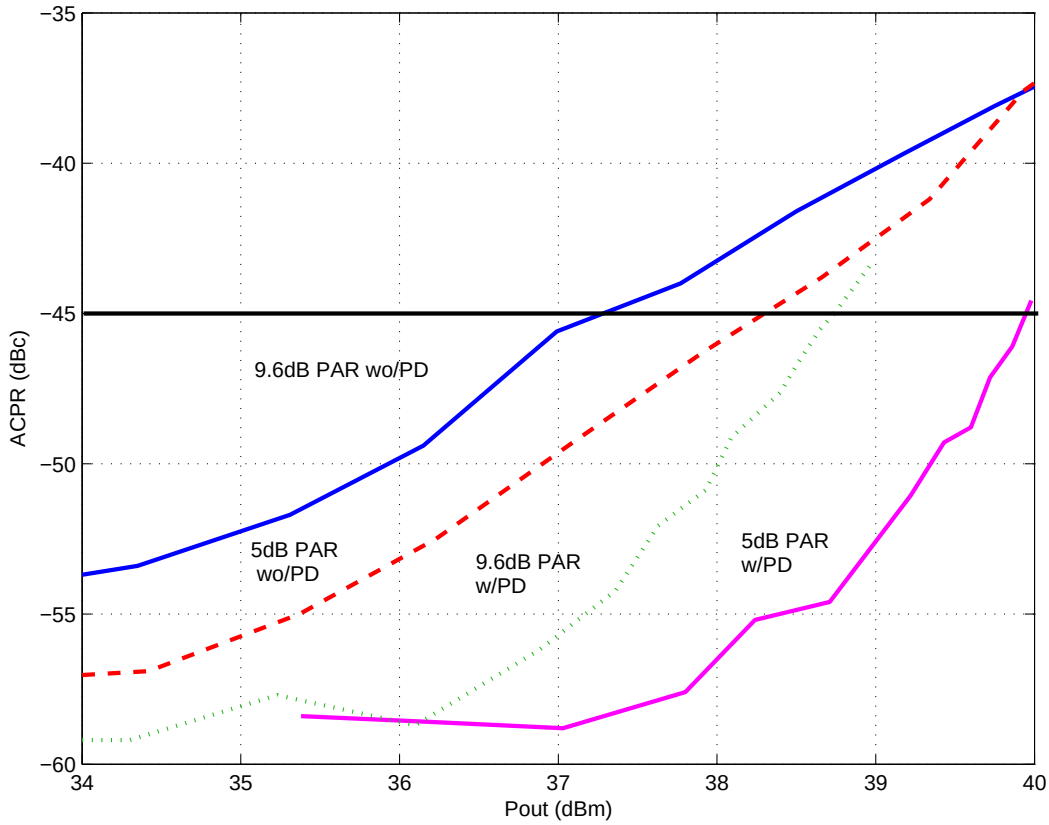

Figure 38: ACPR improvement with respect to output power.

output power levels. The figure suggests that without such limitations the output power improvement would be greater for a lower level of ACP, as may be required for some multi-carrier applications. The results for increased output power and efficiency

for the given ACP are shown in Table 10.

Table 10: Power and efficiency improvement.

	With PD		Without PD	
PAR	9.6dB	5dB	9.6dB	5dB
Pout	38.7dBm	40.0dBm	37.3dBm	38.3dBm
Efficiency	21.5%	23.9%	18.3%	20.5%

The above table suggests that PD is responsible for a greater percentage of efficiency improvement. The CFR of the input signal increases the efficiency by 2.2% in the absence of pre-distortion improvements. With pre-distortion, the improvement due to CFR is 2.4% with an additional 1.2dB of output power. The total added output power due to pre-distortion and crest factor reduction is 2.7dB. Previous work suggests that the efficiency improvement would be greater for input signals with larger PAR.

CHAPTER VI

PRE-DISTORTION OF POWER AMPLIFIERS WITH MEMORY EFFECTS

6.1 Introduction

This chapter investigates the application of genetic algorithms to linearize power amplifiers with strong memory effects using digital pre-distortion. As was explained earlier, the term memory effects refer to the bandwidth-dependant nonlinear effects often present in PAs. These encompass envelope memory effects and frequency memory effects. Spectral regrowth asymmetry in the adjacent and alternate channels indicates the presence of memory effects and is commonly referred to as IMD imbalance. Envelope memory effects are primarily a result of thermal hysteresis and electrical properties inherent to PAs. Frequency memory effects are due to the variations in the frequency spacing of the transmitted signal and are characterized by shorter time constants. Both wideband and narrowband algorithms use the memory polynomial pre-distorter model to achieve optimal linearization performance. The model uses the diagonal kernels of the Volterra series; although there are many terms to solve for, the wideband LMS algorithm is quite capable of solving for them as shown in [49,50]. This work is the first documented attempt at solving these same kernels using only narrowband feedback information. The wideband approach is described next as it applies to a PA model with strong memory effects.

6.2 Memory Polynomial and Wideband Pre-Distortion

The wideband LMS adaptation algorithm described uses an indirect learning architecture and requires little or no characterization of the amplifier. The memory polynomial PD function is described by Equation 47 where $x(n)$ represents the input waveform to the PD and $y(n)$ represents the output of the PD.

$$y(n) = \sum_{k_{odd}=1}^{K} \sum_{d=0}^{D} a_{kd} \cdot x(n-d)|x(n-d)|^{k-1} \tag{47}$$

For Equation 47, the k term defines the order of the PD polynomials and are only permitted to be odd valued. The D term identifies the tap delay, or memory between the polynomials. In the case of memoryless PD, $D = 0$ and the equation resembles those defined by Equations 23 and 24 in Chapter 2 for which the polynomial was restricted to $K = 7$ terms. The previously defined coefficients in Chapter 2 correspond, as follows, to those defined here.

$$\begin{bmatrix} A_a + j \cdot A_\phi \\ B_a + j \cdot B_\phi \\ C_a + j \cdot C_\phi \\ D_a + j \cdot D_\phi \end{bmatrix} = \begin{bmatrix} a_{10} \\ a_{30} \\ a_{50} \\ a_{70} \end{bmatrix} \tag{48}$$

It is evident from the above notation that the a_{kd} coefficients are complex valued. It is also noteworthy that A_ϕ was previously omitted from calculations as constant phase offset should not affect the PA behavior. Figure 39 represents the block diagram for the PD equation described above with $D = 2$.

Adaptation of the a_{kd} coefficients is first accomplished through wideband PD. As such, an LMS algorithm is able to optimize the indirect learning architecture shown in Figure 40. The DPD blocks shown in the architecture are duplicates of one another, the second is used as a training block for the first. The delay, although unimportant in simulations, is critical in a real-world implementation as the analog delay in the signal path must be accounted for to accurately perform sample-by-sample adjustments in

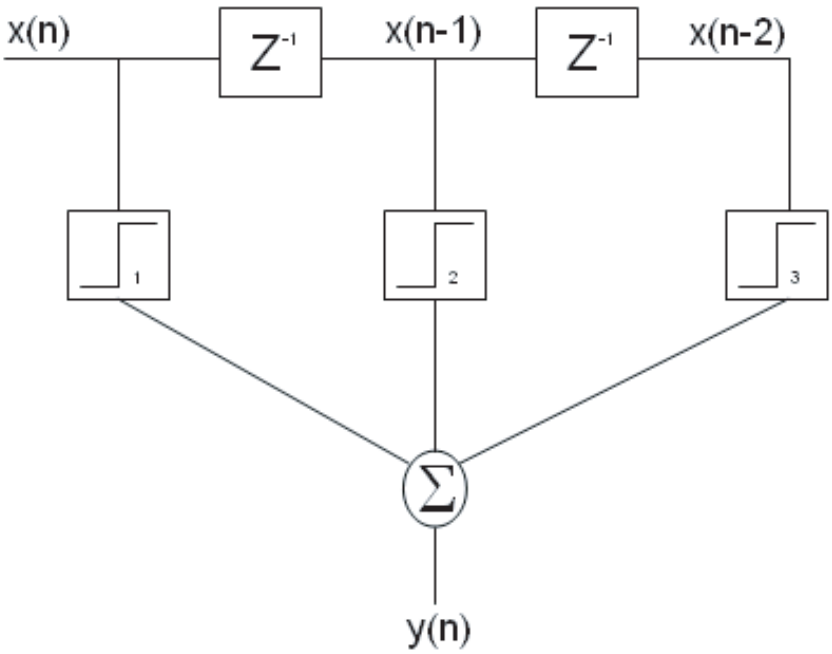

Figure 39: Block diagram for memory PD with D=2.

the PD coefficients. The mean-squared error is used determine the effectiveness of the PD coefficients.

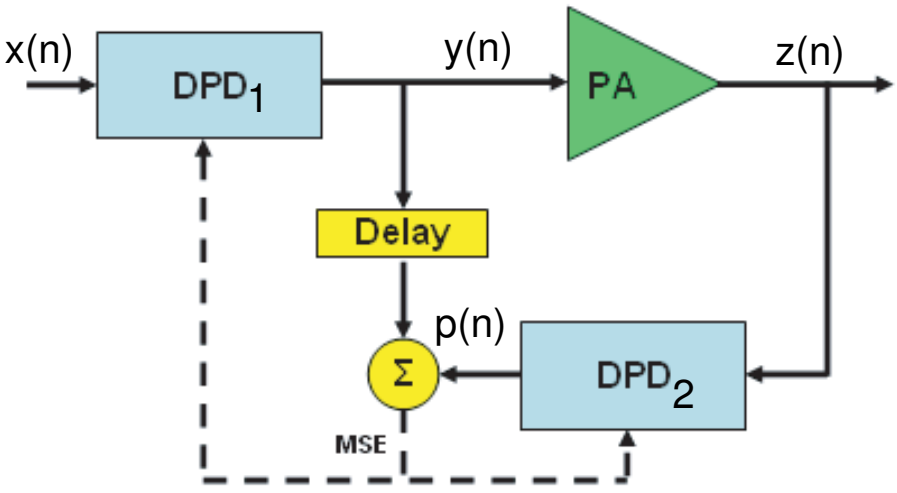

Figure 40: Indirect learning architecture.

Given that all PA and PD gains are normalized, $v_{kd}(n)$ can be defined as follows

$$v_{kd}(n) = z(n-d)|z(n-d)|^{k-1} \tag{49}$$

we further define

$$\begin{aligned}
\mathbf{a} &= [a_{10}, \cdots, a_{K0}, \cdots, a_{1D}, \cdots, a_{KD}]^T \\
\mathbf{u}_{kd} &= [v_{kd}(0), \cdots, v_{kd}(N-1)]^T \\
\mathbf{V} &= [\mathbf{u}_{10}, \cdots, \mathbf{u}_{K0}, \cdots, \mathbf{u}_{1D}, \cdots, \mathbf{u}_{KD}] \\
\mathbf{y} &= [y(0), \cdots, y(N-1)]^T
\end{aligned}$$

As the mean-squared error decreases, $y(n) \simeq p(n)$ the latter being the output of the training PD block. When the algorithm converges, Equation 50 should hold true.

$$\mathbf{y} = \mathbf{V}\mathbf{a} \tag{50}$$

Finally, the LMS solution for the previous equation is described by Equation 51 where ς is used to ensure the stability of the adaptation.

$$\hat{\mathbf{a}} = (\mathbf{V} \cdot \mathbf{V}' + \varsigma \cdot \mathbf{I})^{-1} \cdot \mathbf{V}' \cdot \mathbf{y} \tag{51}$$

The LMS wideband algorithm is applied to a PA model that resembles the memory polynomial pre-distorter. The PA model will be restricted in the number of taps and the order of the polynomials used. In the software implementation of the algorithm, the output of the PA is described by Equation 52. The coefficients of the PA model are represented by b_{kd} while $K = 5$ and $D = 1$; therefore, the PA model is a 5th order model with a single memory delay tap. The coefficients of the PA model are listed in Equation 53.

$$z(n) = \sum_{k_{odd}=1}^{K} \sum_{d=0}^{D} b_{kd} \cdot y(n-d)|y(n-d)|^{k-1} \tag{52}$$

$$\begin{bmatrix}
b_{10} & = & 1.0 + 0i & b_{11} & = & 0 - 0.2i \\
b_{30} & = & -0.2 - 0.2i & b_{31} & = & 0.3 + 0.1i \\
b_{50} & = & -0.1 - 0.1i & b_{51} & = & 0.25 + 0.01i
\end{bmatrix} \tag{53}$$

The memoryless AM-AM and AM-PM characteristics of the PA model are estimated in Figures 41(a) and 41(b), respectively.

To achieve optimal results, the order of the PD polynomials is selected to be greater than the PA model being pre-distorted, or $K_{PD} = K_{PA} + 1$. They are also selected to have more taps than the PA model, or $D_{PD} = D_{PA} + 1$. The PD polynomial order could be greater than that indicated above; the inclusion of additional terms only proves to increase the computational complexity of the algorithm with little performance improvements. The work done in [51] indicates that added performance is achieved by including even ordered terms as well. The added even ordered coefficients are not considered here. The purpose of this work is not intended to determine the optimal PD configuration, it will instead demonstrate that similar performance for a given configuration is achievable with a more cost effective hardware implementation. One distinct advantage of using wideband feedback and an LMS type algorithm is that the coefficients of a_{kd} are all solved simultaneously. The simultaneous processing of coefficients does not guarantee that the ideal PD solution will be determined, only that the time of convergence is optimal. It is interesting to observe the performance of the LMS algorithm while varying D_{PD}. This analysis demonstrates the added improvement for each additional tap and PD polynomial in Figure 42(a) for $D_{PD} = 0$, Figure 42(b) for $D_{PD} = 1$, Figure 43(a) for $D_{PD} = 2$, and Figure 43(b) for $D_{PD} = 3$.

The solution is optimized when using a tap delay of $D_{PD} = 2$ for wideband feedback and an LMS algorithm as shown in Figure 43(a). This figure indicates an ACP3L improvement of approximately 24dB while the ACP3H improvement is approximately 23dB. Typical performance is defined by the worst-case result, consequently the actual ACP improvement from 40dBc to 62dBc gives a net improvement of 22dB. The results are summarized in Table 11 where the improvement is described relative to the original ACP levels. It can be observed that results for the memoryless case

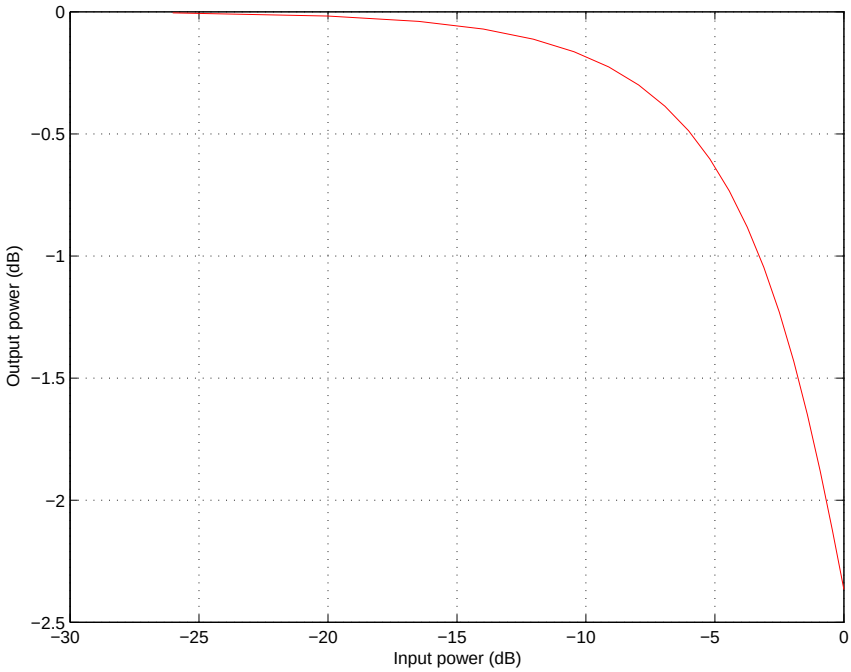

(a) Memoryless AM-AM Characteristic Curve for the PA model.

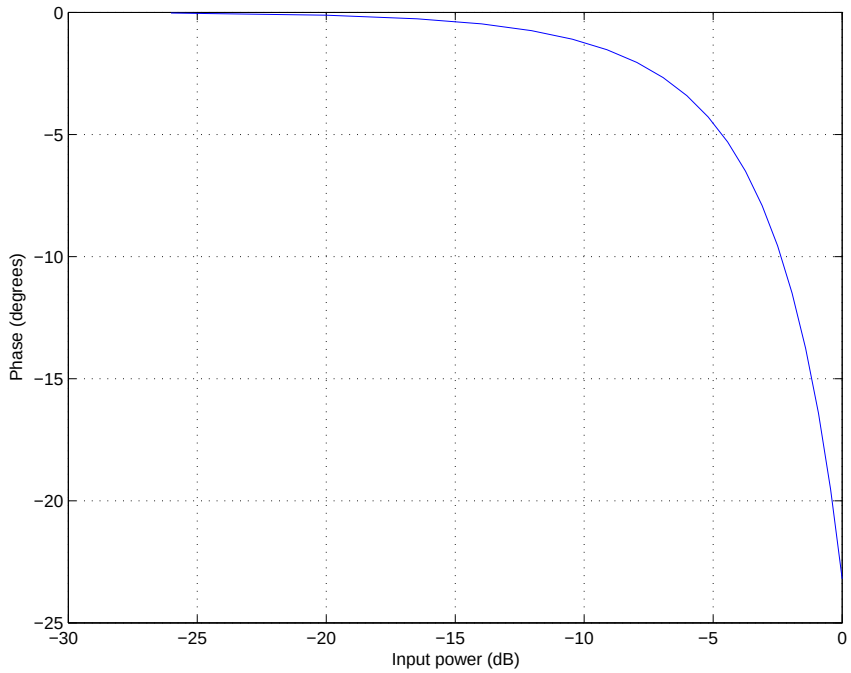

(b) Memoryless AM-PM Characteristic Curve for the PA model.

Figure 41: Characteristic Curves for the memory PA model.

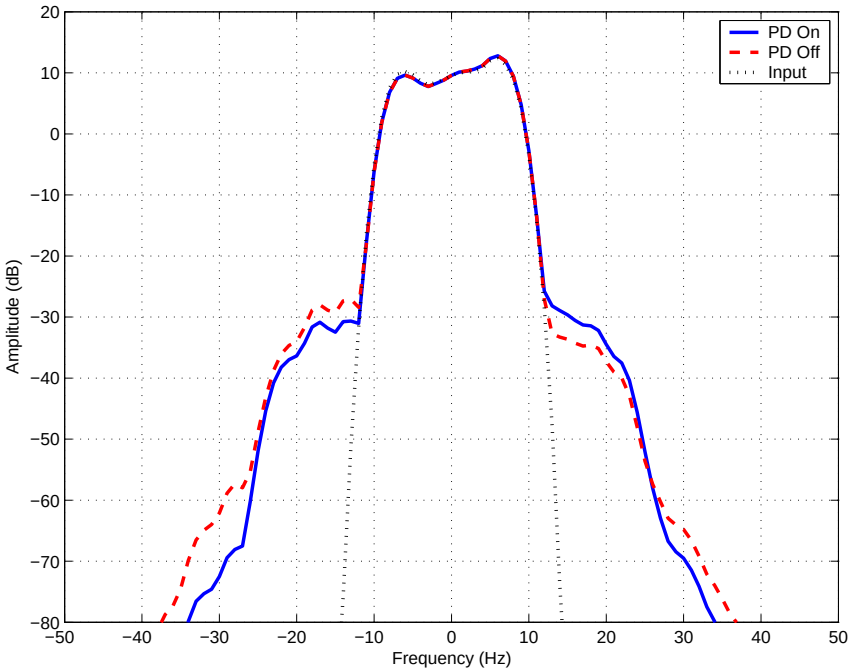

(a) Wideband PD using LMS algorithm and $D_{PD} = 0$.

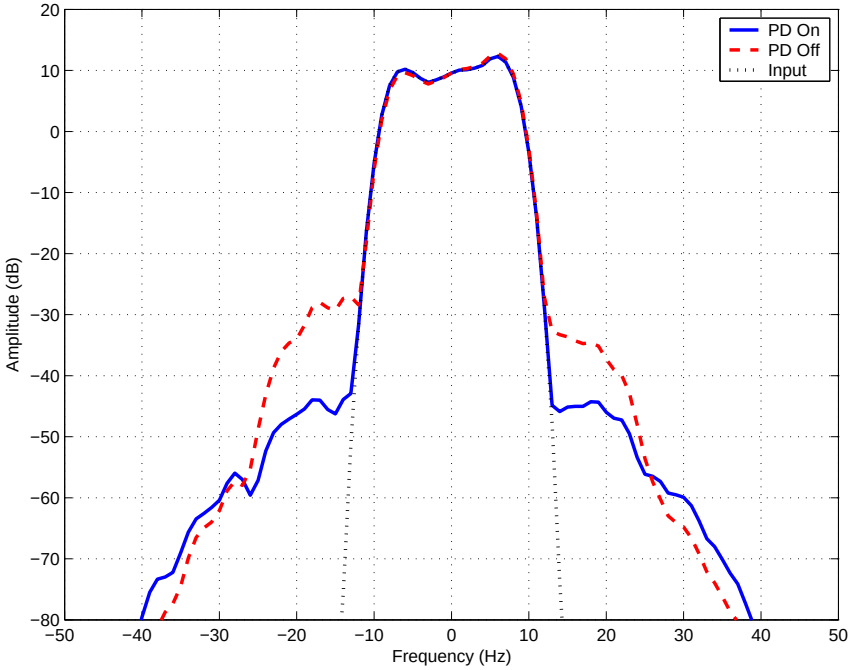

(b) Wideband PD using LMS algorithm and $D_{PD} = 1$.

Figure 42: Spectral output of wideband PD using LMS algorithm.

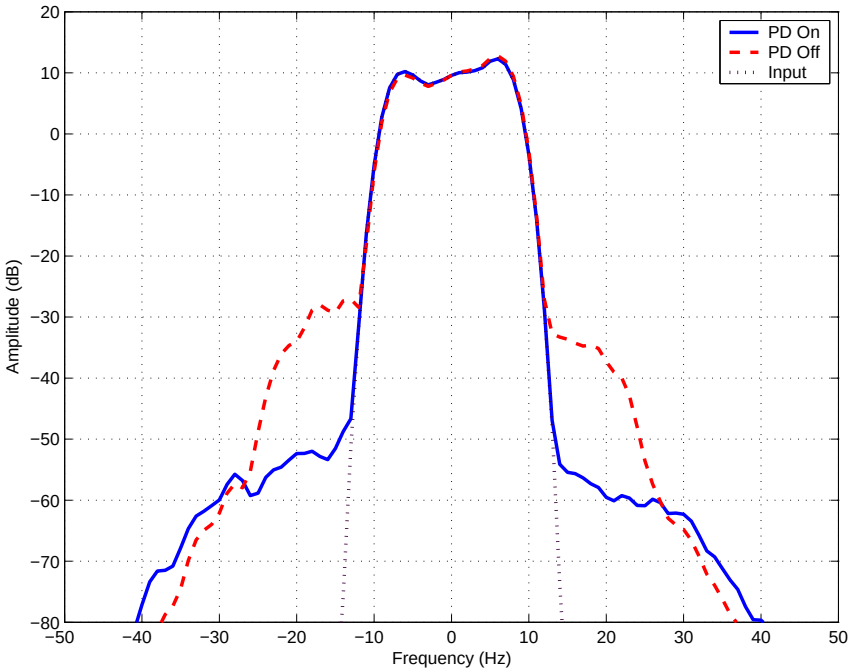

(a) Wideband PD using LMS algorithm and $D_{PD} = 2$.

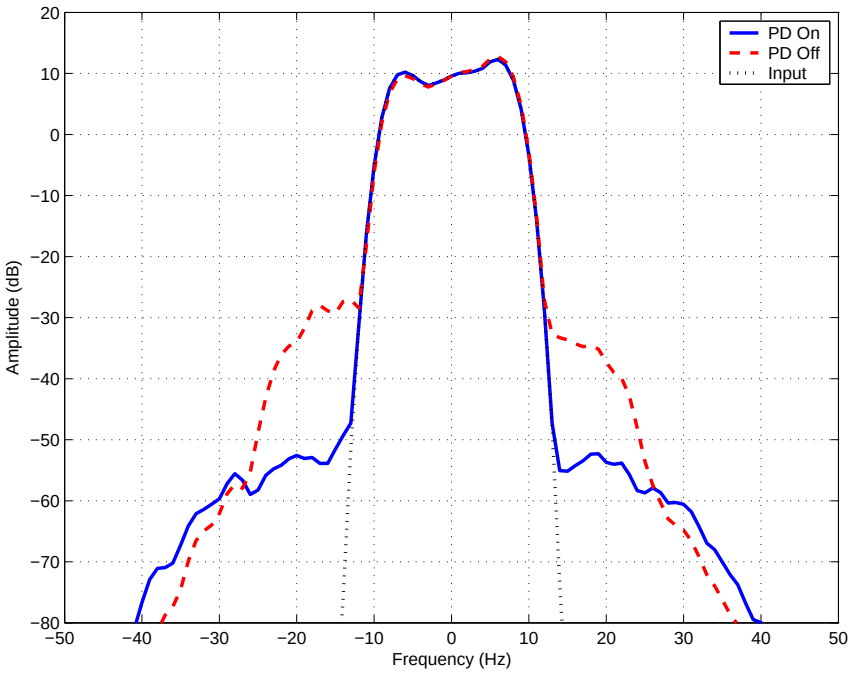

(b) Wideband PD using LMS algorithm and $D_{PD} = 3$.

Figure 43: Spectral output of wideband PD using LMS algorithm. (cont.)

where $D_{PD} = 0$ are not significant, and for $D_{PD} = 3$ the results are worse than those obtained for $D_{PD} = 2$.

Table 11: ACP performance of wideband PD using LMS algorithm.

D_{PD}	**ACP3L**	**ACP3H**
0	-3dB	3dB
1	-15dB	-11dB
2	-24dB	-23dB
3	-24dB	-20dB

Finally, the optimal coefficients determined using wideband feedback and an LMS algorithm are shown in 54 for a tap delay of $D_{PD} = 2$. The following section describes the GA implementation of the memory PD polynomial.

$$\begin{bmatrix} a_{10} = 1.0099 - 0.0064i & a_{11} = -0.0198 + 0.2193i & a_{12} = -0.0276 - 0.0225i \\ a_{30} = 0.1570 + 0.2603i & a_{31} = -0.3381 - 0.2182i & a_{32} = 0.0667 - 0.0252i \\ a_{50} = -0.0403 + 0.0287i & a_{51} = -0.0990 - 0.1127i & a_{52} = 0.0692 + 0.0481i \\ a_{70} = -0.0231 - 0.0025i & a_{71} = -0.0226 - 0.0356i & a_{72} = 0.0266 + 0.0224i \end{bmatrix} \tag{54}$$

6.3 Memory Polynomial and Sequential Narrowband Pre-Distortion

It was shown that the GA, although effective at linearizing memoryless PAs, did not achieve significant performance on a PA with memory effects. Generally, only limited linearization results can be achieved with a memoryless pre-distorter [21]. To meet performance requirements already achieved by conventional linearization approaches, the algorithm was modified to include memory polynomials [59]. The application of the memory polynomials with the GA is computationally identical to the LMS algorithm described in the previous section.

The optimal solution for memoryless PD was determined through the optimization

of a specific cost function. For the memory GA, the cost function is now a measure of the linear power of IMD3L and IMD3H relative to the fundamental linear power or IMD1, as illustrated in Figure 44 and defined by Equation 42 from [Chapter 4]. While the LMS algorithm adapts all 12 of the complex coefficients simultaneously ($a_{10}...a_{73}$), similar adaptation of 3 polynomials ($D_{PD} = 2$) with the GA is ineffective at reducing ACP levels without prior definition of a narrow search space. Regardless of search space definition, the ACP improvement was insignificant compared to the LMS implementation. In the memory GA, the search spaces must adapt sequentially to maintain the overall stability of the algorithm. The algorithm was therefore parameterized to sequentially optimize the 3 polynomial sets.

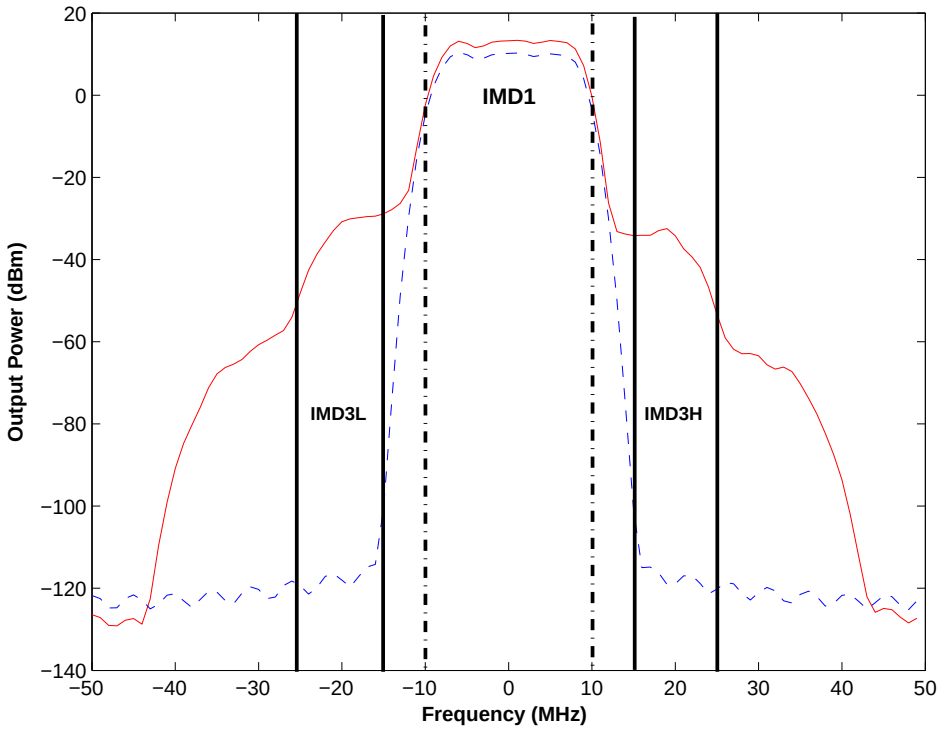

Figure 44: Cost function for the GA.

The sequential adaptation of the memory GA is summarized by the following steps:

1. Characterize approximate P_{1dB} of the amplifier using two-tone test.

2. Optimize coefficients of $P_0(n)$.

   (a) Define search space from P_{1dB} calculations.

   (b) Iterate the 4 complex coefficients.

   (c) Stop if ACP levels are constant.

3. Optimize coefficients of $P_0(n)$ and $P_1(n-1)$.

   (a) Define narrow search space for $P_0(n)$.

   (b) Define search space for $P_1(n-1)$.

   (c) Iterate the 8 complex coefficients.

   (d) Stop if ACP levels are constant.

4. Optimize coefficients of $P_0(n)$, $P_1(n-1)$ and $P_2(n-2)$.

   (a) Define narrow search space for $P_0(n)$.

   (b) Define narrow search space for $P_1(n-1)$.

   (c) Define search space for $P_2(n-2)$.

   (d) Iterate the 12 complex coefficients.

   (e) Stop if ACP levels are constant.

The convergence profile of polynomial PD using the sequential genetic algorithm is shown in Figure 51. For each iteration, the average and best GA solutions are shown along with the minimum attainable performance as defined by the noise floor of the system. Each process is permitted to optimize over a maximum of 20 iterations; however, if the improvement remains constant for multiple iterations the algorithm proceeds to the following step. The PA characterization including P_{1dB} determination are completed in STEP 1 and are not shown in the convergence profile. The results indicate an ACPR improvement of 13dB from the 1st polynomial adaptation, 2dB

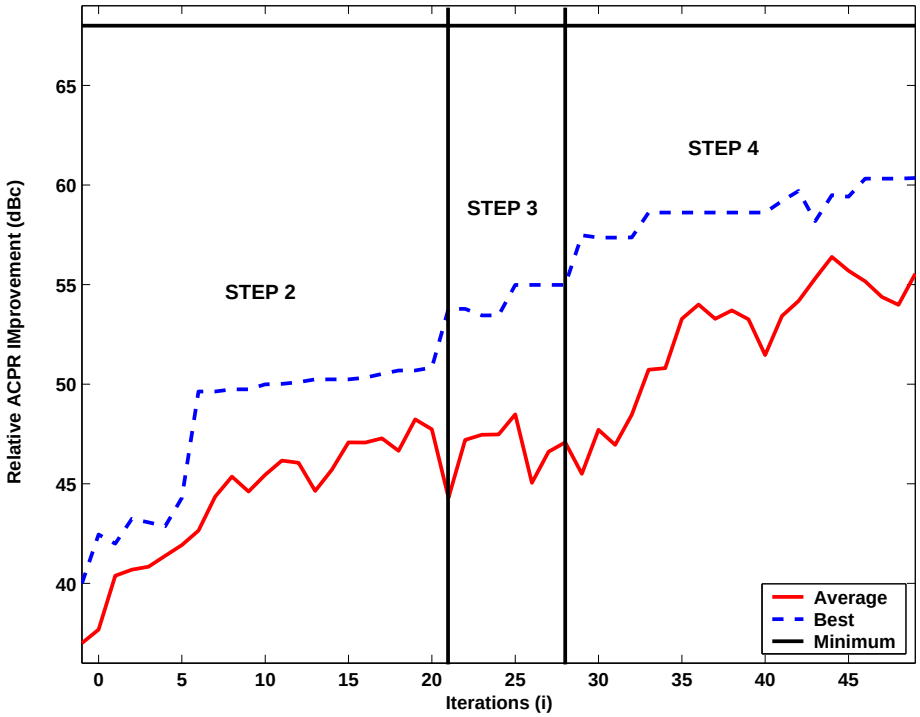

Figure 45: Convergence profile for the sequential GA.

improvement with the inclusion of the 2nd polynomial and 5dB of improvement with the inclusion of the 3rd polynomial. The profile also indicates a trend that would seem to suggest further improvement is possible with the addition of a 4th polynomial.

The GAs sequential linearization performance is illustrated for each additional tap and PD polynomial in Figure 46(a) for $D_{PD} = 0$, Figure 46(b) for $D_{PD} = 1$, and Figure 46(c) for $D_{PD} = 2$. The results using narrowband GA show an ACLR of 40dBc to 60dBc for a net improvement of 20dB, indicating a performance comparable to that of the wideband LMS algorithm.

For the memoryless case, where $D_{PD} = 0$, the initial characterization of the PA model and subsequent adaptation of the PD polynomial show significant ACP improvement contrary to what was observed with wideband feedback and the LMS algorithm. The results are summarized in Table 12 where the improvement is described relative to the original ACP levels.

Finally, the optimal coefficients determined using narrowband feedback and the

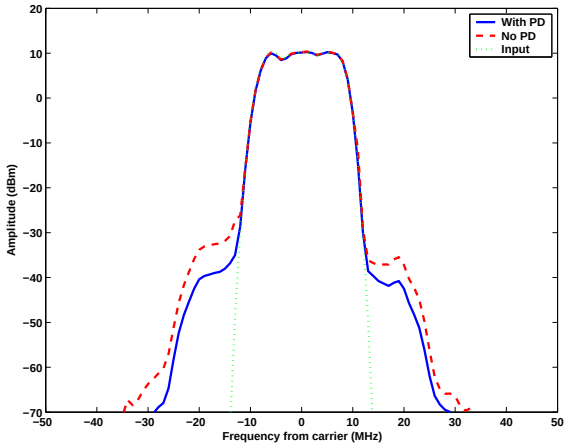

(a) Narrowband PD using the GA and $D_{PD} = 0$.

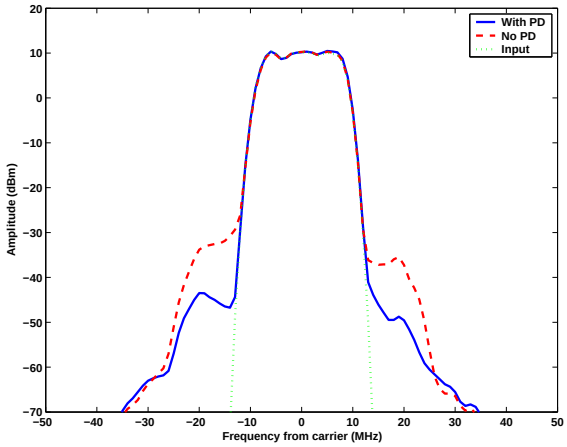

(b) Narrowband PD using the GA and $D_{PD} = 1$.

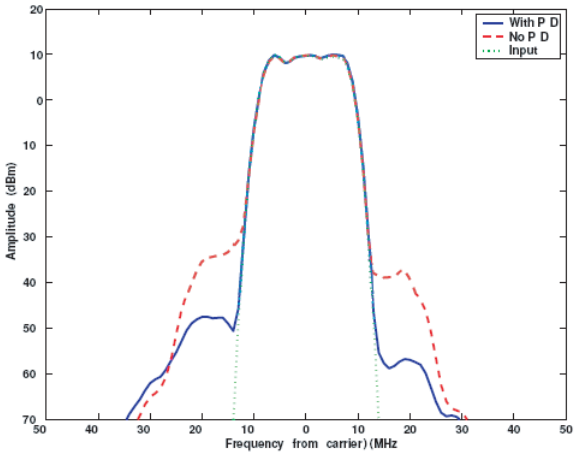

(c) Narrowband PD using the GA and $D_{PD} = 2$.

Figure 46: Spectral output of narrowband PD using the GA.

Table 12: ACP performance of narrowband PD using the GA.

D_{PD}	**ACP3L**	**ACP3H**
0	-8dB	-5dB
1	-15dB	-11dB
2	-24dB	-23dB

GA are shown in 55 for a tap delay of $D_{PD} = 2$. The following section describes the hardware that is assembled to verify performance of the GA as applied to "real-world" PAs.

$$\begin{bmatrix} a_{10} = 0.9482 + 0.0613i & a_{11} = -0.2597 + 0.0165i & a_{12} = 0.0090 + 0.0108i \\ a_{30} = 0.0220 + 0.0197i & a_{31} = -0.0480 - 0.0236i & a_{32} = 0.0230 + 0.0075i \\ a_{50} = 0.0078 + 0.0145i & a_{51} = -0.1630 - 0.2699i & a_{52} = 0.0183 - 0.1876i \\ a_{70} = 0.1543 + 0.0468i & a_{71} = 0.0379 + 0.7060i & a_{72} = -0.0575 + 0.4521i \end{bmatrix} \tag{55}$$

6.4 System Architecture for Wideband Pre-Distortion

The implementation of a LUT-based pre-distortion system was shown in Chapter 4. Although effective at correcting for memoryless non-linearities, the platform was unable to accurately correct the PA memory effects. Consequently, the implementation of this system was only able to guarantee minimal performance improvements. The research efforts now demand the need for a test platform capable of evaluating the performance of a pre-distortion algorithm that includes the implementation of the memory polynomial described in the previous sections. A typical hardware architecture is configured to give 60MHz of feedback bandwidth. Including 3rd and 5th order intermodulation products, the transmitted signal is capable of reaching bandwidths of up to 1/5th of the feedback bandwidth which in this case is 12.5MHz. The system architecture is designed to accommodate feedback bandwidths of up to 100MHz; however, this would require a second ADC in the feedback path and is not the focus

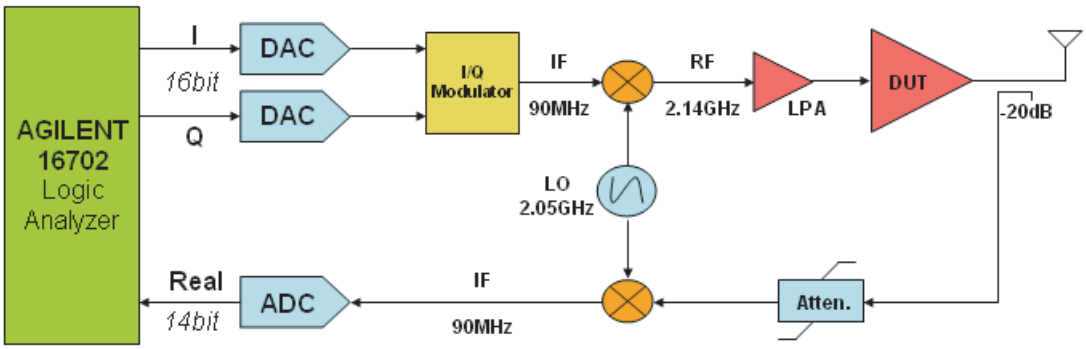

Figure 47: Block Diagram of Wideband Pre-Distortion System.

of this work. The new algorithm evaluation platform is also used to implement a Texas Instruments Corporation (TI) proprietary algorithm which requires wideband feedback. A simplified version of the initial platform is shown in Figure 47.

The application of DPD to the transmitted signal is done within the Matlab environment. The pre-distorted signal is then uploaded to an Agilent l6702-Logic Analyzer with pattern generation capabilities. The complex digital signal is converted to the analog domain through a dual-DAC up to a 92.16MHz intermediate frequency (IF). The signal is filtered, and modulated up to a 2.14GHz frequency. The test platform incorporates a digitally controlled step-attenuator to regulate the RF transmit power. A duplicate device is used to control the RF receive power to maintain optimal performance of the feedback path. The transmit and receive power is measured through dual power meters. The board also includes a switch at the output of the transmit chain. This is used as a PA protection device designed to cut-off the RF transit power. The protection feature is designed to reduce the risk of applying excessive power levels to the PA, thus preventing the damage or destruction of these expensive devices. The receive chain includes an analog mixer to reduce the RF signal back to the 92.16MHz IF frequency. The signal is amplified, filtered and digitized. The digital signal is captured with the logic analyzer and the data is downloaded to

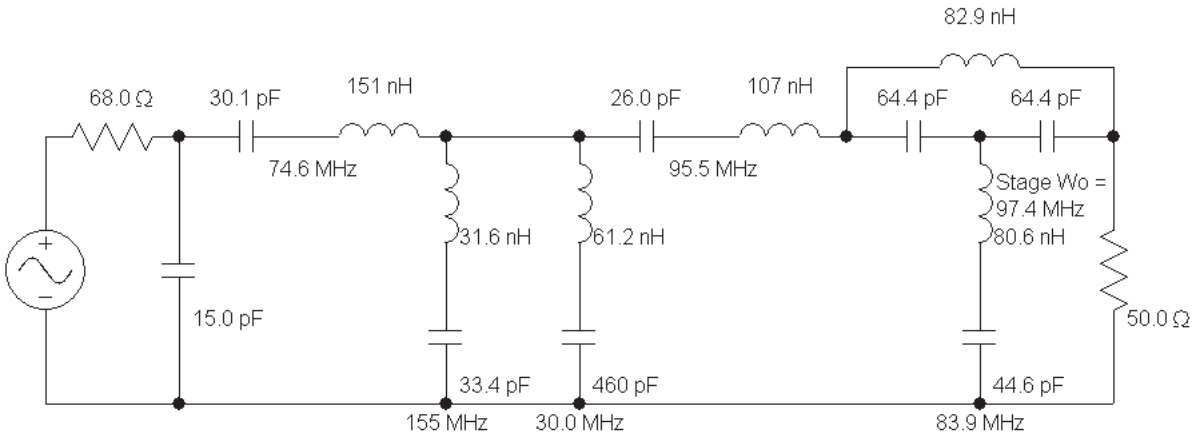

Figure 48: Schematic design for the 90MHz bandbass filter.

the Matlab environment for signal processing. The platform is optimized for UMTS signal encoding. A full frame of UMTS data is 1.2288Msamples while the bandwidth of a single UMTS carrier is 3.84MHz. The carrier spacing, or occupied bandwidth, for the test signal is approximately 5MHz. Consequently, the data converters in the transmit and receive data path are clocked at a frequency of 122.88MHz. The detailed block diagram for this system implementation is shown in Figure 47, and illustrated in Appendix C.

The detailed diagram illustrates the use of a custom analog filter between the mixer and ADC in the feedback path. The filter requires good stop band attenuation to eliminate mixer products while the passband requires a constant phase delay, or a group delay of less than 3ns; as such, a custom filter design was required for this application. The schematics for this filter design are illustrated in Figure 48, the simulated spectral data and group delay performance are also included in Figure 49; finally, the measured filter performance was similar to the simulated results.

For wideband feedback, the input and output data must be time aligned to apply accurate DPD on a sample by sample basis. The digital and analog delay can be determined by applying the cross-correlation of a signal with itself, the result is the

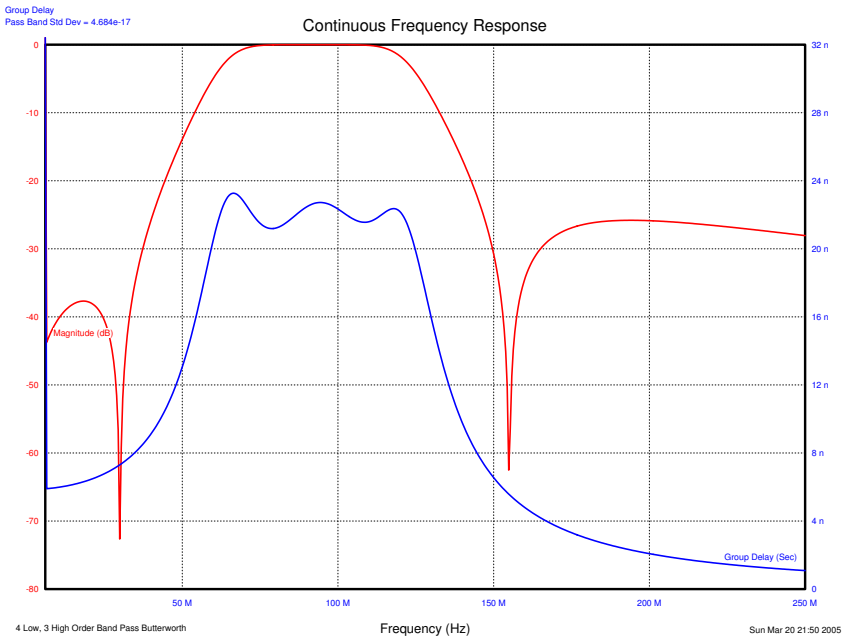

Figure 49: Spectral and group delay performance of the 90MHz bandpass filter.

autocorrelation of the signal which can be represented by Equation 56 and Equation 57. The delay is assumed to remain constant throughout the PA linearization process.

$$\hat{r}_x(l) \triangleq \frac{1}{N}(x \star x)(l) \triangleq \frac{1}{N}\sum_{n=0}^{N-1} \overline{x(n)}x(n+l) \tag{56}$$

The autocorrelation function is Hermitian:

$$\hat{r}_x(-l) = \overline{\hat{r}_x(l)} \tag{57}$$

The above platform illustrates the complexity and accuracy required to achieve optimal linearization performance with wideband feedback. These results further support the development of a narrowband feedback algorithm that is not bounded by strict design specifications.

6.5 Sequential Memory Pre-Distortion using the Genetic Algorithm

The original Volterra series model is often used to represent memoryless PAs with nonlinearities [54]. However, when including memory effects, the added complexity of this model outweighs its usefulness. The work presented here assumes that the actual PA can be accurately represented by a pseudo-Volterra based model [60]. The PD linearization architecture is implemented by cascading the inverse Volterra model with the PA. It is shown through experimentation that the inverse system, for the PAs described in this section, requires three cascaded 4th order polynomials each separated by a variable-tap delay, as shown in Figure 50.

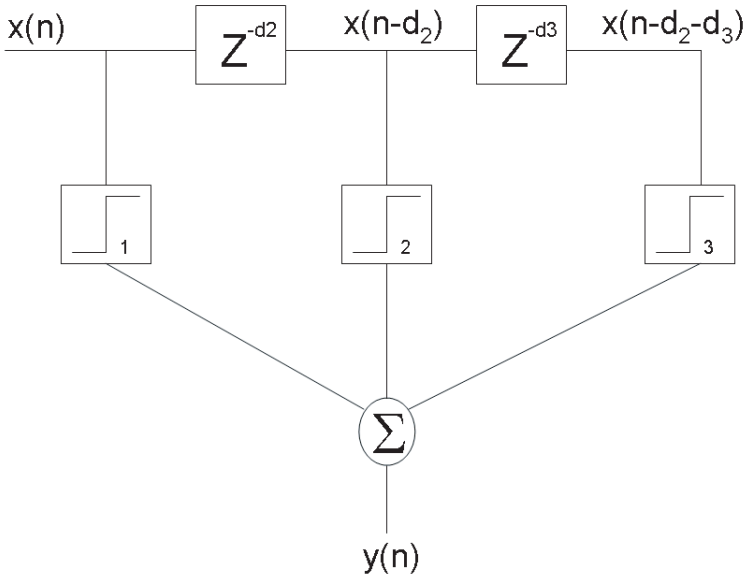

Figure 50: Pre-distortion block diagram.

The general form of the polynomials used to linearize the PA are expressed in Equation 58, where d represents the delay at the input to the summing node. The coefficients described below are complex to include both amplitude and phase information. The input to the PA can be expressed as the sum of the delayed polynomials as shown in Equation 59. Although this truncated polynomial model is only an

approximation, considerable results are achieved through this type of PD implementation.

$$f_d(x(n)) = A_d x(n-d) + B_d x(n-d)x|n-d|^2 + C_d x(n-d)x|n-d|^4 + D_d x(n-d)x|n-d|^6 \quad (58)$$

$$y(n) = f_1(x(n-d_1)) + f_2(x(n-d_2)) + f_3(x(n-d_3)) \quad (59)$$

The application of the memory polynomials, described by Equations 58 and 59, is shown in Figure 50. The GA application of these PD polynomials is similar to that implemented using wideband feedback and an LMS algorithm. However, the LMS algorithm adapts all 12 of the complex coefficients simultaneously. Previous work indicated that similar adaptation of 3 polynomials with the GA was ineffective at reducing ACP levels. As described earlier, the GA adaptation of the polynomials and their individual bounding functions is accomplished in a sequential manner to maintain stability and performance.

The sequential adaptation of the memory GA is summarized by the following steps:

1. Characterize approximate P_{1dB} of the amplifier using two-tone compression test.
2. Determine Output Power $IM1_{woPD}$ and Initial ACP levels.
   (a) Define search space for $P_1(n-d_1)$.
   (b) Iterate the 4 complex coefficients.
   (c) Stop at i iterations or if ACP is minimized.
3. Optimize coefficients of $P_1(n-d_1)$ and $P_2(n-d_2)$.
   (a) Define narrow search space for $P_1(n-d_1)$.

(b) Define search space for $P_2(n - d_2)$.

(c) Iterate the 8 complex coefficients.

(d) Stop at i iterations or if ACP is minimized.

4. Optimize coefficients of $P_1(n - d_1)$, $P_2(n - d_2)$ and $P_3(n - d_3)$.

(a) Define narrow search space for $P_1(n - d_1)$.

(b) Define narrow search space for $P_2(n - d_2)$.

(c) Define search space for $P_3(n - d_3)$.

(d) Iterate the 12 complex coefficients.

(e) Stop at i iterations or if ACP is minimized.

The hardware implementation described in the previous section is now used to evaluate the performance of the memory polynomial GA. The local oscillator (LO) frequency of 2.05GHz results in a transmission frequency of approximately 2.14GHz. A Stealth Microwave SL0825-40 5W laboratory PA is used to drive the device under test (DUT). In this implementation, the DUT is a two-stage PA. The first stage is a CREE Microwave UPF21010 10W amplifier, while the second is a CREE UGF21090 90W amplifier [46].

Although the hardware is designed for wideband PD, the GA requires only narrowband information. It is convenient to test multiple PD solutions, using only narrowband information, with a single frame of data to minimize the total simulation and adaptation time. The performance of individual population members for this implementation is dependant on the average power of each member. To accurately compare the fitness of the N individual population members, the average power (mean square) of each PD member is normalized to the average power of the original input of data $x(n)$, as defined in Equation 60 where F is the number of samples in the frame of data and P is the number of samples for a given population member,

(or $P = F/N$). These conditions help ensure the PA average output power remains constant for a given iteration.

$$\frac{1}{P}\sum_{n=1}^{P}|y(n)|^2 \equiv \frac{1}{F}\sum_{n=1}^{F}|x(n)|^2 \tag{60}$$

The adaptation of the GA is critically dependant on the cost function that indicates the viability or *fitness* of each individual PD solution. For the hardware implementation of the sequential memory GA, the cost function is a measure of the linear power of IM3L and IM3H relative to the fundamental linear power or IM1, as defined in Section 6.3. In actual implementation, certain population members provide solutions with decreased fundamental output power or IMD1, this precipitates the need for cost function modification. First, the fundamental output power for an ideal amplifier is determined. Second, the measured IMD1 output power is compared to the ideal output power. Finally, the fitness of the population members is adversely affected for measured values that are below the expected ideal value. The fitness f of the individual population members is now defined by Equations 61 and 62.

For $IMD1_{Measured} \geq IMD1_{Ideal}$,

$$f = 10^{(IM1-IM3L)/20} + 10^{(IM1-IM3H)/20} \tag{61}$$

while $IMD1_{Measured} < IMD1_{Ideal}$

$$f = 10^{(IM1-IM3L)/20} + 10^{(IM1-IM3H)/20} + \Theta \cdot 10^{(IM1_{Measured}-IM1_{Ideal})/20} \tag{62}$$

where Θ defines an experimentally determined weighting value.

The convergence profile of polynomial PD using the sequential genetic algorithm is shown in Figure 51. For each iteration, the average and best IM3L/IM3H GA solutions are shown along with the minimum attainable performance as defined by the noise floor of the system. Each process is permitted to optimize over 20 iterations. The PA characterization including P_{1dB} determination is completed in STEP 1 and indicates an initial IM3L of approximately 37dBm and an IM3H of approximately

38dBm. The software control interface for the algorithm is illustrated in Appendix C. It is important to note that the progress results are measured from the individual PD solutions contained in a frame and as such, are only an approximation. The optimal solutions are validated over the entire frame of data after the completion of each step described above. These actual ACP optimization results are summarized in Table 13 and the sequential linearization performance is illustrated in Figure 52.

Table 13: Genetic Algorithm Optimization Results

Step	ACP3L	ACP3H
1	33dBc	34dBc
2	42.5dBc	44.5dBc
3	46dBc	49dBc
4	51dBc	50dBc
Total	18dB	16dB

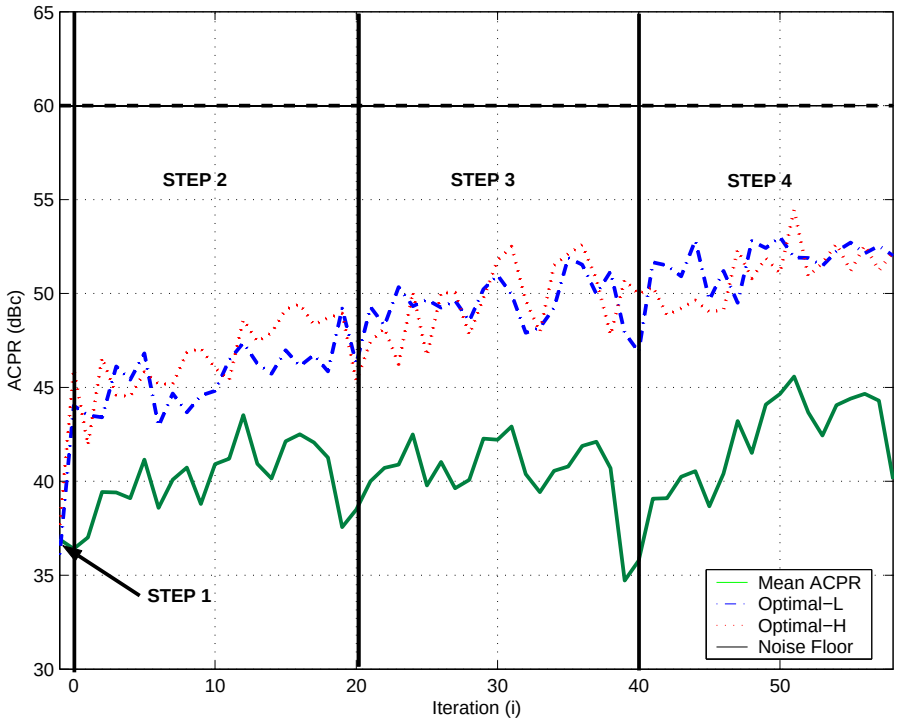

Figure 51: Convergence Profile for the Sequential GA.

The results indicate a total ACP3L improvement of 18dB, while the ACP3H showed a total improvement of 16dB. The tap delay lengths were experimentally

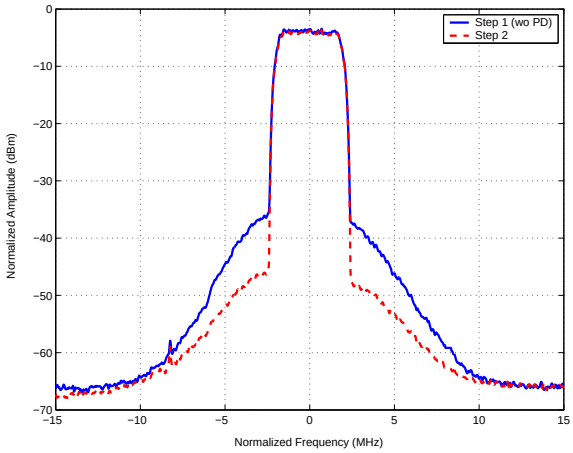

(a) Memoryless PA distortion compensation from P_1 adaptation.

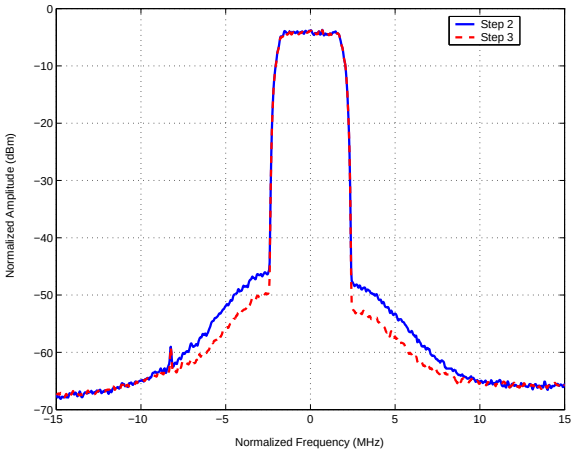

(b) Memory PD with 1st memory tap and P_2 adaptation.

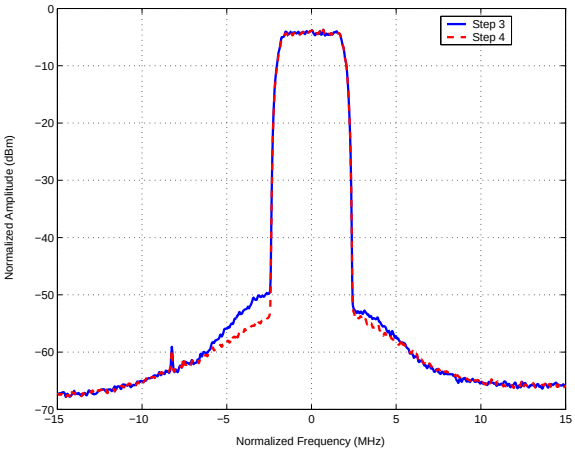

(c) Memory PD with additional taps and P_3 adaptation.

Figure 52: Sequential GA Linearization Performance.

optimized: the first polynomial was used to remove memoryless distortion, thus the delay was 0, a delay of 1 for the second polynomial (or first memory polynomial) and a delay of 4 for the third polynomial (second memory polynomial). The output clock rate of the DAC was 122.88MHz thus a single tap delay is equal to an analog delay of 8.138ns. The profile also indicates a trend that would seem to suggest further improvement is possible with the addition of possibly a 4th polynomial. This concept was not supported by hardware results or software simulations. The additional polynomial adds more degrees of uncertainty, and performance of the algorithm degrades as it did with wideband feedback. The longest pre-distortion polynomial delay is 4*8.138ns or approximately 32.6ns which implies correction is specifically applied to frequency memory effects.

6.6 Sequential Memory Pre-Distortion, Crest Factor Reduction, and the Genetic Algorithm

In the previous section, linearization was applied to the PA module without initially reducing the PAR of the input signal. Previous work had also shown that the combination of an LMS algorithm with CFR yielded greater improvements than the sum of their individual improvements. The purpose of this work is also to determine the effect of applying CFR to the input signal on the GA linearization performance with memory effects. The test platform is now optimized for 2-UMTS carriers thus the total occupied signal bandwidth is 10MHz. In this section, the work is applied to a high efficiency Doherty amplifier. Previous DPD and CFR efforts were applied to class A and AB amplifiers. The specific implementation of this type of PA is not the focus of this work; however, a simple block diagram illustrating the implementation of such a device is included in Figure 53. The drawback to using a Doherty PA is that this PA is not very linear and requires DPD to maintain acceptable levels of ACP. The theoretical efficiency that can be achieved by a Doherty amplifier is shown in Figure 54 as compared to a typical class B amplifier. In theory, efficiencies greater than 50% can be achieved; however, practical results have not shown efficiencies greater than 35%.

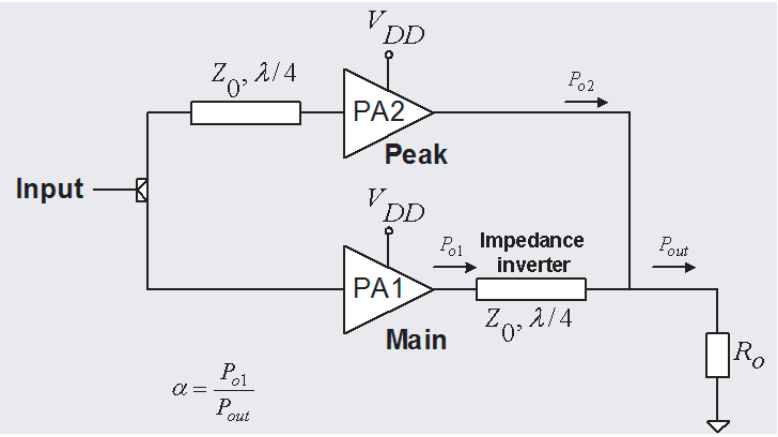

Figure 53: Doherty amplifier implementation.

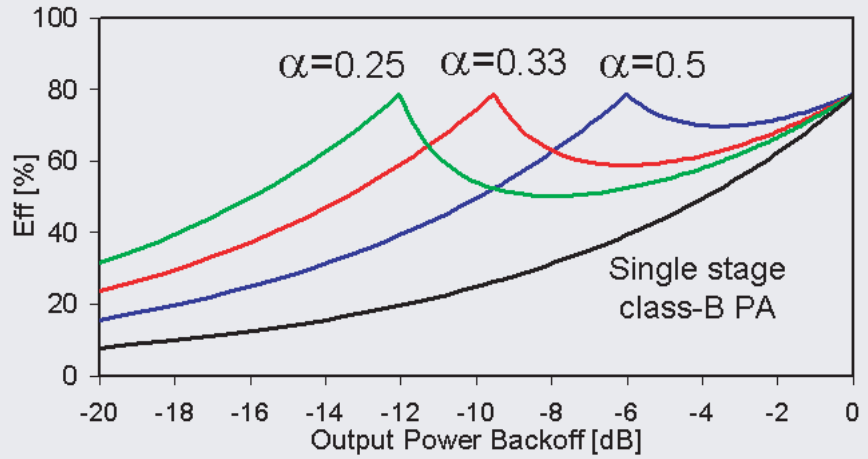

Figure 54: Efficiency of the Doherty amplifier versus a Class B amplifier.

The Doherty amplifier used in this research is a Bravo Tech Inc. 50W amplifier [53]. The amplifier requires a 28V DC supply with currents varying between 1.7A and 4A, depending on the input-output power levels. The system used to evaluate the performance of the GA was introduced in the previous chapter and has minor changes for this evaluation.

The GA with narrowband feedback was applied both with and without CFR. The adaptation coefficients were optimized for varying power levels, Figure 55 illustrates the performance of the algorithm.

The results for the narrowband feedback GA are summarized in Table 14 for an ACP level of 50dBc. These results are 5dB greater than the 3GPP specification of 45dBc. The results indicate that for a given ACP level, the GA was able to increase the output power by approximately 9.5dB. The efficiency was also increased by 24.8%. The considerable improvement is due, in part, to the biasing of the Doherty amplifier which is designed to operate at high efficiency in conjunction with a linearization technique.

The convergence profile of polynomial PD using the sequential genetic algorithm is shown in Figure 56. The results indicate linearization performance results using

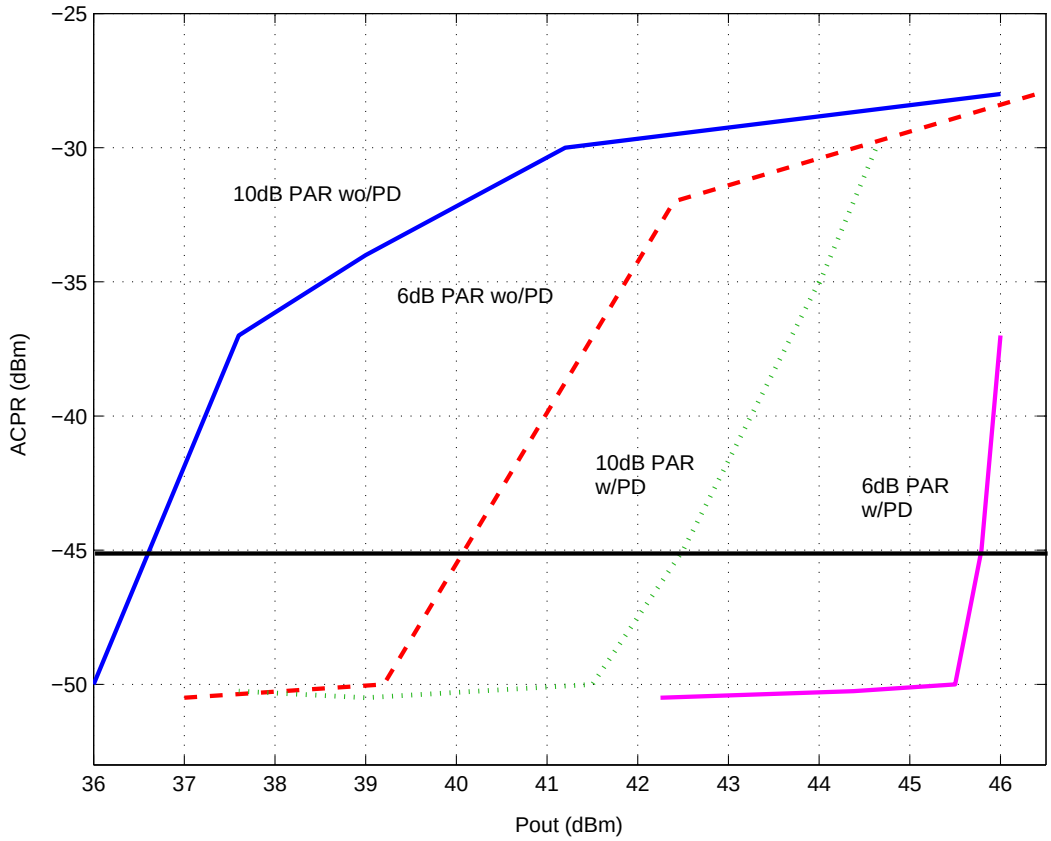

Figure 55: ACPR improvement with respect to output power.

Table 14: Power and efficiency improvement.

	With PD		Without PD	
PAR	10dB	6dB	10dB	6dB
Pout	41.5dBm	45.5dBm	36dBm	39.2dBm
Efficiency	18.6%	32.9%	8.1%	13.4%

a 10MHz bandwidth signal with a PAR of 6dB. The sequential linearization performance is illustrated in Figure 57. The convergence profile for the GA using an input signal of 10dB is shown in Figure 58 and the sequential linearization performance is illustrated in Figure 59.

The performance of the algorithm is limited by the linearity and dynamic range of the transmit and feedback paths. In all applications of linearization using this test platform, the optimal performance was limited to approximately 50dBc. As much as 8dB of additional improvement has been achieved using a TI proprietary linearization

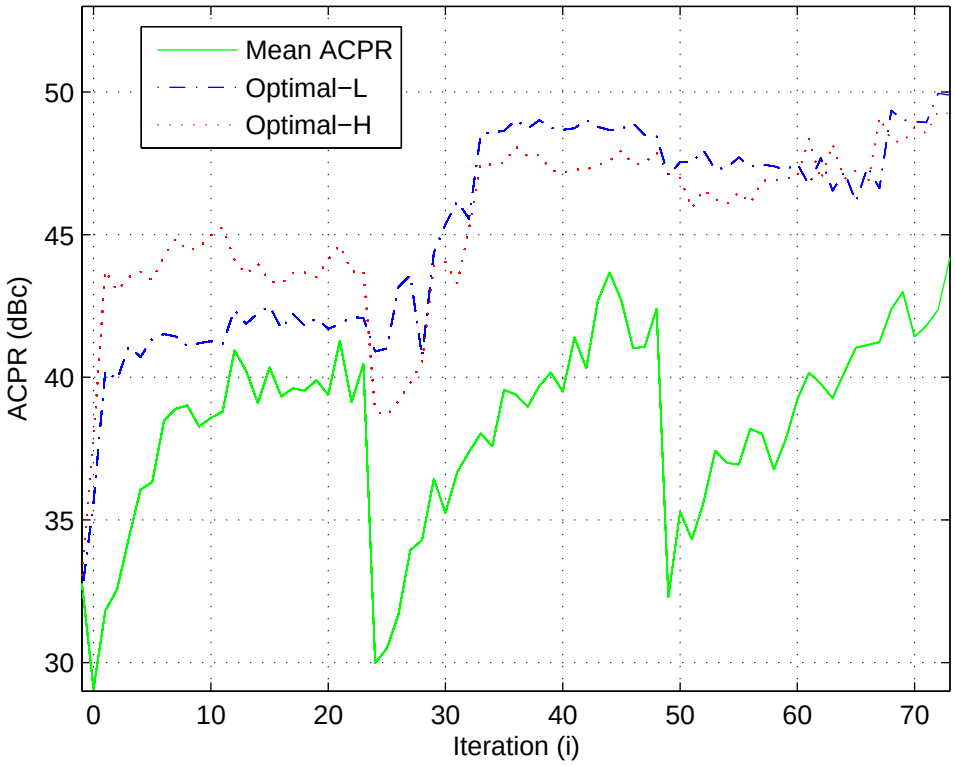

Figure 56: Convergence Profile for the Sequential GA with a 6dB PAR input signal.

technique prior to PD coefficient adaptation. The technique equalizes the signal chain correcting for memoryless nonlinearities and I/Q imbalance. The linear equalization technique is not applied to this work, and is subject to future research efforts. The optimized DPD coefficients for a PAR of 10db and 6dB are included in Equations 63 and 64, respectively.

$$\begin{bmatrix} a_{10} = 0.8640 + 0.3225i & a_{11} = 0.4463 + 0.0015i & a_{12} = -0.4758 + 0.1372i \\ a_{30} = -0.2436 + 0.2244i & a_{31} = -0.2270 + 0.3435i & a_{32} = 0.2366 - 0.1198i \\ a_{50} = 0.4401 + 0.2747i & a_{51} = 0.0984 + 0.1639i & a_{52} = -0.0625 + 0.1005i \\ a_{70} = -0.0361 + 0.4018i & a_{71} = 0.3285 - 0.3180i & a_{72} = -0.2905 - 0.0692i \end{bmatrix} \tag{63}$$

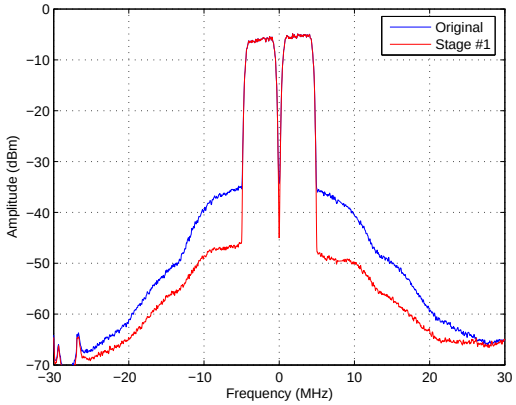

(a) Memoryless PA distortion compensation from P_1 adaptation.

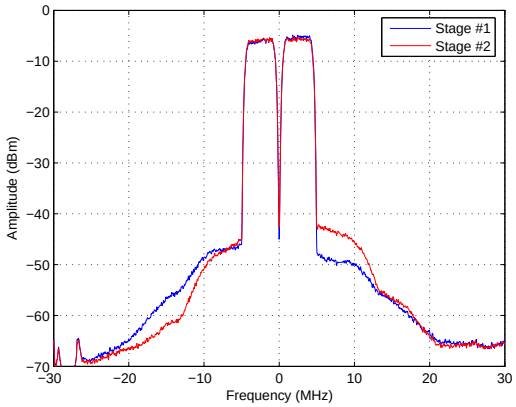

(b) Memory PD with 1st memory tap and P_2 adaptation.

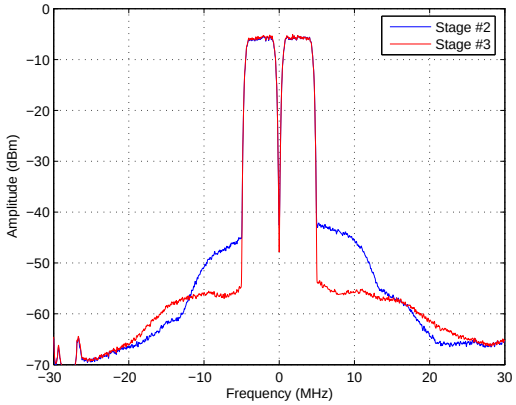

(c) Memory PD with additional taps and P_3 adaptation.

Figure 57: Sequential GA Linearization Performance with a 6dB PAR input signal.

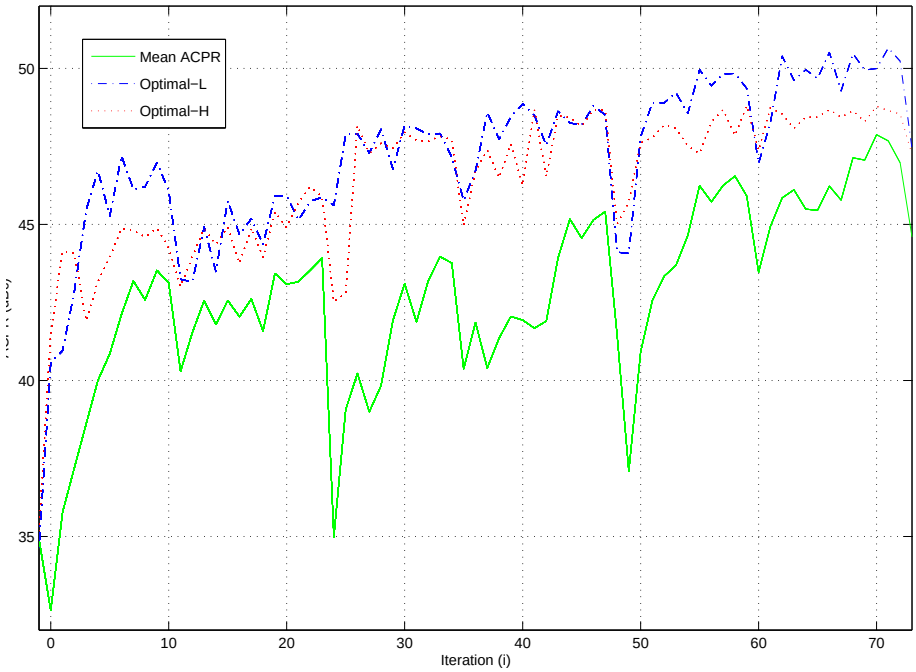

Figure 58: Convergence Profile for the Sequential GA with a 10dB PAR input signal.

$$\begin{bmatrix} a_{10} = 1.0145 + 0.2611i & a_{11} = 0.3476 - 0.1656i & a_{12} = -0.2429 - 0.4326i \\ a_{30} = -0.3044 + 0.0271i & a_{31} = 0.0755 + 0.4095i & a_{32} = 0.0020 + 0.1364i \\ a_{50} = 0.3246 + 0.2723i & a_{51} = -0.2583 - 0.0879i & a_{52} = 0.1160 + 0.0587i \\ a_{70} = 0.1974 + 0.5661i & a_{71} = 0.1009 + 0.0031i & a_{72} = -0.0362 - 0.3576i \end{bmatrix} \tag{64}$$

Contrary to the class AB amplifier tested in the previous section, the coefficients for this correction are separated by unit tap delays for both PAR levels. The implication is that Doherty amplifiers exhibit strong short-term memory effects when a 10MHz bandwidth signal is applied. The sampling rate determines the length of the memory effects which are corrected. The first polynomial is memoryless, the second corrects for memory effects up to 8.138ns, and the final polynomial corrects for memory effects up to 16.276ns. In this implementation, delays of up to 10 taps

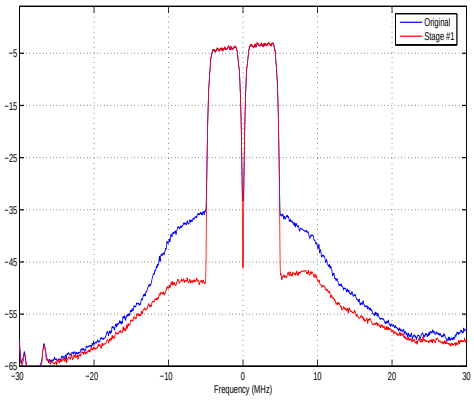

(a) Memoryless PA distortion compensation from P_1 adaptation.

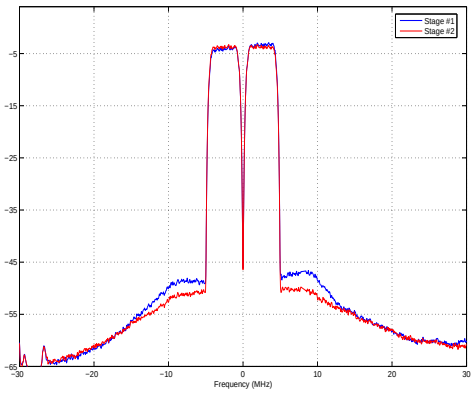

(b) Memory PD with 1st memory tap and P_2 adaptation.

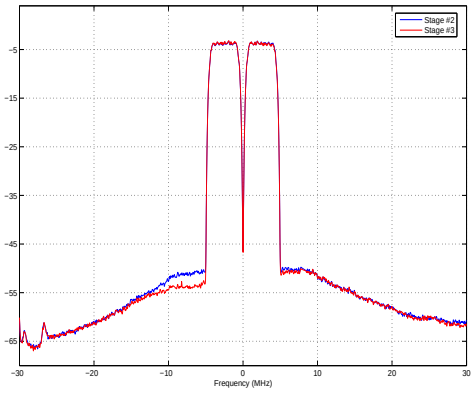

(c) Memory PD with additional taps and P_3 adaptation.

Figure 59: Sequential GA Linearization Performance with a 10dB PAR input signal.

were applied without added improvement which indicated that the remaining memory effects, if any, were greater than 81.38ns in length.

CHAPTER VII

CONCLUSION AND FUTURE WORK

This concluding chapter presents a brief summary of the work presented in this dissertation. This is followed by a discussion of possible applications, a highlighting of the contributions made by the work, and a brief discussion of potential areas of future research.

7.1 Summary

This dissertation presented a study of linearization techniques that have been applied to power amplifiers in the cellular communication industry. Previous techniques, although effective, have significant implementation costs that increase exponentially with the increasing signal bandwidths. In this work, a new technique was proposed that significantly reduces implementation costs and the overall complexity of the design.

The first embodiment of the algorithm was a simple polynomial solver. This was used to determine the curve fitting capabilities of the algorithm. With only limited information, the algorithm was used to simultaneously determine the coefficients of two independent polynomials.

The algorithm was then applied to a power amplifier software model. The exercise was used to demonstrate the algorithm performance versus an exhaustive random search technique. The algorithm was then applied to a closed loop hardware system. The system was implemented using laboratory equipment while adaptation was applied through a sponsor evaluation platform. The entire system was controlled through a software-computer interface. The system was characterized in terms of

adjacent channel power improvement for varying algorithm parameters.

A new system was introduced to validate crest factor reduction. The benefits and consequences of reducing the peak-to-average ratio of a test signal were quantified. The work extended itself to the application of CFR and wideband DPD on a hardware power amplifier.

The performance limitations of the algorithm on power amplifiers with strong memory effects dictated the need for memory pre-distortion. A wideband memory polynomial pre-distorter was introduced in software. The genetic algorithm using narrowband feedback was modified to correct for memory effects and a performance analysis was done between the two embodiments. The work introduced the concept of a sequential adaptation of the memory polynomials to maintain stability.

Finally, a new system was designed capable of implementing both wideband and narrowband pre-distortion. The system closely represents a typical basestation implementation for DPD including memory effects. The sequential genetic algorithm was allowed to adapt the memory polynomials using data with and without CFR. The implementation confirmed the combined benefits of DPD and CFR with greater signal bandwidths. The algorithm performance was indicated through increased output power and efficiency.

The application of genetic algorithms to memory PA linearization is a new approach to adaptive digital pre-distortion using narrowband feedback. The algorithm has been shown to adapt PD polynomials using only ACP feedback on software and hardware platforms. In this work, closed-loop hardware results for the adaption of a sequential memory polynomial have shown performance improvements on an amplifier with memory effects suggesting that this technique can be employed as a lower-cost solution to meet ACP requirements when compared to typical system implementations.

7.2 Comparison to Previous Techniques

In the past, several different techniques have been proposed to handle the problem of PA linearization. Previous implementations and techniques have been shown to achieve significant efficiency improvements. The most effective systems utilized either analog feedforward, analog feedback, or digital pre-distortion with wideband feedback. Although each successive method has achieved noticeable performance at a continually decreasing cost, the trend for cost reduction remains. This trend and the ongoing desire to push the digital domain out closer to analog favors digital pre-distortion. Performance and cost of DPD implementations is driven by the ADCs in the feedback path. These tradeoffs will be even more prevalent with the increasing bandwidth of 3.5G and 4G systems. The linearization efforts of PAs operating under 4th generation orthogonal frequency-domain modulation (OFDM) systems will further illustrate the limitations of DPD algorithms that require wideband feedback to achieve efficiency improvements. The 4G systems will occupy signal bandwidths exceeding 60MHz, these will require over 300MHz of feedback bandwidth to correct 3rd and 5th order intermodulation products. The ADCs required to accomplish this will have to sample at rates exceeding 400MHz. The cost of such devices will outweigh the benefits of pre-distortion.

As compared to previous results, this work produces linearization enhancements that exceed that of published techniques for closed-loop systems. This work acknowledges that many DPD implementations do not publish results to maintain the intellectual property of their proprietary algorithms.

7.3 Applications

One of the motivating factors for this work was the applicability to various modulation schemes with varying signal bandwidths. Implementation cost of the narrowband

feedback DPD using the GA is independent of the bandwidth of the transmitted signal. Power amplifiers, regardless of size, benefit from added efficiency. The application lends itself well to picocell basestations which typically require 5W of transmitted power, 20W PAs are typically used for this type of application at significant levels of backoff. In this case, it is less expensive to operate a PA in significant backoff than to implement wideband feedback DPD. The application is further idealized by the fact that PAs rated for greater than 20W are predominantly affected by frequency or short memory effects.

Any system that requires some form of signal amplification will be subject to distortion. Linearization techniques can be utilized in any of these applications with minimal impact on system performance while achieving considerable cost savings. Linearization could be applied in the field of audio engineering, the implementation would mostly lend itself to high-fidelity systems. The most important tradeoff is the complexity of the design. In the simplest case, backoff is sufficient to achieve acceptable distortion levels. A second tradeoff may be that PA modules were designed to generate and dissipate specific levels of power. Operating a PA outside of these levels may affect the lifetime of the PA module. Therefor to maintain the thermal behavior of the module, the PA may also require additional cooling fans and heat sinks. In most cases, these tradeoffs will still suggest that at least one linearization technique should be employed.

7.4 Contributions

The key contributions of this work are:

1. An novel linearization algorithm that requires only narrowand feedback.
    - The genetic algorithm was parameterized to be used as a polynomial solver.
    - The algorithm was applied to a typical power amplifier model.

- The algorithm parameters and cost function were optimized to significantly reduce distortion levels in the software model.

2. Closed-loop implementations of the algorithm.

   - Software was used to control test equipment capable of representing a closed loop system with narrowband feedback.
   - A second system was implemented capable of supporting larger signal bandwidths and crest factor reduction.
   - A final system was designed capable of supporting significant bandwidths for both narrowband and wideband feedback algorithms.

3. Memory pre-distortion and the genetic algorithm.

   - A sequential adaptation genetic algorithm was proposed in software and validated in hardware.
   - The implementation confirms that the algorithm is not subject to typical system constraints present in wideband feedback architectures.
   - The simple, cost-effective solution is shown to significantly increase the efficiency and output power of a base station power amplifier.

7.5 Future Work

Based on the work presented here, there exist several potential directions for future research. The first extension of this work is to apply the genetic algorithm using only narrowband feedback to correct the I/Q imbalance and LO feedthrough in the transmit chain that are often present in direct upconversion systems. Techniques have been proposed for correcting gain, phase, and offset imbalance [52]. Previous work defines the gain imbalance indicated in Equation 65 where α and β represent

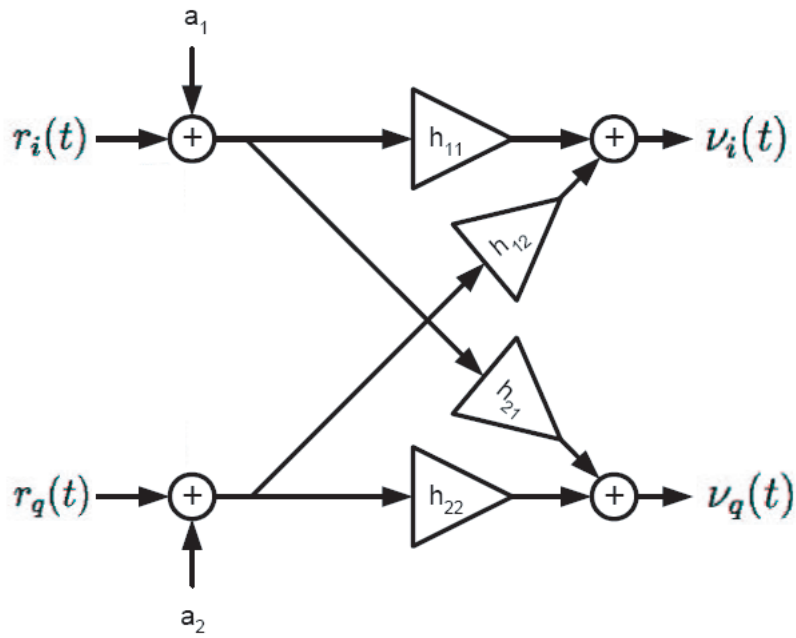

Figure 60: Model of imbalance introduced by a direct upconversion circuit.

the amplitude gains of both the I and Q channels, respectively.

$$\epsilon = \alpha/\beta - 1 \tag{65}$$

Direct upconversion is modeled in Figure 60, where a_1 and a_2 define the resulting DC offset. The input to the direct upconversion model is shown in Equation 66.

$$r(t) = \begin{bmatrix} r_i(t) \\ r_q(t) \end{bmatrix} \tag{66}$$

The direct upconversion output is given by Equation 67

$$\begin{bmatrix} v_i(t) \\ v_q(t) \end{bmatrix} = \begin{bmatrix} h_{11} & h_{12} \\ h_{21} & h_{22} \end{bmatrix} \left(\begin{bmatrix} r_i(t) \\ r_q(t) \end{bmatrix} + \begin{bmatrix} a_1 \\ a_2 \end{bmatrix} \right) \tag{67}$$

where

$$\begin{bmatrix} h_{11} & h_{12} \\ h_{21} & h_{22} \end{bmatrix} = \begin{bmatrix} \alpha cos(\phi/2) & \beta sin(\phi/2) \\ \alpha sin(\phi/2) & \beta cos(\phi/2) \end{bmatrix} \tag{68}$$

A typical correction circuitry is suggested in Figure 61 which requires only 6 parameters to achieve additional performance, the I and Q gain offset parameters, or

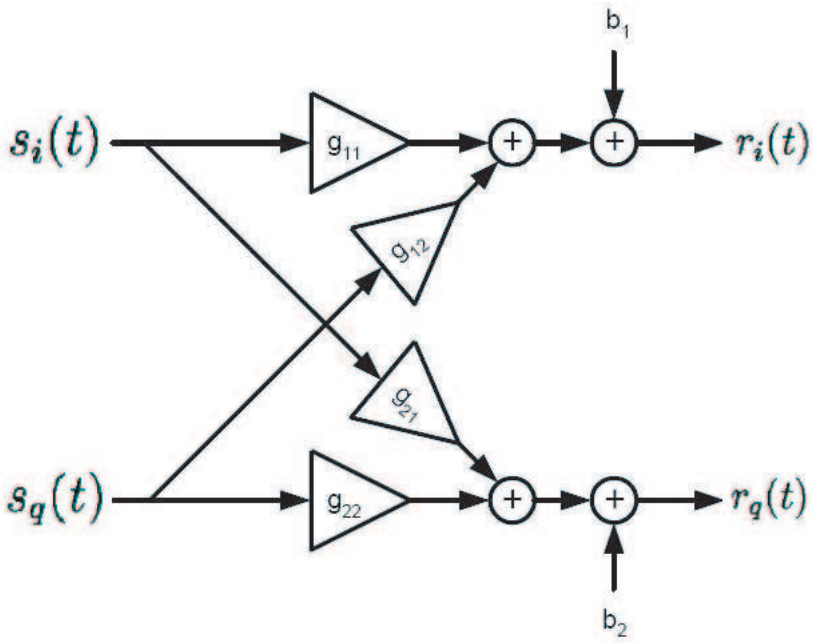

Figure 61: Direct upconversion imbalance correction circuit.

b_1 and b_2 would correct for LO feedthrough while the g_{11}, g_{12}, g_{21}, and g_{22} parameters would correct the I/Q imbalance. The correction implementation is summarized by Equation 69.

$$\begin{bmatrix} r_i(t) \\ r_q(t) \end{bmatrix} = \begin{bmatrix} g_{11} & g_{12} \\ g_{21} & g_{22} \end{bmatrix} \begin{bmatrix} s_i(t) \\ s_q(t) \end{bmatrix} + \begin{bmatrix} b_1 \\ b_2 \end{bmatrix} \tag{69}$$

The LO feedthrough would be measured simply at the LO frequency with a narrowband power detector, the I/Q imbalance would be measured at the carrier location and the image location. Equation 67 can be expressed as $v(t) = H(r(t) + a))$ while Equation 69 is summarized as $r(t) = Gs(t) + b$. The GA could adapt the 6 parameters until $b = -a$ and $G = H^{-1}$.

In a wideband system implementation that was suggested in the previous chapter, there is no method to measure the image of the transmitted versus received signal for a single LO solution. The single LO solution is preferred as it maintains the phase alignment of the transmitted and received signal. As was indicated in the previous chapter, an equalization step would allow for greater algorithm performance

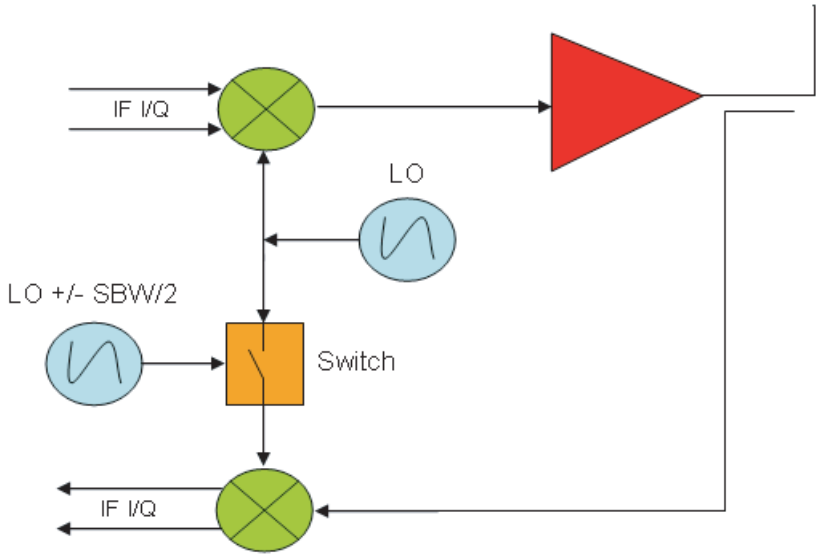

Figure 62: Dual LO configuration for I/Q imbalance correction in a wideband feedback system.

by optimizing the transmit and receive chains. During this calibration process, a novel system implementation would utilize a dual voltage controlled oscillator (VCO) topology to allow measurement of the transmit and receive image. If the VCO offset was marginal there would be little impact on the phase characteristics of the system. It would be simple to measure and eliminate the images of the signals during this calibration. The system implementation is illustrated in Figure 62.

Enhanced characterization of the PA performance and memory effects could also increase the performance of the algorithm. A multi-tone test could be used to accurately predict memory effects by varying the tone-spacing and amplitude. The spectral information could then be used to formulate more accurate search spaces for the three memory polynomials. It may also be desirable to allow the GA adaptation of the tap delay length which, in this case, was optimized experimentally. Future embodiments of the algorithm could also be made to include envelope memory effects which are characterized by their longer time constants, improving the linearization performance of the algorithm.

Fourth generation modulation schemes are now defined to be orthogonal frequency-division multiplexing signals (OFDM). A specific characteristic of these signals is that they are time division duplexing(TDD); thus the PA will transmit frames of data that contain data and no data. The on/off behavior will produce new unquantified memory effects in PAs. A second characteristic of such signals is their large bandwidth, which look to exceed 60MHz. Wideband feedback would require over 300MHz of feedback bandwidth for wideband architectures. The cost advantages of the genetic algorithm and narrowband feedback are evident here.

Finally, the implementation of a physical device which accomplishes DPD using the genetic algorithm and narrowband feedback in an ASIC or FPGA evaluation platform could show the actual cost savings over wideband feedback architectures.

APPENDIX A

TWO-TONE COEFFICIENT EXPANSION

```
y = A1 * Cos[w1 * t] + A2 * Cos[w2 * t]
z = a * y + b * y^2 + c * y^3
Expand[TrigReduce[z]]
```

$$A1\,\text{Cos}[t\,w1] + A2\,\text{Cos}[t\,w2]$$

$$a\,(A1\,\text{Cos}[t\,w1] + A2\,\text{Cos}[t\,w2]) + b\,(A1\,\text{Cos}[t\,w1] + A2\,\text{Cos}[t\,w2])^2 + c\,(A1\,\text{Cos}[t\,w1] + A2\,\text{Cos}[t\,w2])^3$$

$$\frac{A1^2\,b}{2} + \frac{A2^2\,b}{2} + a\,A1\,\text{Cos}[t\,w1] + \frac{3}{4}\,A1^3\,c\,\text{Cos}[t\,w1] + \frac{3}{2}\,A1\,A2^2\,c\,\text{Cos}[t\,w1] + \frac{1}{2}\,A1^2\,b\,\text{Cos}[2\,t\,w1] + \frac{1}{4}\,A1^3\,c\,\text{Cos}[3\,t\,w1] +$$
$$a\,A2\,\text{Cos}[t\,w2] + \frac{3}{2}\,A1^2\,A2\,c\,\text{Cos}[t\,w2] + \frac{3}{4}\,A2^3\,c\,\text{Cos}[t\,w2] + \frac{1}{2}\,A2^2\,b\,\text{Cos}[2\,t\,w2] + \frac{1}{4}\,A2^3\,c\,\text{Cos}[3\,t\,w2] + \frac{3}{4}\,A1\,A2^2\,c\,\text{Cos}[t\,w1 - 2\,t\,w2] +$$
$$A1\,A2\,b\,\text{Cos}[t\,w1 - t\,w2] + \frac{3}{4}\,A1^2\,A2\,c\,\text{Cos}[2\,t\,w1 - t\,w2] + A1\,A2\,b\,\text{Cos}[t\,w1 + t\,w2] + \frac{3}{4}\,A1^2\,A2\,c\,\text{Cos}[2\,t\,w1 + t\,w2] + \frac{3}{4}\,A1\,A2^2\,c\,\text{Cos}[t\,w1 + 2\,t\,w2]$$

```
y = A * Cos[w1 * t] + A * Cos[w2 * t]
z = a * y + b * y^2 + c * y^3
Expand[TrigReduce[z]]
```

$$A\,\text{Cos}[t\,w1] + A\,\text{Cos}[t\,w2]$$

$$a\,(A\,\text{Cos}[t\,w1] + A\,\text{Cos}[t\,w2]) + b\,(A\,\text{Cos}[t\,w1] + A\,\text{Cos}[t\,w2])^2 + c\,(A\,\text{Cos}[t\,w1] + A\,\text{Cos}[t\,w2])^3$$

$$A^2\,b + a\,A\,\text{Cos}[t\,w1] + \frac{9}{4}\,A^3\,c\,\text{Cos}[t\,w1] + \frac{1}{2}\,A^2\,b\,\text{Cos}[2\,t\,w1] + \frac{1}{4}\,A^3\,c\,\text{Cos}[3\,t\,w1] + a\,A\,\text{Cos}[t\,w2] +$$
$$\frac{9}{4}\,A^3\,c\,\text{Cos}[t\,w2] + \frac{1}{2}\,A^2\,b\,\text{Cos}[2\,t\,w2] + \frac{1}{4}\,A^3\,c\,\text{Cos}[3\,t\,w2] + \frac{3}{4}\,A^3\,c\,\text{Cos}[t\,w1 - 2\,t\,w2] + A^2\,b\,\text{Cos}[t\,w1 - t\,w2] +$$
$$\frac{3}{4}\,A^3\,c\,\text{Cos}[2\,t\,w1 - t\,w2] + A^2\,b\,\text{Cos}[t\,w1 + t\,w2] + \frac{3}{4}\,A^3\,c\,\text{Cos}[2\,t\,w1 + t\,w2] + \frac{3}{4}\,A^3\,c\,\text{Cos}[t\,w1 + 2\,t\,w2]$$

Two-tone response of a 3rd order polynomial power amplifier model.

```
y = A1 * Cos[w1 * t] + A2 * Cos[w2 * t]
z = a * y + b * y^3
Expand[TrigReduce[z]]
```

$$A\,\text{Cos}[t\,w1] + A\,\text{Cos}[t\,w2]$$

$$a\,(A\,\text{Cos}[t\,w1] + A\,\text{Cos}[t\,w2]) + b\,(A\,\text{Cos}[t\,w1] + A\,\text{Cos}[t\,w2])^3$$

$$a\,A\,\text{Cos}[t\,w1] + \frac{9}{4}\,A^3\,b\,\text{Cos}[t\,w1] + \frac{1}{4}\,A^3\,b\,\text{Cos}[3\,t\,w1] + a\,A\,\text{Cos}[t\,w2] + \frac{9}{4}\,A^3\,b\,\text{Cos}[t\,w2] + \frac{1}{4}\,A^3\,b\,\text{Cos}[3\,t\,w2] + \frac{3}{4}\,A^3\,b\,\text{Cos}[t\,w1 - 2\,t\,w2] + \frac{3}{4}\,A^3\,b\,\text{Cos}[2\,t\,w1 - t\,w2] + \frac{3}{4}\,A^3\,b\,\text{Cos}[2\,t\,w1 + t\,w2] + \frac{3}{4}\,A^3\,b\,\text{Cos}[t\,w1 + 2\,t\,w2]$$


```
y = A * Cos[w1 * t] + A * Cos[w2 * t]
z = a * y + b * y^3
Expand[TrigReduce[z]]
```

$$A\,\text{Cos}[t\,w1] + A\,\text{Cos}[t\,w2]$$

$$a\,(A\,\text{Cos}[t\,w1] + A\,\text{Cos}[t\,w2]) + b\,(A\,\text{Cos}[t\,w1] + A\,\text{Cos}[t\,w2])^3$$

$$a\,A\,\text{Cos}[t\,w1] + \frac{9}{4}\,A^3\,b\,\text{Cos}[t\,w1] + \frac{1}{4}\,A^3\,b\,\text{Cos}[3\,t\,w1] + a\,A\,\text{Cos}[t\,w2] + \frac{9}{4}\,A^3\,b\,\text{Cos}[t\,w2] + \frac{1}{4}\,A^3\,b\,\text{Cos}[3\,t\,w2] + \frac{3}{4}\,A^3\,b\,\text{Cos}[t\,w1 - 2\,t\,w2] + \frac{3}{4}\,A^3\,b\,\text{Cos}[2\,t\,w1 - t\,w2] + \frac{3}{4}\,A^3\,b\,\text{Cos}[2\,t\,w1 + t\,w2] + \frac{3}{4}\,A^3\,b\,\text{Cos}[t\,w1 + 2\,t\,w2]$$

Two-tone response of a 3rd order polynomial power amplifier model for odd-ordered terms.

```
y = A1 * Cos[w1 * t] + A2 * Cos[w2 * t]
z = a * y + b * y^3 + c * y^5
Expand[TrigReduce[z]]
```

$$A1\,\text{Cos}[t\,w1] + A2\,\text{Cos}[t\,w2]$$

$$a\,(A1\,\text{Cos}[t\,w1] + A2\,\text{Cos}[t\,w2]) + b\,(A1\,\text{Cos}[t\,w1] + A2\,\text{Cos}[t\,w2])^3 + c\,(A1\,\text{Cos}[t\,w1] + A2\,\text{Cos}[t\,w2])^5$$

$$\begin{aligned}
&a\,A1\,\text{Cos}[t\,w1] + \frac{3}{4}A1^3\,b\,\text{Cos}[t\,w1] + \frac{3}{2}A1\,A2^2\,b\,\text{Cos}[t\,w1] + \frac{5}{8}A1^5\,c\,\text{Cos}[t\,w1] + \frac{15}{4}A1^3\,A2^2\,c\,\text{Cos}[t\,w1] + \frac{15}{8}A1\,A2^4\,c\,\text{Cos}[t\,w1] + \frac{1}{4}A1^3\,b\,\text{Cos}[3\,t\,w1] + \\
&\frac{5}{16}A1^5\,c\,\text{Cos}[3\,t\,w1] + \frac{5}{4}A1^3\,A2^2\,c\,\text{Cos}[3\,t\,w1] + \frac{1}{16}A1^5\,c\,\text{Cos}[5\,t\,w1] + a\,A2\,\text{Cos}[t\,w2] + \frac{3}{2}A1^2\,A2\,b\,\text{Cos}[t\,w2] + \frac{3}{4}A2^3\,b\,\text{Cos}[t\,w2] + \\
&\frac{15}{8}A1^4\,A2\,c\,\text{Cos}[t\,w2] + \frac{15}{4}A1^2\,A2^3\,c\,\text{Cos}[t\,w2] + \frac{5}{8}A2^5\,c\,\text{Cos}[t\,w2] + \frac{1}{4}A2^3\,b\,\text{Cos}[3\,t\,w2] + \frac{5}{4}A1^2\,A2^3\,c\,\text{Cos}[3\,t\,w2] + \frac{5}{16}A2^5\,c\,\text{Cos}[3\,t\,w2] + \\
&\frac{1}{16}A2^5\,c\,\text{Cos}[5\,t\,w2] + \frac{5}{16}A1\,A2^4\,c\,\text{Cos}[t\,w1 - 4\,t\,w2] + \frac{5}{8}A1^2\,A2^3\,c\,\text{Cos}[2\,t\,w1 - 3\,t\,w2] + \frac{3}{4}A1\,A2^2\,b\,\text{Cos}[t\,w1 - 2\,t\,w2] + \frac{15}{8}A1^3\,A2^2\,c\,\text{Cos}[t\,w1 - 2\,t\,w2] + \\
&\frac{5}{4}A1\,A2^4\,c\,\text{Cos}[t\,w1 - 2\,t\,w2] + \frac{5}{8}A1^3\,A2^2\,c\,\text{Cos}[3\,t\,w1 - 2\,t\,w2] + \frac{3}{4}A1^2\,A2\,b\,\text{Cos}[2\,t\,w1 - t\,w2] + \frac{5}{4}A1^4\,A2\,c\,\text{Cos}[2\,t\,w1 - t\,w2] + \\
&\frac{15}{8}A1^2\,A2^3\,c\,\text{Cos}[2\,t\,w1 - t\,w2] + \frac{5}{16}A1^4\,A2\,c\,\text{Cos}[4\,t\,w1 - t\,w2] + \frac{3}{4}A1^2\,A2\,b\,\text{Cos}[2\,t\,w1 + t\,w2] + \frac{5}{4}A1^4\,A2\,c\,\text{Cos}[2\,t\,w1 + t\,w2] + \\
&\frac{15}{8}A1^2\,A2^3\,c\,\text{Cos}[2\,t\,w1 + t\,w2] + \frac{5}{16}A1^4\,A2\,c\,\text{Cos}[4\,t\,w1 + t\,w2] + \frac{3}{4}A1\,A2^2\,b\,\text{Cos}[t\,w1 + 2\,t\,w2] + \frac{15}{8}A1^3\,A2^2\,c\,\text{Cos}[t\,w1 + 2\,t\,w2] + \\
&\frac{5}{4}A1\,A2^4\,c\,\text{Cos}[t\,w1 + 2\,t\,w2] + \frac{5}{8}A1^3\,A2^2\,c\,\text{Cos}[3\,t\,w1 + 2\,t\,w2] + \frac{5}{8}A1^2\,A2^3\,c\,\text{Cos}[2\,t\,w1 + 3\,t\,w2] + \frac{5}{16}A1\,A2^4\,c\,\text{Cos}[t\,w1 + 4\,t\,w2]
\end{aligned}$$

Two-tone response of a 5th order polynomial power amplifier model for odd-ordered terms.

```
y = A * Cos[w1 * t] + A * Cos[w2 * t]
z = a * y + b * y^3 + c * y^5
Expand[TrigReduce[z]]
```

$$A\,\mathrm{Cos}[t\,w1] + A\,\mathrm{Cos}[t\,w2]$$

$$a\,(A\,\mathrm{Cos}[t\,w1] + A\,\mathrm{Cos}[t\,w2]) + b\,(A\,\mathrm{Cos}[t\,w1] + A\,\mathrm{Cos}[t\,w2])^3 + c\,(A\,\mathrm{Cos}[t\,w1] + A\,\mathrm{Cos}[t\,w2])^5$$

$$\begin{aligned}
&a\,A\,\mathrm{Cos}[t\,w1] + \frac{9}{4}\,A^3\,b\,\mathrm{Cos}[t\,w1] + \frac{25}{4}\,A^5\,c\,\mathrm{Cos}[t\,w1] + \frac{1}{4}\,A^3\,b\,\mathrm{Cos}[3\,t\,w1] + \frac{25}{16}\,A^5\,c\,\mathrm{Cos}[3\,t\,w1] + \frac{1}{16}\,A^5\,c\,\mathrm{Cos}[5\,t\,w1] + a\,A\,\mathrm{Cos}[t\,w2] + \\
&\frac{9}{4}\,A^3\,b\,\mathrm{Cos}[t\,w2] + \frac{25}{4}\,A^5\,c\,\mathrm{Cos}[t\,w2] + \frac{1}{4}\,A^3\,b\,\mathrm{Cos}[3\,t\,w2] + \frac{25}{16}\,A^5\,c\,\mathrm{Cos}[3\,t\,w2] + \frac{1}{16}\,A^5\,c\,\mathrm{Cos}[5\,t\,w2] + \frac{5}{16}\,A^5\,c\,\mathrm{Cos}[t\,w1 - 4\,t\,w2] + \\
&\frac{5}{8}\,A^5\,c\,\mathrm{Cos}[2\,t\,w1 - 3\,t\,w2] + \frac{3}{4}\,A^3\,b\,\mathrm{Cos}[t\,w1 - 2\,t\,w2] + \frac{25}{8}\,A^5\,c\,\mathrm{Cos}[t\,w1 - 2\,t\,w2] + \frac{5}{8}\,A^5\,c\,\mathrm{Cos}[3\,t\,w1 - 2\,t\,w2] + \frac{3}{4}\,A^3\,b\,\mathrm{Cos}[2\,t\,w1 - t\,w2] + \\
&\frac{25}{8}\,A^5\,c\,\mathrm{Cos}[2\,t\,w1 - t\,w2] + \frac{5}{16}\,A^5\,c\,\mathrm{Cos}[4\,t\,w1 - t\,w2] + \frac{3}{4}\,A^3\,b\,\mathrm{Cos}[2\,t\,w1 + t\,w2] + \frac{25}{8}\,A^5\,c\,\mathrm{Cos}[2\,t\,w1 + t\,w2] + \frac{5}{16}\,A^5\,c\,\mathrm{Cos}[4\,t\,w1 + t\,w2] + \\
&\frac{3}{4}\,A^3\,b\,\mathrm{Cos}[t\,w1 + 2\,t\,w2] + \frac{25}{8}\,A^5\,c\,\mathrm{Cos}[t\,w1 + 2\,t\,w2] + \frac{5}{8}\,A^5\,c\,\mathrm{Cos}[3\,t\,w1 + 2\,t\,w2] + \frac{5}{8}\,A^5\,c\,\mathrm{Cos}[2\,t\,w1 + 3\,t\,w2] + \frac{5}{16}\,A^5\,c\,\mathrm{Cos}[t\,w1 + 4\,t\,w2]
\end{aligned}$$

Simplified two-tone response of a 5th order polynomial power amplifier model for odd-ordered terms.

APPENDIX B

CCDF AND COMPOSITE EVM CALCULATIONS

The following code calculates the complementary cumulative distribution function and the composite error vector magnitude. This can be run as an m-file using Matlab.

```
% ccdf function

function [x_db, ccdf, par, avg] = ccdf(a)

%   function [x_db, ccdf, par, avg] = ccdf(a)
%
%   This function calculates the Complementary Cumulative Distribution Function (CCDF)
%   of the COMPLEX input array a.
%   Output values:  x_db    X axis: dB power array (0 dB = average power of input waveform)
%                   ccdf    Y axis: complementary cumulative distribution function (above 0 dB)
%                   par     peak-to-average ratio, in dB
%

HIST_SIZE = 200;
magsq_a = abs(a).^2;              %   Calculate input mag-squared values
peak = max(magsq_a);              %   Find the peak value;
avg = mean(magsq_a);              %   Calculate the mean power

[h, x] = hist(magsq_a,HIST_SIZE);   %   Histogram the sample values - this generates the PDF
cdf = cumsum(h);                  %   Convert to cumulative distribution function
icdf = 100 * (cdf / max(cdf));      %   Convert cdf to percentages (should have 100% in the last
bin)
ccdf = 100 - icdf;                %   Create the ccdf, in percentages
x_db = 10 * log10(x / avg);         %   Convert mean(a) into dB, where 0 dB = average signal
power
N = 1 + sum(x_db < 0);            %   Ignore those first bins whose power was below 0 dB
x_db = x_db(x_db >= 0);           %   Only keep those mag-squared values above the average
power
ccdf = ccdf(N:HIST_SIZE);         %   Only keep those histogram percentages above the average
power
par = max(x_db);                  %   Save the peak-to-average ratio
return;
```

Figure 67: Complementary cumulative distribution function.

```
function calcevm(rate,samples);
%EVM calculation function
% This function calculates the cEVM using the complex testdata.in and
% testdata.out files. The IO delay is calculated using correlation
% functions for delays up to 2000 samples. The rate is used to define the
% sampling rate to set correct scaling on the frequency axis.
% Samples defines the number of samples to analyze.
% The output also includes PAR information about the input and output signals.
% Type calcevm(80,100000) to look at 100k samples at a 80MSPS sampling rate.

in = load('testdata.in');
out = load('testdata.out');

in = complex(in(:,1), in(:,2));
out = complex(out(:,1), out(:,2));

if samples == 0
in = in(1:end,:);
out = out(1:end,:);
else
in = in(1:samples,:);
out = out(1:samples,:);
end

% Normalize the output data
offset = sqrt(mean(abs(in).^2))/sqrt(mean(abs(out).^2));
out = offset*out;

% avergeIn = 20*log10(mean(abs(in)))
% avergeOut = 20*log10(mean(abs(out)))

%delay calculation
corr = xcorr(in(1:2000),out(1:2000));
[tmp, index] = max(corr);
delay = 2000 - index + 1;
display(['The sample delay is ' num2str(delay)]);

figure;
plot(real(out(delay:delay+200)));
hold on;
plot(real(in(1:201)),'r.-');
hold off;
```

Figure 68: Composite error vector magnitude calculations (Part 1).

```
figure;
% Actual CCDF of signal at 10^-4
[x_db, ccdfi, par, avg] = ccdf(in, 0, 0, 0);hold on;
act = find(ccdfi<.01);
display(['Actual Input CCDF @ 10^-4 is ' num2str(x_db(act(1)))]);

[x_db, ccdfo, par, avg] = ccdf(out(delay:end), 1, 0, 0);
act = find(ccdfo<.01);
display(['Actual Output CCDF @ 10^-4 is ' num2str(x_db(act(1)))]);

%   Generate the error signal
N = min (length(in), length(out));
e = out(delay:N) - in(1:N-delay+1);

figure;psd(e,4096,rate);
tmp = get(gca,'Children');
set(tmp(1),'Color','k');
hold on;
psd(in,4096,rate);
figure;psd(out(delay:end),4096,rate);
tmp = get(gca,'Children');
set(tmp(1),'Color','r');
hold on;
psd(e,4096,rate);
tmp = get(gca,'Children');
set(tmp(1),'Color','k');

%   Calculate evm (ratio of error power to signal power)
errPwr = sqrt(mean(abs(e).^2));
inPwr  = sqrt(mean(abs(in).^2));
EVMrms = 100 * errPwr / inPwr;
display(['RMS Error Vector Magnitude is ' num2str(EVMrms) '%']);

%   Calculate peak EVM
Io  =real(out(delay:N));
I   =real(in(1:N-delay+1));
Qo  =imag(out(delay:N));
Q   =imag(in(1:N-delay+1));
error = (Io-I).^2+(Qo-Q).^2;

EVMpk = 1/N*sqrt(sum(error)/sqrt(max(abs(in).^2)))*100;
display(['Peak Error Vector Magnitude is ' num2str(EVMpk) '%']);
```

Figure 69: Composite error vector magnitude calculations (Part 2).

APPENDIX C

EVALUATION PLATFORM AND GENETIC ALGORITHM GRAPHIC USER INTERFACE

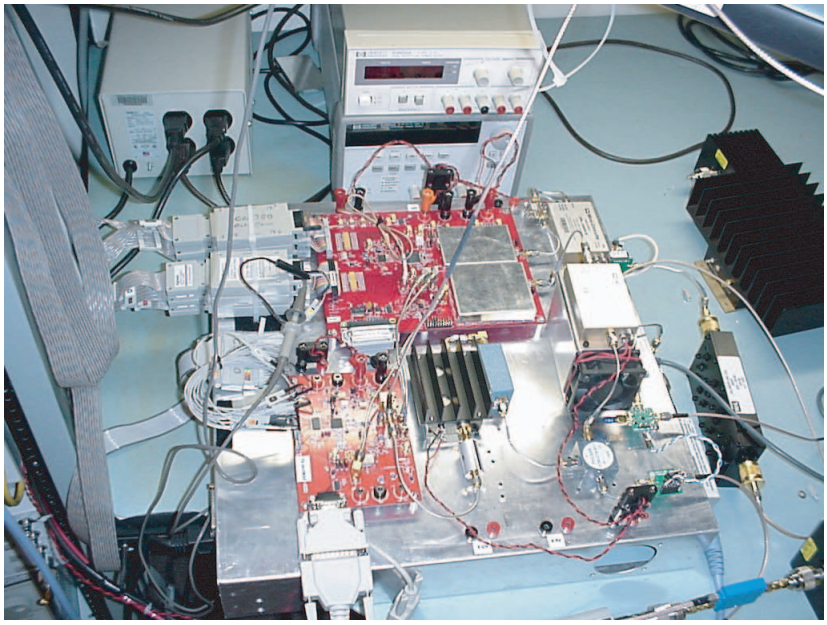

Figure 70: Wideband and narrowband digital pre-distortion evaluation platform.

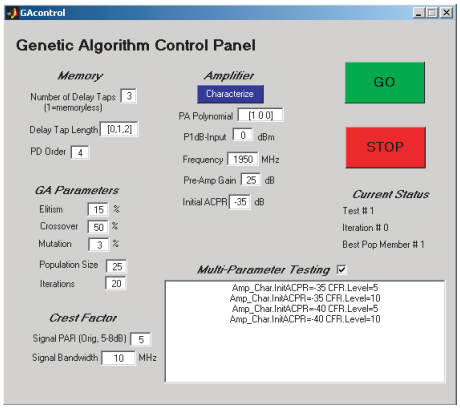

Figure 71: Genetic algorithm graphic user interface.

REFERENCES

[1] CDMA Development Group. http://www.cdg.org

[2] J. S. Kenney, and A. Leke, "Wireless Report: Power amplifier spectral regrowth for digital cellular and PCS applications," *Microwave Journal*, pp. 74-92, Oct. 1995.

[3] F. H. Raab, P. Asbeck, S. Cripps, P. B. Kenington, Z. B. Popovic, N. Pothecary, J. F. Sevic, and N. O. Sokal, "Power amplifiers and transmitters for RF and microwave," *IEEE Trans. Microwave Theory Tech.*, vol. 50, no. 3, pp. 814-826, Mar. 2002.

[4] P. B. Kenington, *High-linearity RF Amplifier Design.* Norwood, MA: Artech House, 2000.

[5] S. P. Stapleton, "Amplifier linearization using adaptive digital predistortion," *Applied Microwave & Wireless*, pp. 72-77, Feb. 2001.

[6] H.S. Black, Translating System, U.S. Patent 1686792, issued Oct. 29, and U.S. Patent 2102671, issued Dec. 1937.

[7] H. Girard, and K. Feher, "A new baseband linearizer for more efficient utilization of earth station amplifiers used for QPSK transmission," *IEEE J. Select. Areas Commun.*, vol. SAC-1, no. 1, 1983.

[8] M. Faulkner, "Adaptive linearization using predistortionexperimental results," *IEEE Trans. on Veh. Tech.*, vol. 43, pp. 323-332, May. 1994.

[9] Y. Park, W. Woo, R. Raich, J. S. Kenney, G. T. Zhou, "Adaptive predistortion linearization of RF power amplifiers using lookup tables generated from subsampled data," *IEEE Radio and Wireless Conference*, RAWCON 2002, pp. 233-236, August 2002.

[10] G. Baudoin, and P. Jardin, "Adaptive polynomial predistortion for linearization of power amplifiers in wireless communication and WLAN," *Eurocon 2001 Trends in Communications*, vol. 1, pp. 157-160, 2001.

[11] S.P. Stapleton, and F.C. Costescu, "An adaptive predistorter for a power amplifier based on adjacent channel emissions," *IEEE Trans. on Veh. Tech.*, vol. 41, no. 1, Feb. 1992.

[12] D. Whitley, "A genetic algorithm tutorial," *Stats. and Comp.*, vol. 4, pp. 65-85, 1994.

[13] R. Haupt, and S. E. Haupt, *Practical Genetic Algorithms.* John Wiley & Sons, Inc., 1998.

[14] M. Mitchell, *An Introduction to Genetic Algorithms*, "A Bradford Book," The MIT Press, 1998.

[15] D. E. Goldberg, *Genetic Algorithms in Search, Optimization & Machine Learning*, Addison Wesley Longman Inc., 1989.

[16] W. Banzhaf, P. Nordin, R. E. Keller, F. D. Francone, *Genetic Programming - An Introduction*, Morgan Kaufman Publishers Inc., 1998.

[17] S. C. Cripps, *RF Power Amplifiers for Wireless Communications*, Artech House, 1999.

[18] J. Sills, *Improved Performance in Power Amplifer Linearization using Digital Predistortion*, Intersil Corporation, 2002.

[19] G. Copeland, *Digital Power Amplifier Linearization*, Texas Instruments Inc., 2003.

[20] J. Vuolevi, and T. Rahkonen, *Distortion in RF Power Amplifiers*, Artech House, 2003.

[21] J. S. Kenney, W. Woo, L. Ding, R. Raich, H. Ku, and G. T. Zhou, "The impact of memory effects on predistortion linearization of RF power amplifiers," *ISMOT 2001*, Montreal, Canada, June 20-22, 2001.

[22] E. Westeson, and L. Sunstrm, *A Complex Polynomial Predistorter Chip in CMOS for Baseband or IF Linearization of RF Power Amplifiers*, Competence Center for Circuit Design, Lund University, 1999.

[23] S. P. Stapleton, and J. K. Cavers, "A new technique for adaptation of linearizing predistorters," *IEEE Veh. Tech. Conf.*, May 1991.

[24] V. Volterra, *Theory of Functionals and of Integral and Integro-Diffferential Equations*, New York: Dover, 1959.

[25] S. C. Cripps, *Advanced Techniques in RF Power Amplifier Design*, Artech House, 2000.

[26] Y. Akaiwa, and Y. Nagata, "Highly efficient digital mobile communications with linear modulation method," *IEEE J. Select. Areas Commun.*, vol. SAC-5, pp.890-895, June 1987.

[27] A. Bateman, D. M. Haines, and R. J. Wilkinson, "Linear transceiver architechtures," Proc. IEEE Veh. Tech. Conf., pp.478-484, 1988.

[28] D. R. Green, Jr., "Characterization and compensation of nonlinearities in microwave transmitters," *IEEE Trans. Microwave Theory Tech.*, vol. MTT-30, pp. 213-217, 1982.

[29] J. K. Cavers, "Convergence behaviour of an adaptive feedforward linearizer," *IEEE Veh. Tech. Conf.*, pp.499-503, 1994.

[30] A. A. M. Saleh, and J. Salz, "Adaptive linearization of power amplifiers in digital radio systems," *Bell Syst. Tech. Jour.*, vol. 62, no. 4, pp. 1019-1033, Apr. 1983.

[31] Y. Seto, S. Mizuta, K. Oosaki, and Y. Akaiwa, "Adaptive predistortion method for linear power amplifiers," *Veh. Tech. Conf.*, 2000.

[32] K. Yamauchi, et al., "A novel series diode linearizer for mobil radio power amplifiers," *Proc. IEEE IMS*, MTT-S, pp.831-834, 1996.

[33] A. Katz, et al., "Passive FET MMIC linearizers for C, X, Ku-band satellite applications,"*Proc. IEEE IMS*, MTT-S, pp.353-356, 1993.

[34] Y. Nagata, "Linear amplification technique for digital mobile communications," *Proc. IEEE Veh. Tech. Conf.*, pp.159-164, 1989.

[35] J. K. Cavers, "Amplifer linearization using a digital predistorter with fast adaptation and low memory requireemnts," *IEEE Trans. on Veh. Tech.*, vol.39, pp.374-382, 1990.

[36] J. Holland, "Adaptation In Natural and Artificial Systems," University of Michigan Press, 1975.

[37] L. Chambers, *The Practical Handbook of Gen etic Algorithms Applications.-2nd ed.*, Chapman & Hall/CRC, 2001.

[38] H. E. Danielson, et al., "Objective analysis of chromatin structure as a tool for diagnosis and prognosis in cancer," *Analytical and Quantitive Cytology and Histology*, Vol. 16, no. 1, pp.40-43, 1994.

[39] A. Wright, *Multi-Carrier WCDMA Basestation Design Considerations-Amplifier Linearization and Crest Factor Control*, PMC-Sierra Inc., 2002.

[40] S. Mizuta, H. Kawaguchi, and Y. Akaiwa, "The peak limiting of a baseband code-division multiplexed signal applied to a predistorted power amplifier," *Proc. IEEE Veh. Tech. Conf.*, vol.3, pp.1953-1957, 2001.

[41] Sirenza Microdevices Inc., Broomfield, CO, 80021.

[42] J. S. Kenney, W. Woo et al., "The impact of memory effects of predistortion linearization of RF power amplifiers," *8th Intl. Symposium on Microwave and Optical Technology (ISMOT'01)*, pp. 189-193, Montreal, Quebec, Canada, June 2001.

[43] Ericsson, Inc., Mountain View Rd., Lynchberg, VA, 24502.

[44] H. Ku and J. S. Kenney, "Behavioral modeling of RF power amplifiers considering IMD and spectral regrowth asymmetries," *IEEE International Microwave Symposium*, IMS 2003, June 2003.

[45] Y. Park, W. Woo, R. Raich, J. S. Kenney, and G. T. Zhou, "Adaptive predistortion linearization of RF power amplifiers using lookup tables generated from subsampled data," *IEEE Radio and Wireless Conference*, RAWCON 2002, pp. 233-236, August 2002.

[46] Cree Microwave Inc., Sunnyvale, California, 94089.

[47] Intersil Corporation, Palm Beach, Florida,.

[48] K. J. Muhonen, M. Kavehrad, and R. Krishnamoorthy, "Look-up table techniques for adaptive digital predistortion: a development and comparison," *IEEE Trans. on Veh. Tech.*, vol.49, pp.1995-2002, 2000.

[49] L. Ding, G. T. Zhou, D. R. Morgan, Z. Ma, J. S. Kenney, J. K Kim, and C. R. Giardina, "A robust digital baseband predistorter constructed using memory polynomials," *IEEE Trans. Communications*, vol.52, no.1, pp.159-165, 2004.

[50] S. Im, and E. J. Powers, "A block LMS algorithm for third-order frequency-domain Volterra filters," *IEEE Signal Processing Letters*, vol.4, no.3, pp.75-78, March 1997.

[51] J. Kim, and K. Konstantinou, "Digital Predistortion of wideband signals based on power amplifiers with memory," Electron Letters, vol.37, pp.1417-1418, Nov. 2001.

[52] J. K. Cavers, and M.W. Liao, "Adaptive Compensation for Imbalance and Offset Losses in Direct Conversion Transceivers," *IEEE Trans. on Veh. Tech.*, vol. 42, no. 4, pp. 581-588, 1993.

[53] Bravo Tech Inc., Cypress, California, 90630.

[54] M. Schetzen, *The Volterra and Weiner Theories of Nonlinear Systems*, New York: Wiley, 1980.

[55] Mini-Circuits, Brooklyn, New York, 11235.

[56] J. A. Sills, and R. Sperlich, "Adaptive power amplifier linearization by digital pre-distortion using genetic algorithms," IEEE Radio and Wireless Conference, RAWCON 2002, pp. 229-232, August 2002.

[57] R. Sperlich, J.A. Sills, J.S. Kenney, "Closed-Loop Digital Pre-Distortion for Power Amplifier Linearization using Genetic Algorithms," *Microwave Symposium Digest*, IEEE MTT-S International, Vol. 1, June 2003.

[58] R. Sperlich, Y. Park, G. Copeland, and J. S. Kenney, "Power Amplifier Linearization with Digital Pre-Distortion and Crest Factor Reduction", International Microwave Symposium, IMS 2004, June 2004.

[59] R. Sperlich, J.A. Sills, and J.S. Kenney, "Power amplifier linearization with memory effects using digital pre-distortion and genetic algorithms," *IEEE Radio and Wireless Conference*, RAWCON 2004, September 2004.

[60] R. Sperlich, J. A. Sills, and J.S. Kenney, "Closed-Loop Digital Pre-Distortion with Memory Effects Using Genetic Algorithms", International Microwave Symposium, IMS 2005, June 2005.

VITA

Roland Sperlich was born in Montreal, Quebec in 1976. He received his B.S. degree in electrical and computer engineering from the Merrimack College, MA in 2000 and his M.S. degree in electrical engineering from Georgia Institute of Technology in 2002.

His interest in power amplifier linearization originated from interests in digital and analog integrated circuit design with a strong background in digital signal processing. These skills and interests naturally extended themselves to system level design and linearization algorithm development.